The Journal of Gemmology
Volume 36 / No. 1 / 2018

SSEF
SCHWEIZERISCHES GEMMOLOGISCHES INSTITUT
SWISS GEMMOLOGICAL INSTITUTE
INSTITUT SUISSE DE GEMMOLOGIE

Gem-A
THE GEMMOLOGICAL ASSOCIATION
OF GREAT BRITAIN

SSEF

SCHWEIZERISCHES GEMMOLOGISCHES INSTITUT
SWISS GEMMOLOGICAL INSTITUTE
INSTITUT SUISSE DE GEMMOLOGIE

ORIGIN DETERMINATION · TREATMENT DETECTION

DIAMOND GRADING · PEARL TESTING

EDUCATION · RESEARCH

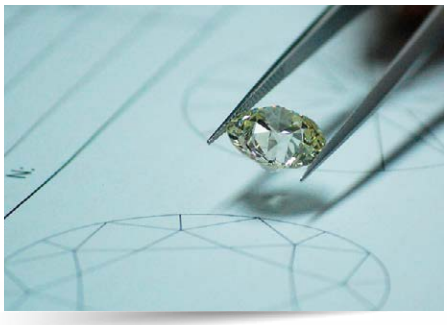

THE SCIENCE OF GEMSTONE TESTING™

Aeschengraben 26, 4051 Basel, Switzerland Tel. +41 61 262 06 40 Fax + 41 61 262 06 41 admin@ssef.ch www.ssef.ch

The Journal of Gemmology

Volume 36 / No. 1 / 2018

COLUMNS

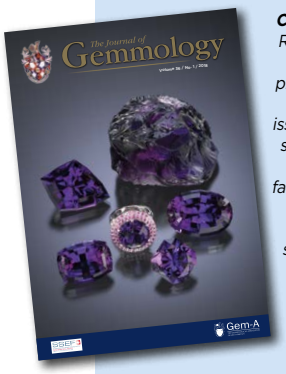

Cover photo: *Amethyst from Rwanda may display unusual optical and microscopic properties, as described in an article on pp. 26–36 of this issue. The Rwandan amethyst shown here includes a rough piece weighing 101 g, loose faceted gems of 26.62–63.41 ct and an 11.61 ct centre stone that is surrounded by pink sapphires in a 14-carat white gold ring. Courtesy of Steve Moriarty, Moriarty's Gem Art, Crown Point, Indiana, USA; photo by Jeff Scovil.*

ARTICLES

The Journal is published by Gem-A in collaboration with SSEF and with the support of AGL.

Gem-A THE GEMMOLOGICAL ASSOCIATION OF GREAT BRITAIN

SSEF SCHWEIZERISCHES GEMMOLOGISCHES INSTITUT SWISS GEMMOLOGICAL INSTITUTE INSTITUT SUISSE DE GEMMOLOGIE

AGL AMERICAN GEMOLOGICAL LABORATORIES

The Journal of Gemmology

CONTENT SUBMISSION

The Editor-in-Chief is glad to consider original articles, news items, conference/excursion reports, announcements and calendar entries on subjects of gemmological interest for publication in *The Journal of Gemmology*. A guide to the various sections and the preparation of manuscripts is given at www.gem-a.com/index.php/news-publications/publications/journal-of-gemmology/submissions, or contact the Editor-in-Chief.

SUBSCRIPTIONS

Gem-A members receive *The Journal* as part of their membership package, full details of which are given at www.gem-a.com/membership. Laboratories, libraries, museums and similar institutions may become direct subscribers to *The Journal*.

ADVERTISING

Enquiries about advertising in *The Journal* should be directed to advertising@gem-a.com. For more information, see www.gem-a.com/index.php/news-publications/publications/journal-of-gemmology/advertising.

DATABASE COVERAGE

The Journal of Gemmology is covered by the following abstracting and indexing services: Australian Research Council academic journal list, British Library Document Supply Service, Chemical Abstracts (CA Plus), Copyright Clearance Center's RightFind application, CrossRef, EBSCO (Academic Search International, Discovery Service and TOC Premier), Gale/Cengage Learning Academic OneFile, GeoRef, Index Copernicus ICI Journals Master List, Mineralogical Abstracts, Cambridge Scientific Abstracts (ProQuest), Scopus and the Thomson Reuters' Emerging Sources Citation Index (in the Web of Science).

COPYRIGHT AND REPRINT PERMISSION

Design & production by Zest Design, www.zest-uk.com

Printed by DG3 Group (Holdings) Ltd

ISSN: 1355-4565

Gem-A
THE GEMMOLOGICAL ASSOCIATION OF GREAT BRITAIN

21 Ely Place
London EC1N 6TD
UK
t: +44 (0)20 7404 3334
f: +44 (0)20 7404 8843
e: information@gem-a.com
w: www.gem-a.com

Registered Charity No. 1109555
A company limited by guarantee and registered in England No. 1945780
Registered office: Palladium House, 1–4 Argyll Street, London W1F 7LD

Editorial

AN UPDATED DESIGN FOR *THE JOURNAL OF GEMMOLOGY*

With this issue of *The Journal*, we begin a new volume (36) and also introduce a fresh new design. Unfortunately, however, we also see the departure of Mary Burland as production editor. Mary states, "I am sorry to be leaving *The Journal* after over 50 years working in various capacities from typing copy to production manager. In recent years I also have been responsible for the layout, which I have really enjoyed. I wish *The Journal* luck for the future—may it go from strength to strength." Thank you, Mary, for your many decades of dedication to ensuring that *The Journal* is informative, looks good and free of typos!

Gem-A has now appointed Zest (in London) for the design and production of *The Journal*. While the range of content will remain the same, you will notice a more contemporary look to the pages, particularly the Feature Articles. As shown by the images on this page, the design of *Journal* articles has evolved several times over the years. One aspect that has remained the same, though, is the care and attention given to manuscripts throughout the review, revision and editing process to maintain their educational value and scientific rigor. For this I particularly thank *The Journal*'s Associate Editors for their expertise, advice and constructive comments, and the authors for their perseverance and commitment to ensuring the high quality of their contributions.

I also would like to take this opportunity to acknowledge the valuable financial support of our sponsors and advertisers, which helps make it all possible—thank you.

Brendan Laurs
Editor-in-Chief

Updated Feature Article design alongside article pages from *The Journal* spanning 1947–2014

What's New

INSTRUMENTATION

ABCD Gem Testing Set

In June 2017, the Asian Gemmological Institute and Laboratory Ltd in Hong Kong released a compact portable kit consisting of 13 gem-testing instruments: polariscope, handheld incandescent lamp, darkfield and diffuse adaptors for the lamp, rotating plate for the polariscope, loupe, long-wave UV lamp, tweezers, four-claw stone holder, conoscope, reflective diffuse block, lanyard and gem cloth. For additional information, including a guide for use, visit www.agil.com.hk/en/gemtesting.php?gemtestingid=13. *CMS*

Jewellery Inspector

Manufactured by Gemetrix (Perth, Australia), the Jewellery Inspector debuted January 2018. This cousin of the Melee Inspector (see Vol. 35, No. 8, p. 687 of *The Journal*) features a tray that can hold jewellery to allow observation of both short- and long-wave UV luminescence and phosphorescence of mounted or unmounted samples through the unit's 45 × 45 mm viewing area. For more information, visit www.gemconference.com/store/instruments/jewellery-inspector. *CMS*

GemoAid Universal Microscope Upgrade Kit

Released in late 2017, this useful set of gemmological microscope accessories includes four dock bases (to accommodate various models of microscopes) for placing accessories over the light well, a diffuser lens, a glass immersion cell, mounting rods of two different heights, two polarizing lenses, and yellow and blue colour filters. The kit is structured in a modular way that allows mounting of several accessories at the same time (e.g. diffuser, immersion cell and colour filter). The kit is compatible with most current gemmological microscopes, and is available for US$139.00 plus $6 shipping. For additional information and online ordering, visit www.gemoaid.com/universal-microscope-upgrade-kit-special-price or email instruments@gem-a.com. *CMS*

NEWS AND PUBLICATIONS

AGTA GemFair Tucson Seminars

From 30 January to 4 February 2018, the American Gem Trade Association hosted an array of seminars during the gem shows in Tucson, Arizona, USA. Presenters from around the world discussed various aspects of the industry, including marketing, mining, appraising, identification and jewellery. The lectures also covered various gem materials, including ruby, sapphire, pearl, jade, coral and more. A flash drive containing recordings and slides of 22 of the 26 seminars can be purchased for US$50.00. Visit www.agta.org/education/seminars.html for a summary of the presentations, a list of the speakers and an order form. *CMS*

Gem Testing Laboratory (Jaipur, India) Newsletter

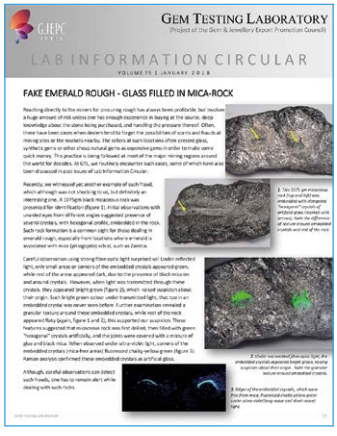

GTL Jaipur's latest *Lab Information Circular* (January 2018) features reports on a black micaceous rock embedded with hexagonal-shaped artificial glass imitating emerald crystals, faceted specimens of eudialyte, purple 'Morado' opal from Mexico, resin-filled amazonite beads, quartz with abundant graphite inclusions, and photos of various gem materials from Namibia. Download the issue at www.gtljaipur.info/ProjectUpload/labDownLoad/LIC_January2018.pdf. *CMS*

Global Diamond Industry 2017

The seventh annual report prepared by Antwerp World Diamond Centre and Bain & Co. was released in December 2017, titled *The Global Diamond Industry Report: The Enduring Story in a Changing World*. The report covers 2016 and the first half of 2017, and includes a forecast of the diamond industry through 2030. Diamond jewellery sales were fairly stagnant through 2016 and appeared to remain so for 2017, and mid-2016 revenues fell slightly. Key challenges include declining demand for diamond jewellery, the impact of laboratory-grown diamonds and financial instability of certain sectors of the trade. Download the report at www.bain.com/Images/bain_diamond_report_2017_pages.pdf. *CMS*

Gold Demand Trends 2017

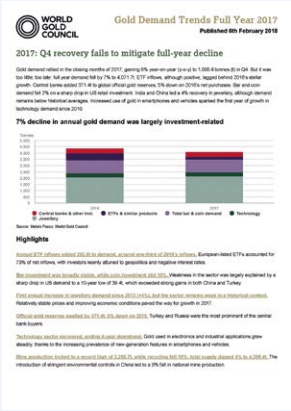

This annual report from the World Gold Council, released in February 2018, includes a section that focuses on gold jewellery. In 2017, gold jewellery demand rose 4% globally, with notable recovery in India, despite an overall decline in demand for gold worldwide. This was the first increase in gold jewellery demand since 2013. The gold jewellery market in the USA and China climbed at gradual rates. However, demand in Europe, and especially the UK, continued to decline. Download the report at www.gold.org/research/gold-demand-trends.

CMS

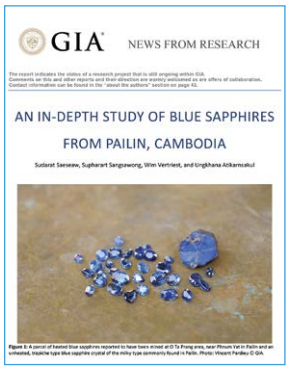

Sapphires from Pailin, Cambodia

In this Research News release from December 2017, titled 'An In-Depth Study of Blue Sapphries from Pailin, Cambodia', authors from the Gemological Institute of America's Bangkok laboratory analyse 68 heated and unheated blue sapphires from Pailin, Cambodia, presenting LA-ICP-MS chemical analysis, UV-Vis-NIR and FTIR spectroscopy, and inclusion studies using microscopy and Raman spectroscopy. Download the report at www.gia.edu/gia-news-research/blue-sapphires-pailin-cambodia. *CMS*

SSEF *Facette*

In February 2018, the Swiss Gemmological Institute SSEF released No. 24 of its annual publication *Facette Magazine*. This issue covers padparadscha-like sapphires with unstable coloration; an excursion to Paraíba tourmaline mines in Brazil; emerald and sapphire from Ethiopia; Afghan emeralds with properties similar to Colombian stones; artificial resin fillers in Burmese rubies and Paraiba tourmalines; detection of sapphire heat treatment using Fe-hydroxide transformation; GemTOF analysis of sapphires from Madagascar and Kashmir; age dating of sapphires and their inclusions; SIMS analysis of carbon isotopes in natural and synthetic diamonds; natural diamonds mixed into batches of synthetic diamonds; collector's stones including grandidierite, fluorite and musgravite; 'Sannan-Skarn' resembling maw-sit-sit; identification of jadeite and related samples; 'Mini Ming' cultured pearls from China; impact of water pollution regulations on Chinese freshwater cultured pearl production; a cultured pearl with an Fe-rich core; a hollow pearl containing metallic beads; SSEF-affiliated research projects and publications; several exceptional items with SSEF reports sold at auction in 2017; recaps of SSEF courses; SSEF news and instrumentation; conference reports; and more. Download this and previous issues of *Facette* at www.ssef.ch/ssef-facette. *BML*

SSEF Trade Alert: Artificial Resin in Rubies

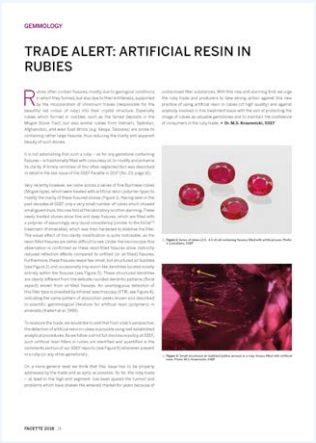

SSEF issued a trade alert in February 2018 about a series of relatively high quality Burmese rubies recently encountered in their laboratory that were fracture-filled with artificial resin to improve their clarity. The resin-filled fissures were rather difficult to see, with only a few small air bubbles, and sometimes tiny worm-like dendrites in the fissures that appeared much different from the rounded dendritic patterns often displayed by oil-filled fissures. FTIR spectroscopy confirmed the presence of the resin filler. Download the report at www.ssef.ch/wp-content/uploads/2018/03/2018_artificial_resin_rubies.pdf. *BML*

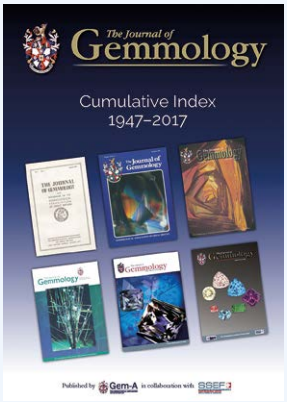

Updated Cumulative Index for *The Journal*

In March 2018, *The Journal of Gemmology's* cumulative index was updated to cover issues from 1947 to 2017 (Vols. 1–35). In addition, issue numbers have been included for the listings, making it easier to locate corresponding information in *The Journal*'s online archive. The contents are listed alphabetically by subject, and the file also can be searched electronically for specific authors as well as topics. The cumulative index is available in electronic (PDF) format only, and can be freely downloaded at https://gem-a.com/news-publications/publications/journal-of-gemmology#the-journal-index. *CMS*

What's New provides announcements of new instruments/technology, publications, online resources and more. Inclusion in What's New does not imply recommendation or endorsement by Gem-A. Entries were prepared by Carol M. Stockton (CMS) or Brendan M. Laurs (BML), unless otherwise noted.

The Fire Within

"For in them you shall see the living fire of the ruby, the glorious purple of the amethyst, the sea-green of the emerald, all glittering together in an incredible mixture of light."

– Roman Elder Pliny, 1st Century AD

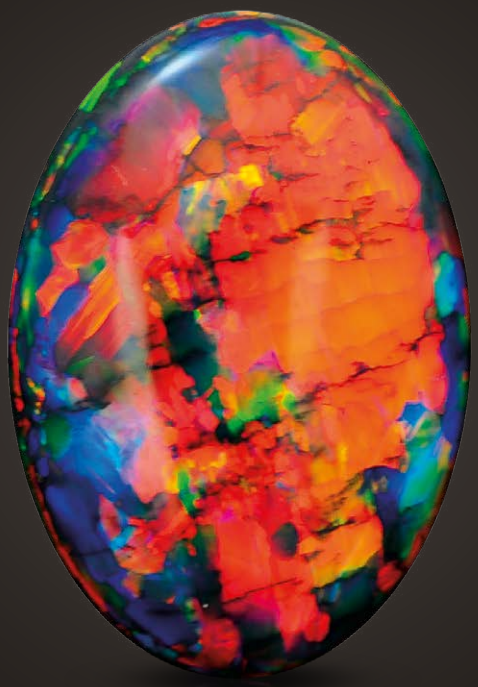

Black Opal 15.7 Carats

Suppliers of Australia's finest opals to the world's gem trade.

CODY OPAL

Level 1 - 119 Swanston Street Melbourne Australia

T. +61 3 9654 5533 E. info@codyopal.com

www.codyopal.com

ICA International Colored Gemstone Association Member

JOG

Gem Notes

COLOURED STONES

Figure 1: Artisanal mining is ongoing at the 2017 find of amethyst in an arid region of Santo Se municipality, Bahia State, Brazil. Photo by Adilton Venegeroles.

Amethyst Discovery in Bahia, Brazil

In April 2017, a new amethyst deposit was discovered by accident near the top of Serra da Quixaba, Santo Se municipality, in the far north-west of Bahia State, Brazil (Figure 1). Word spread quickly, and by June as many as 8,000 people had converged on the locality, including miners and individuals with supporting activities.

Personnel from Brazil's National Department of Mineral Production (DNPM) in Bahia soon visited the area and decided to allow the ongoing extractive activity, while quickly helping to formalize the area into a 200 Ha artisanal mining preserve and establish miners' cooperatives. This locality's biome, *caatinga*, is extremely arid and the area is one of the poorest in Brazil. DNPM's actions of encouraging the mining of amethyst served to benefit the municipality and avoid the 'social chaos' that might have occurred if the rush was shut down.

Buyers from Brazil, China and India quickly established themselves in the town of Santo Se. Nowadays, Wi-Fi connectivity is enabled by using solar panels in even the most remote areas of Brazil, and news spreads rapidly via platforms such as WhatsApp.

The amethyst crystals range up to 130 g, and clean, cobbed pieces typically weigh 5–50 g. The material varies from pale to saturated purple and commonly exhibits colour zoning (e.g. Figure 2). Some zones may display a bluish violet appearance, which adds to the overall desirability of this material.

Brian Cook (bc@naturesgeometry.com)
Nature's Geometry, Tucson, Arizona, USA

Figure 2: Representative examples of amethyst from Santo Se, Bahia, Brazil, are shown by this 53.25 ct carved 'Aromajewel' and 5.2-cm-tall crystal specimen. Photo by Jeff Scovil.

Yellow Brucite from Balochistan, Pakistan

Brucite is a layered magnesium hydroxide, $Mg(OH)_2$, that typically forms compact aggregates with a vitreous, waxy or pearly lustre. Until recently, it has not been encountered in the gem trade except as an imitation of nephrite jade and Shoushan stone in China (Li Jianjun et al., 2010). At the February 2018 gem shows in Tucson, Arizona, USA, yellow brucite from a relatively new find in Pakistan was available as faceted stones (e.g. Figure 3) and beads. However, the vast majority of this brucite was offered as mineral specimens (e.g. Figure 4).

The brucite comes from Pakistan's Balochistan (Baluchistan) Province, with both the Killa Saifullah and Khuzdar districts being reported as the area where mining takes place. A photo and video of one such mine is available at www.irocks.com/brucite-a-chemists-treasure. Pale yellow brucite from Balochistan first appeared in the mineral specimen market in 2015, followed by pale to bright yellow material in 2016. Many of the aesthetic yellow specimens offered at this year's Tucson shows were mined in mid-2017. They typically consisted of coarse-grained translucent aggregates of yellow brucite on a matrix of hydromagnesite and/or altered serpentinite.

Brucite has been documented in the literature from magnesite deposits in the Khuzar area, where ultramafic rocks were serpentinized and then hydrothermally altered into assemblages of magnesite, hydromagnesite and brucite (Bashir et al., 2009). The colour of the brucite, however, was not specified, and it is unknown to the present author if the recent finds of yellow brucite are related to these deposits.

Figure 3: These faceted brucites weigh 3.33–3.45 ct and the specimen measures 19 × 21 × 4 mm. Photo by Mauro Pantò.

Figure 4: This brucite specimen from Pakistan measures approximately 11 cm wide and 9 cm tall. The brucite formation at the top resembles the profile of a woman wearing a tiara, leading some to refer to it as 'Queen Elizabeth'. Courtesy of Ghulam Mustafa, Fine Art Minerals, Peshawar, Pakistan; photo by Joaquim Callen.

The faceted brucite was displayed in Tucson by Mauro Pantò (The Beauty in the Rocks, Sassari, Italy), who kindly donated one cut stone to Gem-A. He had approximately 60 brucites (total weight ~150 carats) that mostly ranged from 1 to 3 ct each. With a Mohs hardness of 2½–3 and perfect cleavage on {0001}, brucite is challenging to facet. In addition, the brucite aggregates typically form rather thin layers and often contain some white areas, so Pantò estimates that 70% of the rough material cannot be used for faceting unless very small stones are cut.

Brendan M. Laurs FGA

References

Bashir E., Naseem S., Akhtar T. and Shireen K., 2009. Characteristics of ultramafic rocks and associated magnesite deposits, Nal area, Khuzdar, Balochistan, Pakistan. *Journal of Geology and Mining Research*, **1**(2), 34–41.

Li Jianjun, Yu Xiaoyan, Cai Jia, Liu Xiaowei, Fan Chengxing and Cheng Youfa, 2010. The gemmological properties and infrared spectra of brucite, an imitation of nephrite and Shoushan stone. *Journal of Gemmology*, **32**(1–4), 67–73, http://dx.doi.org/10.15506/jog.2010.32.1-4.67.

Figure 5: At the Katjanga tourmaline deposit, miners use a pneumatic drill to prepare the pegmatite for blasting, while a front-end loader removes waste rock from the pit. The inset shows the pure greenish blue hue of a tourmaline preform from this mining area. Photos by B. M. Laurs.

Update on Some Coloured Stone Mining in Namibia

After attending the 35th International Gemmological Conference on 12–15 October 2018 in Windhoek, Namibia, this author visited some coloured stone deposits to obtain updated information on the mining and production there. Guided by Markus Wild (Paul Wild OHG, Kirschweiler, Germany), we saw active mining for tourmaline at Katjanga and Neu Schwaben, and for demantoid at the Parrot mine.

The Katjanga mining area has produced blue to blue-green gem tourmaline over the past two decades. It is situated on a private farm owned by Jeano Foelscher that is located approximately 40 km south-east of Omaruru. Several granitic pegmatites are present in an area measuring approximately 4 km^2, and the largest one was being mined in an open cut during our visit (Figure 5). The pit was being worked by a crew of 4–5 miners, who drill and blast the pegmatite with explosives. Most of the pegmatite that we saw was relatively fine grained, and it locally contained elongate coarse-grained segregations that were typically up to 1 m (rarely up to 2 m) wide and 3–6 m long; they dipped ~35° south-east. The miners look for areas where these 'veins' are cross-cut by near-vertical iron-stained joints or fractures, since this is where 'pockets' or cavities seem to occur. Most of the pockets contain only quartz, feldspar and mica, and perhaps 20% of them are mineralized with gem tourmaline. Such cavities are typically small and may produce up to ~1.5 kg of tourmaline, of which ~5% is gem quality in some cases and ~30% in others. Fine gem tourmaline also has been produced from eluvial deposits overlying the pegmatites. Most of the tourmaline from Katjanga is pure blue to blue-green and lacks any greyish or brownish hues (e.g. Figure 5, inset),

Figure 6: Numerous open pits explore the Neu Schwaben pegmatite for tourmaline, but only a few of them were being actively mined in October 2017. The prismatic greenish blue crystals in the inset are typical of tourmaline from this locality. Photos by B. M. Laurs.

Figure 7: Demantoid is mined from a hard layer of calc-silicate rock at the Parrot mine using hand tools. Photo by B. M. Laurs.

and also has an 'open' c-axis that is prized by gem cutters and connoisseurs.

The Neu Schwaben mining area has been known for decades, and in 1996–1997 it produced large quantities of tourmaline in attractive blue-to-green colours from secondary deposits associated with a large pegmatite (Johnson and Koivula, 1997). Subsequent production has been mostly rather small and inconsistent due to the disorganized nature of the mining; this was noted by Laurs (2002) and this situation continues to the present time. During our visit we saw numerous pits (e.g. Figure 6) ranging up to 8–10 m deep over an area of approximately 3–4 km^2. The pits were located on both sides of a prominent north/south-trending ridge that is formed by the pegmatite, and four of them were actively being mined by separate groups of 3–5 people. We saw two air compressors used to power pneumatic drills (although it was not clear if they were both in use), but otherwise no mechanized equipment was present. The geology was quite similar to that seen at Katjanga, with a large relatively fine-grained pegmatite that locally contained coarse-grained 'veins' ~0.5 to 1.5 m thick that dipped shallowly to moderately south-east. According to the local miners, the pockets typically vary from 10 to 60 cm long, and may contain tourmaline that is blue to green (e.g., Figure 6, inset) or black. Although some of the tourmaline from Neu Schwaben shows an 'open' c-axis, such material is less commonly encountered than in tourmaline from Katjanga.

Demantoid and brownish to greenish yellow andradite is mined from Tubussis Farm 22 in the Erongo region of west-central Namibia. We visited the Parrot mine, which is owned by Manfred Lehrl (Esme Fine Gemstones, Omaruru) and is located adjacent to the Green Dragon mine (Reif, 2017). The main open pit extended to a depth of ~18 m, and in early October Lehrl had shifted to shallower workings that were ~7 m deep. A crew of four workers was following the steeply-dipping mineralized zone using pry-bars and feathers-and-wedges (Figure 7). The garnets were hosted by a narrow ~0.5 m layer of calc-silicate rock (skarn) adjacent to marble that had been locally intruded by granitic veins. Lehrl preferred not to use explosives near the mineralized zone to avoid breaking the garnets, and therefore mining proceeded slowly. Most of the production consisted of small broken crystals (e.g. Figure 8), although larger stones are occasionally found.

Brendan M. Laurs FGA

References

Johnson M.L. and Koivula J.I., 1997. Gem News: Tourmaline from the Neu Schwaben region, Namibia: A major new player. *Gems & Gemology*, **33**(1), 66–67.

Laurs B.M., 2002. Gem News International: Update on some Namibian gem localities. *Gems & Gemology*, **38**(3), 266–268.

Reif S., 2017. Green Dragon mine demantoid from Namibia. *InColor*, No. 36, 48–52.

Figure 8: Most of the Parrot mine demantoid production consists of broken crystals such as these. Photo by B. M. Laurs.

Copper-bearing Opal from West Java, Indonesia

West Java in Indonesia has long been known as a source of opal, with much of it displaying play-of-colour (e.g. Einfalt, 2007). More recently, common opal showing various body colours (mostly greenish blue to bluish green) was found as pebbles and cobbles in streams, and subsequently the primary source was discovered (e.g. Figure 9). The deposit is located in the Garut Regency of West Java, which is south of the city of Bandung. What makes this material particularly interesting is that is it commonly associated with fossilized wood (Figure 10) in the remnants of an ancient petrified forest, and also some pieces of the opal contain concentrations of native copper (Figure 11). Fossilized (silicified) tree remains are well known in West Java and elsewhere in Indonesia, and some of these deposits are hosted by Late Miocene–Pliocene volcaniclastic strata (van Gorsel, 2014). The volcanic material was ejected during major eruptions that locally smothered and preserved entire forests. According to geologist Joel Ivey (IndoAgate.com, Bangkok, Thailand), the opal-bearing silicified wood in the Garut area formed as a result of hydrothermal solutions associated with an epithermal system circulating through the volcanic sequence. The solutions contained various metallic impurities (Cu, Mn and Fe) that resulted in the colourful appearance of the opal.

Figure 9: A relatively new deposit of mostly blue-to-green opal associated with petrified wood is located in steep jungle terrain in West Java, Indonesia. The opal-bearing material is mined from several small tunnels. Photo courtesy of Dace Irwan.

Figure 10: A lensoidal shape and layered pattern are displayed by this specimen of greenish blue opal from West Java. The top photo shows a cross-section of the piece, and the bottom image views the top portion of the sample with surface textures that would be expected for fossilized wood material. The specimen weighs 10.2 kg and measures approximately 40 × 26 × 11 cm. Courtesy of Joe Jelks; photos by B. M. Laurs.

The mining area is located at an elevation of 394 m in steep terrain that is cloaked by jungle (Figure 9), making exploration and extraction difficult, particularly when large petrified logs are recovered (see photo at www.interweave.com/?p=414313&preview=1&_ppp=1496058d6c). The opal is locally concentrated in specific layers within the logs (e.g. Figure 10) and also is found in veins and structures in the associated tuffaceous deposits. According to

Figure 11: Abundant flecks of native copper decorate this sawn slab of West Java opal. Photo courtesy of Joel Ivey; image width ~10 cm.

Figure 12: This opal cabochon from West Java, Indonesia contains various bluish green and brown hues in a layered arrangement. Photo by Joe Jelks.

Dace Irwan (coralagate.com, Sukabumi, Indonesia), approximately 500 kg of mixed-quality opal is produced monthly, and Ivey estimates that more than a tonne of rough opal material has been recovered so far.

Both rough and cut opal were offered at the February 2018 Tucson gem shows, and Joe Jelks (Horizon Mineral Lapidary, Lewes, Delaware, USA) showed this author some interesting pieces that he obtained from two shipments in November 2017. The first batch weighed 63 kg and consisted mostly of small-to-medium sized rough, from which he cut approximately 300 cabochons ranging from 12 to 50 mm in maximum dimension. They typically showed a banded brown and blue-green appearance, as seen in Figure 12. The next shipment consisted of larger rough, and in Tucson he displayed pieces weighing 1.85–10.2 kg (e.g. Figure 10). The opal in most of the rough pieces ranged from greenish blue to bluish green with some light-to-dark brown and black areas, although pieces containing white, orange and yellowish green areas also have been recovered.

Furuya (2017) characterized one rough and two cabochon-cut samples (bluish green ± dark brown). Most of the material was identified as opal, although some portions of the rough sample showing better transparency were chalcedony. Energy-dispersive X-ray fluorescence spectroscopy revealed enriched copper contents (10–20 wt.% CuO). Although it is likely that the greenish blue to bluish green material is coloured by impurities of Cu-bearing minerals such as chrysocolla, the exact origin of the coloration has not yet been confirmed.

This Cu-bearing opal may resemble the chrysocolla-bearing quartz and chalcedony from Indonesia that was documented by Einfalt (2006), particularly when cut as homogenously coloured cabochons. However, most of the opal samples show patterning that is distinctly different from that material.

Brendan M. Laurs FGA

References

Einfalt H.C., 2006. Chrysocolla quartz from the Bacan Archipelago, South Halmahera Regency, North Maluku Province, Indonesia. *Journal of Gemmology*, **30**(3), 155–168, http://dx.doi.org/10.15506/jog.2006.30.3.155.

Einfalt H.C., 2007. Some observations on the composition and origin of opals from Java. *Journal of Gemmology*, **30**(7), 383–398, http://dx.doi.org/10.15506/jog.2007.30.7.383.

Furuya M., 2017. Gem News: Chrysocolla opal from Java Island, Indonesia. *J.G.G.L. Gem Information*, No. 45, 15 (in Japanese).

van Gorsel J.T., 2014. An introduction to Cenozoic macrofossils of Indonesia. *Berita Sedimentologi—Indonesian Journal of Sedimentary Geology*, **30**, 63–76.

Figure 13: Front and oblique side views are shown of a gold ring featuring a sapphire (15 × 12 × 1.5 mm) that displays conspicuous growth zoning. Specimen BM.89462; courtesy of NHM London, © The Trustees of the Natural History Museum, London.

A Sapphire Ring in the Natural History Museum Collections

The author recently had the pleasure to view a historical sapphire ring (Figure 13) from the gem collection of the Natural History Museum (NHM), London. The ring is listed in the handwritten mineralogy registers as BM.89462 and described as 'Corundum, pale-blue, faceted, showing hexagonal markings. India.'

The ring features a medium violetish blue sapphire, 15 × 12 × 1.5 mm, with a large flat table, facets around the edges and a very shallow pavilion. The stone is set in unmarked gold, with a thin band and a decorative bezel setting. What makes this gem so interesting are the prominent, alternating transparent blue and silky white bands, which outline two sides of the hexagonal growth pattern. As the ring is moved, the silky layers reflect light and highlight the zoning. The silk is formed of fine clouds of particles (likely rutile; Palke and Breeding, 2017) that follow the host sapphire's growth zones. Interestingly, the alternating transparent and silky layers do not match up on adjacent hexagonal prism faces (Figure 14), seemingly forming preferentially on one face and then the other as the crystal grew. Other inclusions include clusters of transparent euhedral crystals, negative crystals and partially healed fractures.

The specimen came to the museum as part of the Allan-Greg Collection. This mineral and gem collection was begun by Thomas Allan (1777–1833), a natural scientist based in Edinburgh. After Allan's death, Robert Hyde Greg (1795–1875) of Manchester purchased the collection, and his son Robert Philip Greg (1826–1906), then of Norcliffe Hall near Manchester, added to it. The collection was global in its coverage, but was famed for its British minerals and formed the basis for the *Manual of the Mineralogy of Great Britain and Ireland* (Greg and Lettsom, 1858). For nearly 150 years this was the only attempt at a complete catalogue of the mineralogical diversity of the British Isles, and it stands as one of the most important books on British Mineralogy ever published.

The Trustees of the British Museum purchased the Allan-Greg Collection in 1860 (British Museum, 1904), at which time it consisted of approximately 9,000 specimens and was thought to be the finest collection in the UK. The collection is beautifully catalogued in three volumes, with chronological entries written by Thomas Allan (up to 1833) and by R. P. Greg (during 1850–1859). The catalogue is arranged by mineral species, and the sapphire ring is listed as no. 116 under 'Rhombohedral Corundum'. (This is one of four lists of corundum groups, the first being 'Dodecahedral Corundum', which is in fact spinel; red spinels were commonly mistaken for rubies.) The entry for this sapphire ring does not give much further information, stating only, 'Ring stone set; of a pale blue colour + transparent, showing

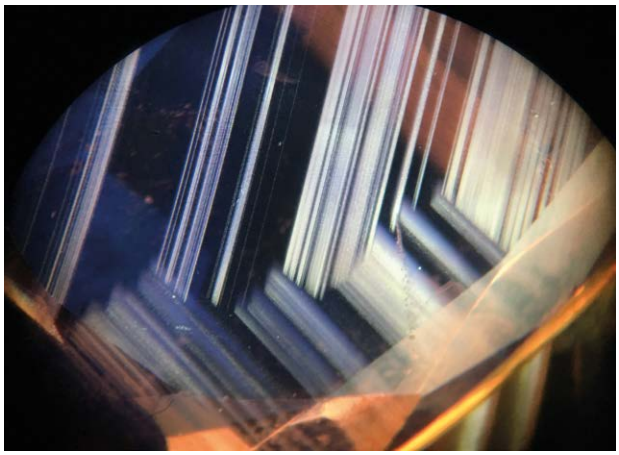

Figure 14: Alternating bands of 'silk' follow the hexagonal growth zoning in the sapphire pictured in Figure 13. Photomicrograph by R. Hansen; magnified 60×. Courtesy of NHM London, © The Trustees of the Natural History Museum, London.

the hexagonal markings – £4. India'. The previous catalogue entry, no. 115, has the year 1857 written next to it, so it is likely that the ring was purchased by R. P. Greg between 1857 and 1860, when the collection was sold.

India has long been known for its gemstones, including sapphire and ruby. It is most famed for its Kashmir blue sapphires; however, these were discovered around 1880 (Hughes, 1997), which post-dates this ring. India also was an important cutting centre and trade route for gems, so it is likely that the present sapphire was cut and the ring purchased in India, with the rough originating from another location such as Sri Lanka or Burma.

This ring is one of several early and important sapphires held in the NHM collection that are listed as being from India (and similarly were probably cut and sold in India, but mined elsewhere). Three others include a rose-cut sapphire mounted in a Mughal turban button acquired by Sir Han Sloane (whose collection founded the British Museum, dating this gem before 1753), a blue sapphire carved as a Buddha and mounted on a pin (the stone thought to originate from Burma) and an 88 ct star sapphire bead with a drill-hole at one end (purchased by NHM in 1825, thought to come from Sri Lanka). The ring is currently displayed in the newly redeveloped corundum case in NHM's Earth's Treasury gallery, and the other three sapphires mentioned here are displayed in the Vault (although one of them is currently on tour).

Robin Hansen FGA *(r.hansen@nhm.ac.uk)*
Earth Science Department
Natural History Museum, London

References

British Museum, 1904. *The History of the Collections Contained in the Natural History Departments of the British Museum*. Trustees of the British Museum, London, 472 pp.

Greg R.P. and Lettsom W.G., 1858. *Manual of the Mineralogy of Great Britain and Ireland*. John Van Voorst, London, 514 pp.

Hughes R.W., 1997. *Ruby & Sapphire*. Chapter 12, World Sources: India [extract], www.ruby-sapphire.com/r-s-bk-india.htm, accessed 24 February 2018.

Palke A.C. and Breeding C.M., 2017. The origin of needle-like rutile inclusions in natural gem corundum: A combined EPMA, LA-ICP-MS, and nanoSIMS investigation. *American Mineralogist*, **102**(7), 1451–1461, http://dx.doi.org/10.2138/am-2017-5965.

Cat's-eye Indicolite Tourmaline from Afghanistan

Chatoyant tourmaline with sharp well-developed 'eyes' is uncommonly encountered in the gem trade, and when such stones are available they typically show green or pink body colours (e.g. Laurs, 2004).

It was therefore surprising to encounter a rather large amount of fine-quality cat's-eye indicolite at the February 2018 Tucson gem shows. The stones were displayed by Wali Beekzad of Five Lions Gems, San Jose, California, USA. They were cut from a 1.5 kg parcel of rough material that was mined in late 2016 in Laghman, Afghanistan. The cutting was performed in July 2017 by a Brazilian gem cutter with expertise in manufacturing cat's-eye stones. He produced 373 cabochons with a total weight of 2,435 carats, which ranged from approximately 2 to 66 ct each.

The stones displayed an attractive greenish blue colour and sharp 'eyes' that were caused by growth tubes oriented parallel to the c-axis (Figure 15). A few well-formed crystals from this find were preserved as mineral specimens, but otherwise the remainder of the production was cut. Given the rarity of cat's-eye indicolite, it seems unlikely that significant further production of this material will take place in the future.

Brendan M. Laurs FGA

Reference

Laurs B.M., 2004. Gem News International: Tucson report. *Gems & Gemology*, **40**(1), 66.

Figure 15: These chatoyant tourmalines from Laghman, Afghanistan, measure 4.2 cm tall (crystal specimen with quartz) and weigh 31.65 ct (cabochon). Photo by Jeff Scovil.

Cat's-eye Tremolite from Badakhshan, Afghanistan

In recent years there have been descriptions of transparent gem-quality tremolite from apparently two different locations in Tanzania (Zwaan and Hawthorne, 2015; Williams et al., 2017), and now this report covers tremolite that is from a different locality—Afghanistan—which also displays chatoyancy. Gem dealer Dudley Blauwet (Dudley Blauwet Gems, Louisville, Colorado, USA) first encountered this material in 2015, and obtained a total of four parcels during various visits to the gem and mineral bazaar in Peshawar, Pakistan. According to his Afghan supplier, the specimens originated from the Dar-e-Zu mine, Sar-e-Sang, Kokcha Valley, Badakhshan Province, Afghanistan. The material in the parcels ranged from pale greyish green or brownish green to black, and Blauwet was particularly interested in selling any unbroken well-formed crystals as mineral specimens. Since much of the rough material was opaque and lacked strong schiller, only a small proportion of the parcels were suitable for cutting cat's-eye gemstones. Furthermore, the narrow cross-section of those crystals showing the most desirable coloration restricted the size of any cut stones. Nevertheless, after initial efforts to cut a 4.1 g piece yielded a 4.70 ct cat's-eye cabochon, Blauwet then sent 16 pieces weighing 96.5 g to his cutting factory in July 2017, and they successfully produced six cabochons with a total weight of 33.58 carats. The largest was a translucent black gem weighing 11.26 ct, and the smallest was a pale greyish green stone that was ~0.90 ct.

Figure 16: A prismatic crystal (1.4 g) and an oval cat's-eye (2.09 ct) tremolite from the Dar-e-Zu Mine, Afghanistan, were gemmologically characterized for this report. Photo by Orasa Weldon.

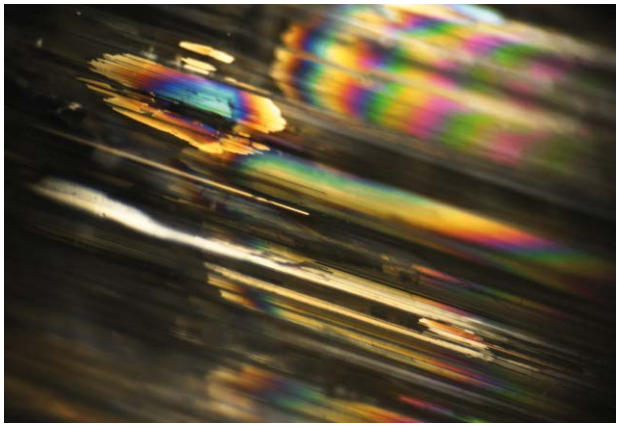

Figure 17: The Afghan cat's-eye tremolite contains growth tubes, incipient cleavage planes and fissures showing bright rainbow colours when viewed with magnification and oblique illumination. Photomicrograph by J. C. Zwaan; image width 5.0 mm.

During the February 2017 Tucson gem shows, Blauwet supplied some rough and cut samples of the chatoyant tremolite to the authors for examination.

A gemmological characterization was performed by author JCZ of the samples in Figure 16. The prismatic crystal and the oval cabochon were transparent to translucent and were light greyish green to greyish brown; in addition, a dark brown zone was present at one end of the crystal. The specimens respectively weighed 1.4 g and 2.09 ct and measured 20.53 × 9.40 × 3.83 mm and 12.71 × 6.68 × 2.88 mm.

The crystal had broken terminations, and on one side there was a small piece of matrix. Parallel to the longitudinal direction, striations were visible on the crystal faces and ran parallel to many straight fibres present inside the crystal. Incipient cleavage planes additionally ran parallel to the length of the crystal, which also contained small partially healed fissures. The oval cabochon essentially showed the same inclusions, with parallel fibres along its length being responsible for the cat's-eye. Viewed with magnification, some fissures in the cabochon showed bright iridescence with oblique illumination (Figure 17). Some slightly thicker fibres in the stone appeared to be lined with limonite or filled with diamond polishing residues where they reached the surface (confirmed by Raman analysis), which indicates that the parallel fibres consist of hollow growth tubes.

Clear RI readings were obtained from the flat base of the cabochon: 1.610–1.638, yielding a birefringence of 0.028. The hydrostatic SG was 3.01. The dichroscope revealed weak-to-distinct trichroism in greenish yellow, pale grey-green and greyish green. Both specimens were inert to long- and short-wave UV radiation.

Comparing these properties with those of amphiboles in the tremolite-actinolite-ferroactinolite series (Deer et al., 1997), the relatively low SG corresponds to tremolite, although distinct trichroism indicates the presence of some iron. Raman spectra most closely matched the spectra of tremolite recorded in the RRUFF database. Furthermore, electron microprobe analysis of another sample by authors FCH and MD confirmed that the material is indeed tremolite, with the formula: $(Na_{0.14}K_{0.01})_{0.15}(Ca_{1.95}Fe^{2+}_{0.03}Na_{0.02})_2(Mg_{4.68}Fe^{2+}_{0.20}Al_{0.10}Ti_{0.01}Mn_{0.01})_{5.00}(Si_{7.70}Al_{0.30})_8O_{22}(OH_{1.91}F_{0.09})_2$. This is well within the compositional range of tremolite, which extends from $\square Ca_2Mg_5Si_8O_{22}(OH)_2$ to $\square Ca_2Mg_{4.5}Fe^{2+}_{0.5}Si_8O_{22}(OH)_2$ (with $\square$ = A-site vacancy; Hawthorne et al., 2012).

In conclusion, the Dar-e-Zu mine in Afghanistan is one of the few known occurrences of gem-quality tremolite, apart from localities in Tanzania (see references above and also Fritz et al., 2007).

Dr J. C. (Hanco) Zwaan FGA
(hanco.zwaan@naturalis.nl)
Netherlands Gemmological Laboratory
National Museum of Natural History 'Naturalis'
Leiden, The Netherlands

Dr Frank C. Hawthorne and Maxwell Day
Geological Sciences, University of Manitoba
Winnipeg, Manitoba, Canada

Brendan M. Laurs FGA

References

Deer W.A., Howie R.A. and Zussman J., 1997. *Rock-Forming Minerals: Double-Chain Silicates*, 2nd edn. Geological Society of London, London, 784 pp.

Fritz E.A., Laurs B.M., Downs R.T. and Costin G., 2007. Yellowish green diopside and tremolite from Merelani, Tanzania. *Gems & Gemology*, **43**(2), 146–148, http://dx.doi.org/10.5741/gems.43.2.146.

Hawthorne F.C., Oberti R., Harlow G.E., Maresch W.V., Martin R.F., Schumacher J.C. and Welch M.D., 2012. Nomenclature of the amphibole supergroup. *American Mineralogist*, **97**(11–12), 2031–2048, http://dx.doi.org/10.2138/am.2012.4276.

Williams C., Williams B. and Laurs B.M., 2017. Gem Notes: More tremolite from Tanzania. *Journal of Gemmology*, **35**(7), 710–702.

Zwaan J.C. and Hawthorne F.C., 2015. Gem Notes: Tremolite from Mwajanga, Tanzania. *Journal of Gemmology*, **34**(7), 569–571.

Wavellite and Drusy Variscite from Arkansas

Wavellite and variscite are both aluminium phosphate minerals with a Mohs hardness of approximately 3½–4 (up to 4½ for variscite). Although variscite is commonly slabbed to show its attractive coloration and patterns, wavellite is typically appreciated for its botryoidal formations and radiating textures.

Since at least 1870, wavellite has been collected near the town of Avant in Garland County, Arkansas, USA (Smith, 2010). The area also is a source of drusy variscite, and both minerals are hosted by brecciated sedimentary rock of the Big Fork Chert Formation (Barwood and de Linde, 1989). The wavellite occurs in a range of colours (blue, blue-green, green, greenish yellow and yellow), which have been attributed to variations in the amounts and valence states of vanadium (Foster and Schaller, 1966).

One of the most important sources of wavellite and variscite in Arkansas is the de Linde mine (also known as the H. de Linde No. 3 or the Stuart Schmidt deposit), and many specimens from this claim have been cut for use in jewellery over the past decade. In 2009 the property was purchased by Avant Mining LLC (Paramus, New Jersey, USA), and they started extracting rough material in early 2010. According to owner James Zigras, the company recently expanded its production of jewellery material, and at the February 2018 Tucson gem shows they had multiple booths that displayed cut stones ranging from 10 to 500 ct each.

Both the wavellite and variscite are cut into various freeform shapes. While the variscite consists of pure drusy green coatings (Figure 18), the wavellite is

Figure 18: Various pieces of drusy variscite (up to 68 × 45 mm) from the de Linde mine are displayed on a background of Arkansas quartz. Photo by Jeff Fuller.

polished on the surface and sometimes includes areas of the breccia matrix material. Most of the wavellite ranges from greenish yellow to yellowish green, and it often exhibits intergrown radiating and concentric textures (Figure 19). It is commonly stabilized with Opticon.

Zigras reported that the de Linde deposit is worked in an open pit with a single trackhoe, and mining typically takes place twice annually for a two-week period, producing about one tonne of good specimen- and cutting-quality material. Several hundred stones have been cut from the variscite and about 1,000 pieces of wavellite have been polished.

Brendan M. Laurs FGA

References

Barwood H.L. and de Linde H., 1989. Arkansas phosphate minerals—A review and update. *Rocks & Minerals*, **64**(4), 294-299, http://dx.doi.org/10.1080/00357529.1989.11761770.

Foster M.D. and Schaller W.T., 1966. Cause of colors in wavellite from Dug Hill Arkansas. *American Mineralogist*, **51**, 422–428.

Smith A.E., 2010. Exploration and mining history of the de Linde wavellite mine—east Dug Hill area, near Avant, Garland County, Arkansas. *Rocks & Minerals*, **85**(4), 346–351, http://dx.doi.org/10.1080/00357529.2010.492298.

Figure 19: This pendant features a cabochon of Arkansas wavellite that measures 25 × 20 mm. Photo by Jeff Fuller.

DIAMONDS

Diamond Mining at Namdeb's Southern Coastal Mines, Namibia

In conjunction with the 35th International Gemmological Conference in Windhoek, Namibia, this author joined a pre-conference tour that took place on 8–11 October 2018 with approximately 30 participants in attendance. A highlight of this excursion was a visit to Namdeb Diamond Corporation's Southern Coastal Mines to witness active mining of a series of old raised beach deposits (Figures 20–22). This concession is situated in an area previously known as Mining Area No. 1, which extends along ~120 km of Namibia's coast from the Orange River at Oranjemund northward to Chameis Bay.

Our tour leader was geologist Dr Jurgen Jacob (Namdeb, Oranjemund, Namibia), who started by giving an informative presentation on the geology, exploration, mining and production of Namibia's diamond deposits (both marine and onshore). Then, after passing through an extensive security facility, the group boarded a Namdeb bus for the trip to the pit that was being worked. As we passed through the historic diamond mining area called the *Sperrgebiet*, we saw abandoned mining pits, dormant and active processing plants, and conveyor belts that were used to transport sand to enormous seawalls designed to keep the Atlantic Ocean from flooding the pits.

A linear beach deposit extends for 110 km along the Sperrgebiet, but 95% of it has been mined out in a series of pits that extend down to 25 m below sea level. Through a process called *accretion*, Namdeb has pushed back the shoreline using sand walls that typically are 50–60 m wide (and locally

Figure 20: In October 2017, diamond mining was taking place at this pit in Namdeb's Southern Coastal Mines. The pit is flanked by sand walls, and ocean water is held back by the seawall to the far left. Previously mined bedrock gullies are visible in the centre of the photo, and on the right side is a series of transvac units and bins located adjacent to the current mining area. Photo courtesy of Namdeb.

Figure 21: To recover diamond-bearing gravels from the bedrock trapsites, excavators and bulldozers first remove overlying sediments, as well as some areas of the bedrock itself, and then transvac machines (each with an accompanying bin) are used to vacuum any remaining sediments from the bedrock surface. Photo courtesy of Namdeb.

Figure 22: A portion of the exposed bedrock (right side) has been vacuumed to remove any diamond-bearing sediments, while on the left an excavator prepares the area for the transvac crews. Photo courtesy of Namdeb.

Figure 23: Members of the transvac crew work in pairs. They will stop vacuuming to pick up any diamonds that they see in the bedrock gullies, although such 'pick ups' typically occur only about twice per week. Photo courtesy of Namdeb.

up to 150 m wide). Adjacent to the active mining pit we visited, the seawall towered 8 m above the beach and was being replenished by 40 tonne dump trucks. Namdeb also constructs sand walls along the flanks of each mining pit (e.g. Figure 20), so if the seawall is breached by the ocean during intense storms then only a small portion of the entire pit system is flooded.

After sand overburden is removed to within 1–2 m of the underlying bedrock (which consists of schist of the Gariep Belt), the pits are then mined in a two-step proces. First, the *bulking* team uses bull-dozers and excavators to remove the remaining sediments and some of the bedrock protuberances, and then the *transvac* team uses powerful vacuums to suction any remaining sediments from the bedrock (Figure 23). The diamonds were deposited within gravels hosted by scour deposits along gullies and potholes in the bedrock (see Jacob et al., 2006, for details), so particular attention is paid to such trapsites. The vacuumed material is discharged into collection bins that are mounted on trailers and hauled to a treatment plant for processing. The material removed by the bulking team also is processed, while the overlying 15–18 m of sand is used for the seawall construction mentioned above.

The bedrock gullies in the linear beach deposits range from 1 to 4 m deep and have variable grade, but overall they tend to produce ~6 carats per 100 tonnes. Diamonds are actually seen by the transvac crews only about twice per week. The diamonds average ~0.7 ct per stone, and typically about 5–10 carats may be recovered by hand from gravels in some trapsites. However, the vast majority of the diamonds are recovered at the processing plant, which treats material ranging from 2 to 30 mm. A concentrate is produced using dense media separation, and this material then undergoes X-ray sorting.

At the time of our visit, the Southern Coastal Mines employed a total of 700 people who worked in three 8-hour shifts (although the transvac crews were only active in the daytime).

In total, Namdeb is currently producing 500,000 carats/year from its onshore operations and 1.3 million carats/year from its marine concessions. The diamonds are 95%–98% gem quality, since most of the lower quality stones broke down during the extensive journey along the Orange River and while being transported northward along the Atlantic coast in longshore currents. Although Namdeb's mine plan for its onshore operations is scheduled to last for five years, there is the potential to explore and extend the diamond reserves until at least 2050.

Brendan M. Laurs FGA

Reference

Jacob J., Ward J.D., Bluck B.J., Scholz R.A. and Frimmel H.E., 2006. Some observations on diamondiferous bedrock gully trapsites on Late Cainozoic, marine-cut platforms of the Sperrgebiet, Namibia. *Ore Geology Reviews*, **28**(4), 493–506, http://dx.doi.org/10.1016/j.oregeorev.2005.03.010.

SYNTHETICS AND SIMULANTS

Feldspar-Sapphirine Rock as a Grandidierite Imitation

Grandidierite is a rare Mg-Fe-Al-borosilicate, which was first described by Lacroix (1902) and named after the French scientist Alfred Grandidier (1836–1912). The type locality is Cap Andrahomana in southern Madagascar.

Chemically, grandidierite [$MgAl_3O_2(BO_3)(SiO_4)$] forms a solid-solution series with the iron end-member ominelite [$Fe^{2+}Al_3O_2(BO_3)(SiO_4)$]. Grandidierite ranges from bluish green to greenish blue with strong pleochroism (due to iron), and is found as an accessory phase in aluminium-bearing, boron-rich pegmatites. Standard gemmological properties are reported as n_x = 1.583–1.602, n_y = 1.620–1.636 and n_z = 1.622–1.639, with a birefringence of 0.037–0.039 and an SG ranging from 2.85 to 3.00 (Henn, 2012).

Recently the authors have examined an increasing number of grandidierite gemstones from a new find in Madagascar (cf. Bruyére et al., 2016; Laurs, 2016). Most of the material has been translucent, but some rare transparent samples also have been investigated, including a bright greenish blue specimen weighing 1.26 ct. We also examined a stone that drew attention because of its unusual appearance (Figure 24), which had been purchased by the client as grandidierite from Madagascar. The refractometer gave values of 1.548–1.555 with a maximum birefringence of 0.007. The hydrostatic SG was 3.03. The RIs and birefringence correspond to the typical values of plagioclase feldspars, although the SG is close to that of grandidierite.

Figure 24: This 2.61 ct feldspar-sapphirine rock was sold as grandidierite from Madagascar. Photo by S. Müller.

In the microscope, we observed numerous greenish blue tabular inclusions (Figure 25) that showed a higher lustre than the surrounding matrix in reflected light (Figure 26). Analyses with a Renishaw inVia Raman spectroscope confirmed plagioclase as the matrix material. Most of the inclusions were identified as sapphirine, although some mica grains were present. Figure 26 shows that the material consists of approximately 50% sapphirine.

Figure 25: With magnification, tabular greenish blue sapphirine inclusions can be seen in the feldspar matrix of the grandidierite imitation. Photomicrograph by T. Stephan, transmitted light; field of view 2.8 mm.

Figure 26: With reflected light on the table facet of the feldspar-sapphirine rock, the sapphirine inclusions show a brighter reflection than that of the plagioclase matrix. Photomicrograph by T. Stephan, reflected light; field of view 5.0 mm.

Although the stone showed typical RIs for plagioclase, it actually is a rock consisting of both plagioclase and sapphirine. This is consistent with the SG that we measured, which lies between the values for plagioclase (2.61–2.77) and sapphirine (3.42–3.51) reported in the literature (cf. Henn, 2012). It is interesting to note that grandidierite occurs together with both plagioclase and sapphirine in the Madagascar deposit (Bruyére et al., 2016).

Tom Stephan (t.stephan@dgemg.com)
German Gemmological Association, Idar-Oberstein

Dr Claudio C. Milisenda and Stefan Müller
DSEF German Gem Lab, Idar-Oberstein

References

Bruyére D., Delor C., Raoul J., Rakotondranaivo R., Wille G., Maubec N. and Lahfid A., 2016. A new deposit of gem-quality grandidierite in Madagascar. *Gems & Gemology*, **52**(3), 266–275, http://dx.doi.org/10.5741/gems.52.3.266.

Henn U., 2012. *Gemmologische Tabellen zur Bestimmung von Edelsteinen, Synthesen*, künstlichen Produkten und Imitationen, 3rd edn. German Gemmological Association, Idar-Oberstein, Germany, 40 pp.

Lacroix A., 1902. Note préliminaire sur une nouvelle espèce minerale. *Bulletin de la Société Francaise de Minéralogie*, No. 25, 85–86.

Laurs B.M., 2016. Gem Notes: New production of grandidierite from Madagascar. *Journal of Gemmology*, **35**(1), 12–13.

Glass Doublets Simulating Rutilated and Tourmalinated Quartz

During the February 2018 Tucson gem shows, some new variations of simulated rutilated and tourmalinated quartz were offered as pendants at the JOGS Gem & Jewelry Show by Amulete Gems Inc. (based in Manteca, California, USA). The company disclosed the fact that they were not natural, and indicated that the host material is manufactured in China, where it is called 'hydroquartz'. However, rather than being constructed of some type of quartz, these doublets consisted of two pieces of glass that were cemented together along with flat gold metallic or black strips (probably plastic) to imitate the appearance of rutile or tourmaline inclusions in rock crystal quartz. In addition, another variety containing iridescent strips was available. The doublets were faceted in a checkerboard style, and were cut into round, pear and teardrop shapes. The finished pendants ranged from 0.6 to 3.0 cm wide, and the pear/teardrop shapes were up to about 5 cm tall. The doublets were mounted in a yellow, white or oxidized metal bezel, with one to three bails for suspending them in jewellery. The metals reportedly consisted of sterling silver, but this was not confirmed by the author.

Gem-A purchased six of the pendants for its teaching collection (Figure 27). At first glance, the 'tourmalinated' simulants were rather convincing. Upon examination with a loupe, however, it was clear that the long strips imitating the inclusions

Figure 27: Both 'rutilated' and 'tourmalinated' glass doublets are mounted in these pendants (approximately 0.6–3.0 cm wide). Photo by Henry Mesa.

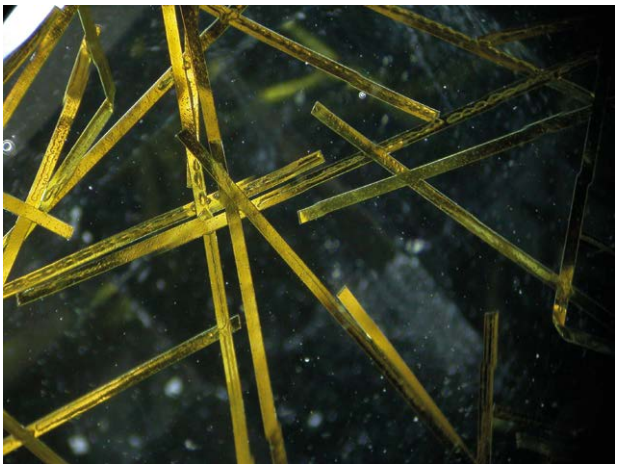

Figure 28: The 'inclusions' in the glass simulants of rutilated quartz consist of tinsel-like flat gold metallic strips with squared ends. Note the gas bubbles and films along some of the strips. Photomicrograph by L. Faber; magnified 30×.

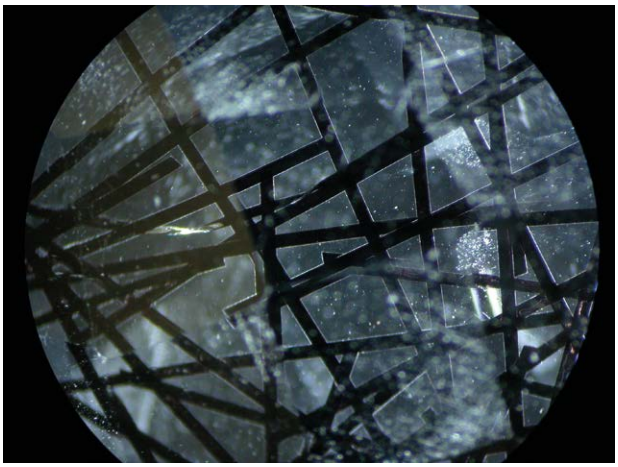

Figure 29: The pendants simulating tourmalinated quartz contain dark-coloured strips between the two layers of glass. These strips also displayed squared ends. Photomicrograph by L. Faber; magnified 30×.

were flat and had squared ends, much like pieces of cut tinsel (Figures 28 and 29). Also, the glass making up some of the samples contained gas bubbles. In addition, flattened and elongated gas bubbles were seen along just one side of the 'inclusions' in both types of doublets. One sample displayed iridescence as well as large, flattened areas that appeared to be air pockets where the two halves of glass had been partially adhered.

When examined with a polariscope, the host glass either stayed dark through a full 360° rotation of the sample or exhibited some strain, consistent with the isotropic optic character of glass. The black-appearing 'inclusions' often appeared light and dark through a 360° rotation, but the gold metallic ones did not allow any light to pass through them. Testing with a refractometer further revealed that the material was singly refractive, with RIs ranging from 1.516 to 1.520, which are well within the range for artificial glass. Polishing lines were present on each of the six examples, as well as some abrasions, indicating a relatively soft material that was not polished with close attention.

The pendants debuted in early 2016, and according to the seller they have been very popular, particularly in the past year or so. At the JOGS show there were several hundred pieces available for purchase at a fraction of the price expected for natural examples of comparable size.

Although the joint lines between the glass halves were obscured by the bezel settings, these doublets could be easily identified by a close examination of their 'inclusions'. A similar type of doublet manufactured from natural quartz with metallic foils was documented by Hänni and Henn (2015).

Lily Faber FGA (lilyfaber@gem-a.com)
Gem-A, London

Reference

Hänni H.A. and Henn U., 2015. Gem Notes: Modern doublets, manufactured in Germany and India. *Journal of Gemmology*, **34**(6), 479–482.

More on Black Star Rutile Imitations

In the previous issue of *The Journal*, this author reported on a 10.67 ct black star cabochon that was purchased by a Canadian gem collector as star rutile from Sri Lanka but proved to be black cubic zirconia (Deljanin, 2018). After receiving the results on this sample, the same client submitted for identification two more black star cabochons that were sold to him as 'natural star rutile from Sri Lanka'.

Both samples displayed six-rayed stars, and their RIs were over the limits of the refractometer. One of them weighed 38.82 ct (Figure 30, left) and appeared translucent dark red with strong transmitted illumination. It had a hydrostatic SG of 4.23, consistent with natural rutile (4.20–4.30). However, star rutile has been documented only as very rare four-rayed stones (Steinbach, 2017, pp. 667–670). Raman spectroscopy performed at the GRS lab in Hong Kong with a GemmoRaman-532SG instrument yielded a spectrum that matched garnet. The other sample, a 41.12 ct opaque black star cabochon

Figure 30: Both the 38.82 ct garnet (left) and the 41.12 ct hematite-magnetite (right, of probable manufactured origin) shown here were sold as natural black star rutile. Photos by Matthias Alessandri.

(Figure 30, right), revealed a higher SG of 5.01, and featured a metallic lustre composed of light and dark grey domains; it also was strongly magnetic. Clearly it was not composed of rutile, and additional testing was needed to identify it (see below).

Microscopic examination using overhead lighting revealed parallel scratches on the surface of both samples (e.g. Figure 31) that were responsible for the perceived asterism (cf. Schmetzer and Steinbach, 2002; Steinbach, 2017, pp. 274–281). Re-examination of the two black star CZ samples reported by Deljanin (2018) showed that similar grooves had been scratched on their surfaces (Figure 32). Thus, the asterism in all of these samples was artificially induced.

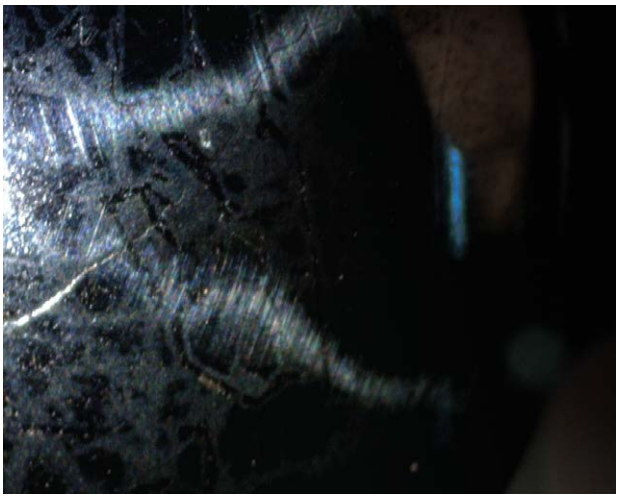

Figure 31: Parallel scratches on the surface of the 41.12 ct hematite-magnetite cabochon (shown here with two of the three orientations scratched on the sample) were responsible for its six-rayed star. Photo by B. Deljanin.

X-ray powder-diffraction (XRD) data were collected on the 38.82 and 41.12 ct samples at University of British Columbia using a Bruker D8 Advance diffractometer. With the client's permission, small amounts of powder were scraped from the 38.82 ct cabochon using a diamond file and from the 41.12 ct sample using SiC abrasive paper. The data were collected with Bragg-Brentano geometry over a range of 10°–140° 2Θ with Co*K*α radiation, an Fe monochromator foil, a 0.6 mm (0.3°) divergence slit, incident- and diffracted-beam Soller slits and a LynxEye XE detector. The 38.82 ct sample consisted mainly of almandine with minor pyrope, grossular and spessartine components. Energy-dispersive spectroscopy recorded with a scanning electron microscope confirmed it to be primarily almandine with minor Mg, Ca and Mn, and a trace of Ti. XRD analysis of the 41.12 ct cabochon revealed it to be hematite-magnetite (2:1 content; Figure 33). The absence of trace rock-forming minerals such as quartz, goethite, etc. might suggest a synthetic origin (Prof. Mati Raudsepp, pers. comm., 2017). According to Marion (2012), natural hematite is rare, expensive and generally not suitable for lapidary work, and therefore most of the 'hematite' beads and cabochons on the market are actually simulants (e.g. formed from powdered hematite).

These two additional cases of imitation black stars are reminders that standard and advanced testing are necessary for non-transparent black stones. While chemical analysis is sometimes needed to reveal a natural or synthetic origin of such material, simple observation using a microscope with proper lighting should reveal if a star is

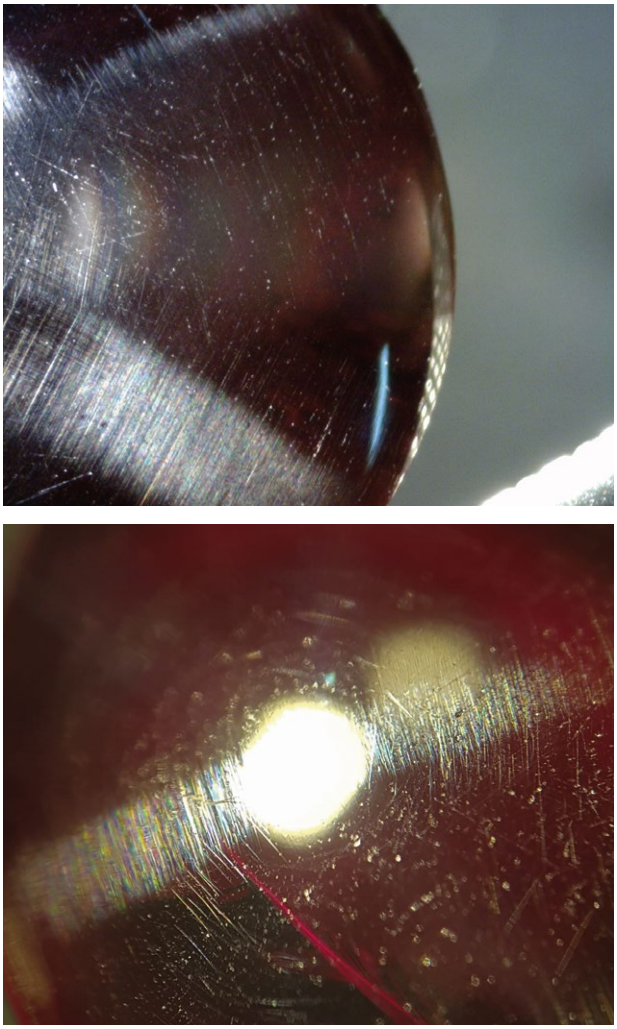

Figure 32: Upon close examination, the CZ imitations of black star rutile reported by Deljanin (2018) also showed surface scratches that created their asterism. Photos by B. Deljanin (left, 10.67 ct) and Alberto Scarani (right, 8.77 ct).

naturally or artificially induced. While garnets have been previously documented with artificial stars (see references cited above), this is the first time to the author's knowledge that hematite-magnetite has been reported with a scratch-induced star.

Acknowledgements: The author thanks Prof. Mati Raudsepp (Department of Earth, Ocean and Atmospheric Sciences, University of British Columbia, Vancouver, Canada) for XRD and SEM-EDS testing and useful feedback; Matthias Alessandri (GRS Lab Ltd., Hong Kong) for Raman spectroscopy of the 38.82 ct sample and for photos of both cabochons; Alberto Scarani (Magilabs, Rome, Italy) for the photomicrograph of the 8.77 ct star CZ that he encountered; and John Chapman (Gemetrix, Perth, Australia) for helpful comments and editing.

Branko Deljanin (branko@cglgrs.com)
CGL-GRS Swiss Canadian Gemlab
Vancouver, British Columbia, Canada

References

Deljanin B., 2017. Gem Notes: Black star cubic zirconia sold as natural star rutile. *Journal of Gemmology*, **35**(8), 704–706.

Marion R., 2012. Gem Profile Sept. 28: About Hematite. www.wirejewelry.com/jewelry-making-blog/8168/what-is-hematite, accessed January 2018.

Schmetzer K. and Steinbach M.P., 2002. Fake asterism – two examples. *Journal of Gemmology*, **28**(1), 41–42, http://dx.doi.org/10.15506/JoG.2002.28.1.41.

Steinbach M.P., 2017. *Asterism—Gems with a Star*. MPS Publishing and Media, Idar-Oberstein, Germany, 896 pp.

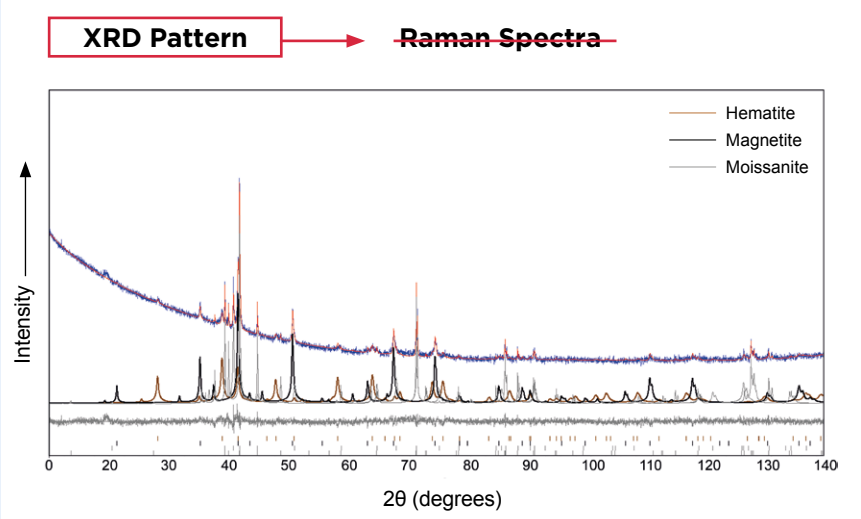

Figure 33: XRD analysis of the 41.12 ct sample proved that it consists of hematite-magnetite. This Rietveld refinement plot shows various patterns (blue line = observed intensity at each step; red line = calculated pattern; solid grey line below = difference between observed and calculated intensities; vertical bars = positions of all Bragg reflections). The differently coloured baseline-corrected peaks correspond to individual diffraction patterns of the detected phases (hematite and magnetite, as well as some contamination by synthetic moissanite from abrading the sample with SiC paper).

MISCELLANEOUS

Mid-Year 2017 Myanma Jade & Gems Emporium and Yangon Gems & Jewellery Fair

The Mid-Year 2017 Myanma Jade & Gems Emporium was held 12–21 December in Nay Pyi Taw, Myanmar. Gems that were offered included parcels of ruby (e.g. Figure 34, left), sapphire, spinel, peridot (Figure 34, right), amber, aquamarine, danburite, garnet and assorted coloured stones. Lot no. 111, consisting of 1.1 g of rough ruby, fetched €63,229. Mong Hsu rough ruby lot no. 176, weighing 2.50 kg, sold for €65,431. The highest price paid for rough sapphire—€40,099—was for lot no. 63, which had two pieces weighing a total of 18.2 g. Rough spinel lot no. 53, consisting of one 5.6 g piece, brought €100,088. Lot no. 168, a parcel of rough peridot weighing 720 g, sold for €51,550. This particular Emporium also had finished products manufactured from Myanmar 'jade', including a tree constructed of carved jadeite; jadeite necklaces, bangles, cabochons and beads; semi-cut jadeite and quartzite; and quartzite bangles, cabochons and beads.

A 14 December 2017 Burmese newspaper article reported that the Emporium was attended by foreign visitors from China, Thailand, Macao and Canada, as well as 1,339 local attendees, for a total of 3,999 participants. Table I summarizes the Emporium's offerings and sales.

From 11 to 14 January 2018, the 1st Yangon International Gems & Jewellery Fair (organized by Yangon Gems & Jewellery Entrepreneurs Association) was held at the Lotte Hotel in Yangon. There were 76 stalls with 104 exhibitors displaying their products (e.g. Figure 35). A total of 6,774 domestic buyers and 686 foreigners attended. Sales of loose stones were US$250,000 and jewellery sales totalled $294,602.50. A seminar programme included two

Figure 34: Gems offered at the Mid-Year 2017 Myanma Jade & Gems Emporium included heat-treated cabochons of Mong Hsu ruby (left, 1,142 carats total weight) and rough Burmese peridot (right, 772.8 g). Photos by T. Hlaing.

foreign presenters: Tay Thye Sun (Far East Gemological Laboratory, Singapore) discussed Burmese amber from Hti Lin and the use of Raman spectroscopy for separating amber from copal and other imitations, and Richard Hughes (Lotus Gemology, Bangkok, Thailand) described the internal features of ruby.

Dr U Tin Hlaing (p.tinhlaing@gmail.com)
Dept. of Geology (retired)
Panglong University, Myanmar

Table I: Sales at the Mid-Year 2017 Myanma Jade & Gems Emporium.

Material	Total Lots	Sold Lots	Total sales (million €)
Jade*	6,660	4,050	438.58
Gems	190	32	0.767

* Consists of rough and semi-cut pieces.

Figure 35: The 1st Yangon International Gems & Jewellery Fair provided a meeting place for vendors and buyers of Burmese gems. Photo by T. Hlaing.

Figure 1: These faceted amethysts from the Ngororero District of Rwanda weigh 7.30 ct (left) and 10.91 ct (right). Courtesy of Jack Lowell; photo by Jeff Scovil.

Gem-Quality Amethyst from Rwanda: Optical and Microscopic Properties

Karl Schmetzer and Bear Williams

Recent years have witnessed the emergence of reports regarding new finds of amethyst in Rwanda. A study of Rwandan material by the present authors shows that the majority of samples displayed characteristic features distinct from those considered typical of most amethyst from other localities. In particular, light violet to almost colourless rhombohedral growth sectors frequently exhibited Brazil-law twinning, while purplish violet or intense violet growth sectors were untwinned. Distinct pleochroism when viewed parallel to the c-axis also was notable, even in samples that showed no Brazil-law twinning. However, a small fraction of the material examined from Rwanda instead showed properties that were generally consistent with those commonly seen in amethyst. This suggests that amethyst has entered the market from different Rwandan sources, and recent finds in both the Ngororero and Ruhango Districts have been cited.

The Journal of Gemmology, **36**(1), 2018, pp. 26–36, http://dx.doi.org/10.15506/JoG.2018.36.1.26

INTRODUCTION

Since late 2015, various reports have emerged regarding new finds of amethyst in Rwanda, and faceted stones of high quality (e.g. Figure 1) have entered the international market. The gems are primarily violet in colour, occasionally appearing slightly purplish violet in daylight and somewhat more intensely purplish violet in incandescent light.

Two areas of Rwanda have been cited as potential sources for the new material: the Ngororero and Ruhango Districts (Figure 2). Ngororero is located in Western Province, about 40 km south-east of Goma (W. Radl, pers. comm., 2017). Internet news reports pertaining to this amethyst deposit further specified the Kavumu Sector of Ngororero District as the source of the occurrence (Rwanda News

Figure 2: The approximate locations of the two recent finds of Rwandan amethyst are shown on this map. The red symbol refers to the Kavumu Sector of the Ngororero District (see National Institute of Statistics of Rwanda, 2010; Tuyisabe, 2015) and is located about 40 km south-east of Goma. The centre of the Ruhango District is represented by the blue symbol.

Agency, 2017; see Tuyisabe, 2015, for the subdivision of provinces and districts in Rwanda), and they showed images of workings located on a sloped grassy terrain (e.g. Figure 3A) where local miners used hand tools to search for amethyst (e.g. Figure 3B). Internet resources also indicated that the deposit was discovered in 2015 (e.g. *Hope Magazine*, 2017).

The second area referenced as a potential source of gem-quality amethyst in Rwanda, likewise discovered in 2015, is the Ruhango District in Southern Province (Footprint to Africa, 2015; Kigali Today, 2015). Samples said to have originated from this find were described by Stephan and Schmitz (2016, 2017). Those authors noted distinct colour zoning with intense violet and colourless areas. They also mentioned observing polysynthetic twinning on the Brazil law, a typical feature of natural amethyst.

Following the initial reports in November 2015, samples of the new Rwandan amethyst reportedly from the Ngororero District were supplied by rough stone dealer Farooq Hashmi, and a preliminary examination by one of the authors (BW) revealed interesting optical and spectroscopic characteristics. It was then decided to conduct a more detailed study with additional samples to identify and better understand the underlying properties. This article describes the optical and microscopic aspects, and a future paper by one of the authors (BW) is planned to examine the spectroscopic properties of the Rwandan amethyst.

Figure 3: (A) The recently discovered amethyst deposit within the Ngororero District is located on sloped terrain. (B) Local miners use hand tools to search for amethyst. The photos were taken by a local miner and are courtesy of Farooq Hashmi.

MATERIALS AND METHODS

This study began with 28 amethyst crystals and crystal fragments, ranging from ~1 × 1 × 0.5 cm (0.6 g) to 7 × 5 × 4 cm (171 g), and 14 faceted gemstones weighing 1.45–16.17 ct. The samples, represented as being from the Ngororero District, were provided by Farooq Hashmi, John Garsow, Jack Lowell and Werner Radl (see Acknowledgements). With permission from the owners, eight of the rough samples were sawn approximately perpendicular to the c-axis, generally yielding three to five slices per sample.

For comparison, the study was subsequently augmented with 10 rough (5.6–28.7 g) and four faceted (5.20–25.67 ct) amethysts from the same German company that had supplied the research material described by Stephan and Schmitz (2016, 2017). The supplier reported that the samples had originated from the western part of Rwanda, but the company had no further information about the particular source locality (E.-O. Sahm, pers. comm., 2017).

All samples were examined microscopically, with and without immersion, using standard gemmological techniques. Some of the rough material was encrusted with white or black material adhered to the surface, and a small quantity of these coatings was analysed by X-ray powder diffraction using a Philips PW1800 diffractometer.

RESULTS

Samples Reportedly from the Ngororero District

Morphology of the Rough and Characterization of Encrustations: The complete crystals generally showed six rhombohedral **r** and **z** faces (Figure 4, occasionally with some prismatic m faces (Figure 5A). The relative proportions of each group of symmetry-equivalent rhombohedral **r** and **z** faces varied (Figures 5B–D), insofar as all crystals were highly distorted (Figure 4).

X-ray diffraction of the encrustations on the crystals identified them as opal-CT (whitish coatings; Figure 4) and lithiophorite (black coatings). Their presence indicated that, subsequent to amethyst crystal growth, the deposit experienced conditions allowing for the deposition of minerals formed at relatively low temperatures.

Figure 4: Amethyst crystals from Rwanda display six rhombohedral faces, occasionally in combination with short prism faces. The rhombohedral **r** and **z** faces are highly distorted, with symmetry-equivalent faces differing in size. The whitish encrustation was identified as opal-CT. The sample weighs 68 g and measures 50 × 45 mm. Photo by K. Schmetzer.

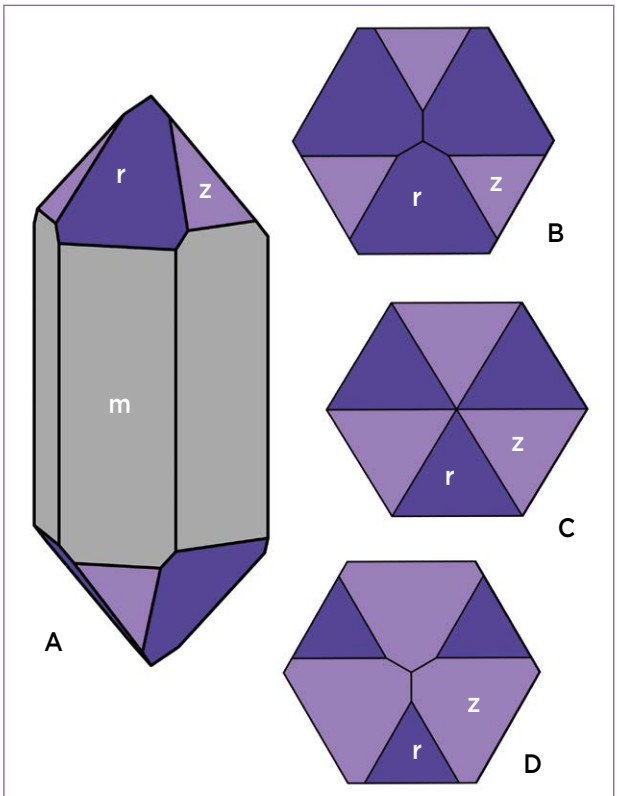

Figure 5: The morphology of amethyst crystals from Rwanda comprises primarily rhombohedral **r** and **z** faces, occasionally in combination with prismatic **m** faces. Shown here are (A) an idealized clinographic projection and (B–D) idealized (non-distorted) projections viewed parallel to the c-axis showing different sizes of **r** and **z** faces. Normally, the Rwandan amethyst crystals are distorted and broken (i.e. samples with two ends were not seen by the authors). Drawings by K. Schmetzer.

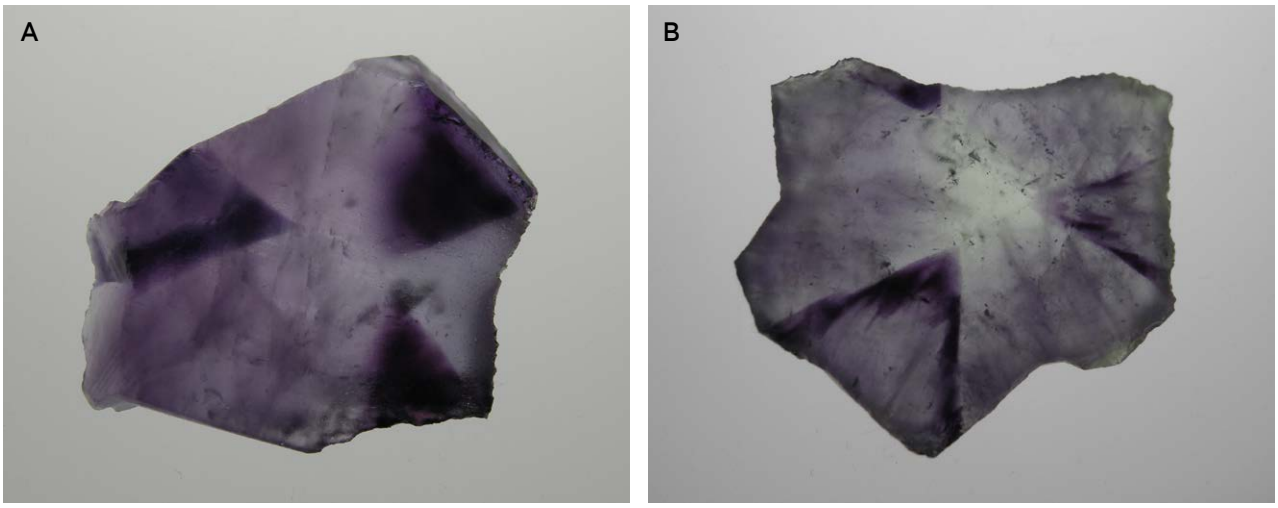

Figure 6: Slices of amethyst from Rwanda, cut perpendicular to the c-axis, show growth sectors that vary from intense violet to lighter violet to almost colourless. The slices measure (A) 36 × 23 × 6 mm and (B) 40 × 34 × 5 mm. Photos by K. Schmetzer.

Colour Zoning of Rhombohedral Growth Sectors: All rough and faceted samples displayed colour zoning that corresponded to the different rhombohedral growth sectors. Such sectorial colour zoning was best seen in slices cut perpendicular to the c-axis, using transmitted light (Figure 6). Frequently, larger light violet areas were observed in combination with smaller triangular growth sectors exhibiting a more intense purplish violet or violet colour (Figure 6A). Within these deeply coloured sectors, lighter and darker stripes also were seen (Figure 6B). In faceted samples, the sectorial colour zoning was more apparent when viewed from the pavilion (Figure 7).

Figure 7: Faceted Rwandan amethyst commonly displays sectorial colour zoning, which typically consists of intense violet to purplish violet and lighter violet to almost colourless zones. The zoning may be visible in views toward the table facet (top), but it is more apparent in views toward the pavilion of the samples (bottom). The stones weigh 7.71 ct (left) and 10.03 ct (right). Photos by K. Schmetzer.

Figure 8: This schematic representation of the pleochroism in amethyst demonstrates that, in a view parallel to the c-axis, symmetry-equivalent rhombohedral growth sectors (violet and light purple) ideally show identical pleochroism after rotation about the c-axis through an angle of 120°. The labels X1, X2, Y1 and Y2 represent the colours observed within the different growth sectors using one polarizer between the sample and the observer. Drawing by K. Schmetzer.

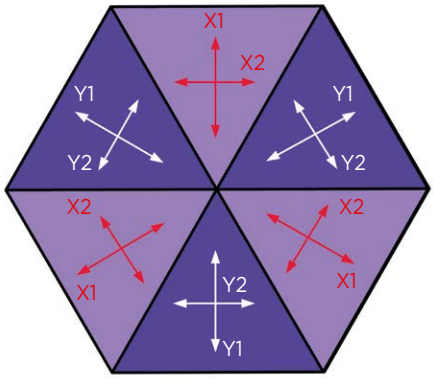

Pleochroism of Rhombohedral Growth Sectors: It has been demonstrated that some amethyst—despite being α-quartz and therefore belonging to the trigonal system—shows pleochroism when viewed parallel to the optic axis in slices cut perpendicular to the c-axis (Pancharatnam, 1954; Lietz and Münchberg, 1956). In such slices, the three symmetry-equivalent **r** or **z** growth sectors exhibit identical pleochroism and colour. Consequently, when a sample is viewed in plane-polarized light and rotated about the c-axis, each rotation through 120° will reveal an identical growth sector with identical pleochroism (Figure 8). Some of the present samples from the Ngororero District exhibited this property, which was especially evident in slices cut from the crystals.

Table I: Pleochroism typical of Rwandan amethyst, viewed parallel to the c-axis.*

Type	Sector colour	Pleochroism
I	Light violet to almost colourless	Light violet and colourless
II	Purplish violet	Intense purplish violet and yellow to light orange-yellow
III	Intense violet	Intense violet and lighter slightly purplish violet

* In views perpendicular to the c-axis of the samples available for this study, the light path always traversed multiple types of rhombohedral growth sectors. To evaluate and accurately describe the pleochroism in such orientation, and for each of the three different types of growth sectors, it would be necessary to obtain numerous slices parallel to the c-axis that each contained only a single growth sector. Slices of that nature were not available for the present research.

Three different types of pleochroism were seen in the triangular growth sectors, depending on their coloration (Table I). In general, a particular specimen showed two of the three types of growth sectors/pleochroism—that is, a combination of type I and type III growth sectors (Figures 9 and 10A) or a combination of type I and type II growth sectors (Figure 10B). However, in some samples all three types of growth sectors were found (Figure 11). Nevertheless, because most samples featured a high degree of distortion, there were frequently fewer than the ideal six rhombohedral growth sectors. Examples with just four discernible rhombohedral growth zones are depicted in Figures 9 and 11.

Other types of zoning—possibly related to twinning—are discussed below.

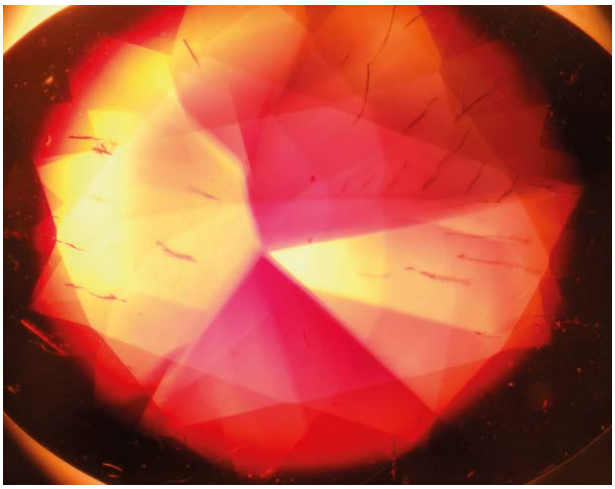

Figure 9: Viewed parallel to the c-axis, this amethyst from Rwanda shows sectorial colour zoning with two light violet to almost colourless growth sectors (type I) and two intense violet growth sectors (type III). Photomicrograph by K. Schmetzer, in immersion; field of view 12.8 × 10.0 mm.

Brazil-law (Optical) Twinning: Natural amethyst normally shows colour zoning with somewhat more intense violet **r** growth sectors and somewhat lighter violet **z** growth sectors. Viewed parallel to the c-axis with crossed polarizers, the intense violet **r** growth sectors typically exhibit interference patterns consisting of more-or-less regular black stripes (Brewster fringes). This pattern is a result of Brazil-law polysynthetic twinning in these sectors. No such pattern was found in the purplish violet or intense violet growth sectors of the Ngororero amethyst. In contrast, the samples revealed three scenarios with respect to Brazil-law twinning features:

- Pattern A: No interference patterns with Brewster fringes were seen in any of the growth sectors

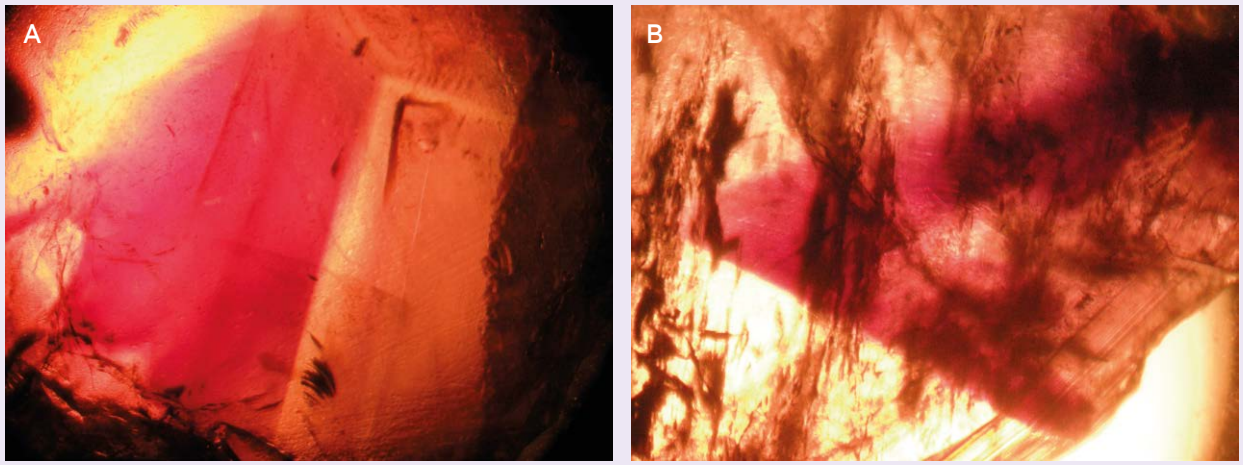

Figure 10: With plane-polarized light, in a view parallel to the c-axis, the rhombohedral growth sectors of Rwandan amethyst exhibit different combinations of colour and pleochroism: (A) a combination of light violet to almost colourless (type I) and intense violet (type III) sectors, and (B) a combination of light violet to almost colourless (type I) and purplish violet (type II) sectors. Photomicrographs by K. Schmetzer, in immersion; field of view 14.5 × 10.9 mm.

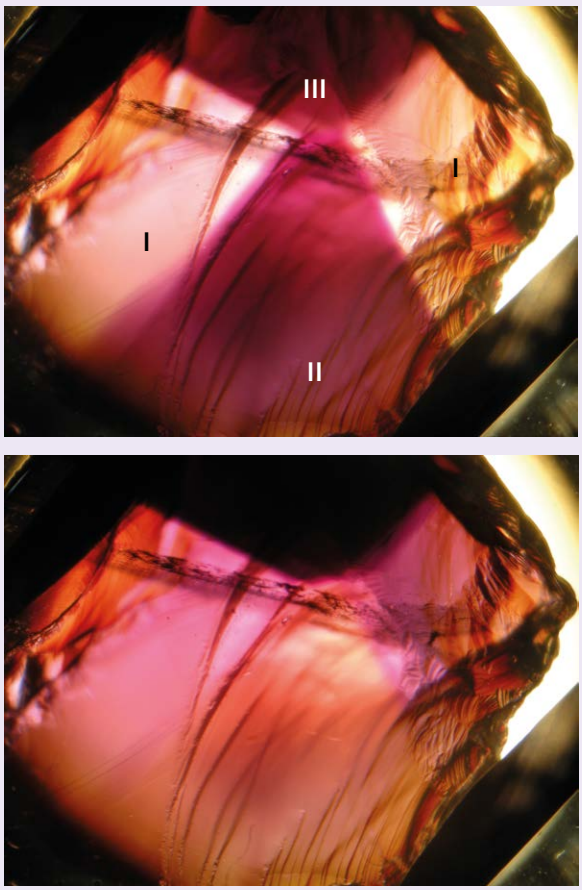

Figure 11: In a view parallel to the c-axis, this distorted Rwandan amethyst sample shows three different types of rhombohedral growth sectors with varying colour and pleochroism. The two views show the pleochroism that is seen upon rotation of the polarizer. In the two type I growth sectors, the pleochroism is light violet and colourless; in the single type II growth sector, the pleochroism is intense purplish violet and yellow; and in the single type III growth sector, the pleochroism is intense violet and a somewhat lighter, slightly purplish violet. Photomicrographs by K. Schmetzer, in immersion; field of view 14.5 × 10.9 mm.

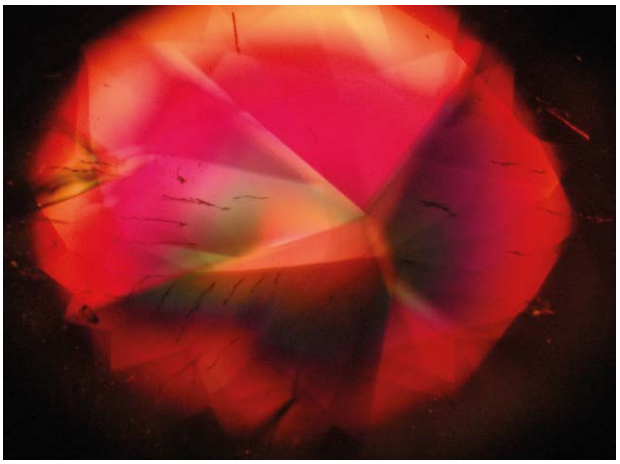

Figure 12: Viewed parallel to the c-axis with crossed polarizers, this amethyst from Rwanda shows different rhombohedral growth sectors but no Brewster fringes indicative of polysynthetic Brazil-law twinning. Photomicrograph by K. Schmetzer, in immersion; field of view 14.5 × 10.9 mm.

(Figure 12), despite the presence of different types of rhombohedral growth zones as described above.

- Pattern B: Single Brewster fringes confined to the boundaries between different growth sectors were observed (Figure 13).
- Pattern C: In addition to Brewster fringes following the boundaries between different growth sectors as described in pattern B, polysynthetic twinning on the Brazil law was observed in the light violet to almost colourless growth zones, at times resulting in highly complex patterns (Figure 14).

Dauphiné Twinning: Certain samples also contained irregularly shaped domains displaying coloration (more intense violet or more purplish violet) and pleochroism that were different from the surrounding host material (Figure 15). These domains and the surrounding material showed no interference patterns with crossed polarizers and are most likely related to Dauphiné twinning.

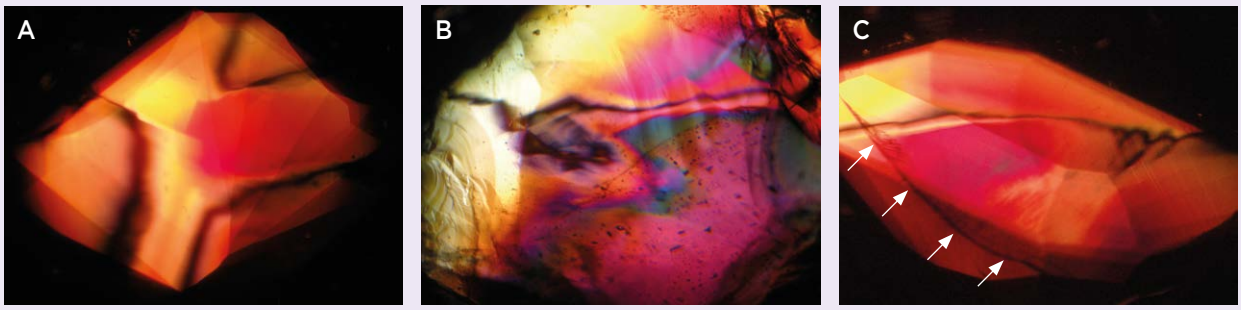

Figure 13: A single black interference line (Brewster fringe) confined to the boundaries between various rhombohedral growth sectors is commonly seen in Rwandan amethyst when viewed parallel to the c-axis with crossed polarizers. (The dark line highlighted with arrows in photo C is a partially healed fracture.) Photomicrographs by K. Schmetzer, in immersion; field of view (A) 12.4 × 9.3 mm, (B) 11.5 × 8.7 mm and (C) 9.5 × 7.2 mm.

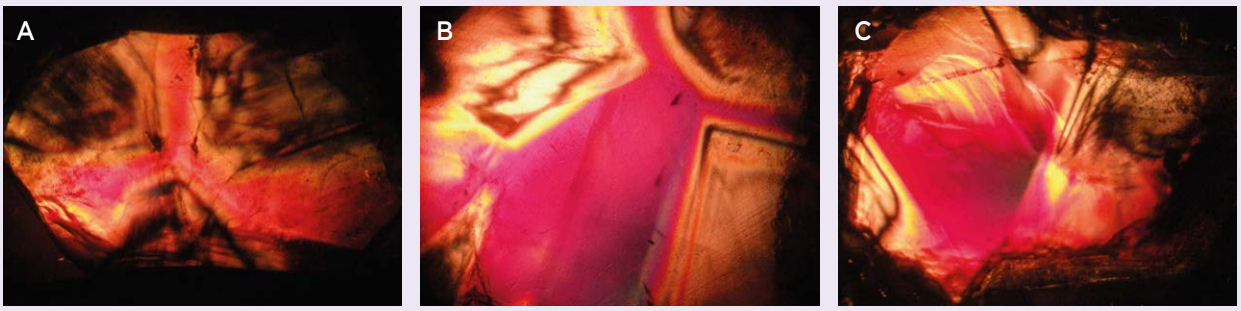

Figure 14: In several Rwandan amethyst samples, complex arrangements of optical twinning features are evident. In these views parallel to the c-axis with crossed polarizers, single black interference lines (Brewster fringes) follow the boundaries between various rhombohedral growth sectors and are accompanied by dense patterns of Brewster fringes indicating Brazil-law polysynthetic twinning in the light violet to almost colourless sectors. Photomicrographs by K. Schmetzer, in immersion; field of view (A) 13.5 × 10.1 mm, (B) 11.9 × 9.0 mm and (C) 14.0 × 10.5 mm.

Other Zoning: One sample displayed another type of colour zoning and pleochroism that was seen in a view inclined 42° to the c-axis as a thin growth zone (Figure 16). It was apparently related to the boundary between two rhombohedral growth sectors. This zoning also might be related to twinning, but the pattern is not completely understood (see also the pleochroism in different rhombohedral growth sectors described in the next paragraph).

Rhombohedral Growth Zoning and Striations: Striations parallel to the external rhombohedral faces of the amethyst crystals were frequently observed within the rhombohedral growth sectors. In a view inclined 42° to the c-axis, these striations occasionally were found in two different rhombohedral growth sectors. The two series of parallel striations formed an angle of 133.7° with each other (Figure 17). In this orientation, the two different rhombohedral growth sectors also showed different pleochroism.

For faceted gems, it should be reiterated that stones cut from significantly larger rough material may consist of only one rhombohedral growth sector (Figure 18). Such gems would present only a single series of parallel growth striations (Figure 19).

Inclusions: The rough samples showed abundant inclusions, primarily in the form of partially healed fractures, negative crystals and two-phase inclusions (liquid/gas; e.g. Figure 20). Conversely, the faceted material was very clean, only rarely incorporating inclusions. The implication therefore would be that, as is common practice for amethyst, the rough material was processed (sawn and/or cobbed by hammering) to remove impure parts and obtain clean areas for faceting.

In some samples, reddish brown solid inclusions were seen as well (Figure 21). Features with a similar appearance have been described in the gemmological literature as 'beetle-legs' and have been attributed to platelets or fibres of hematite (White, 2000; Troilo et al., 2015).

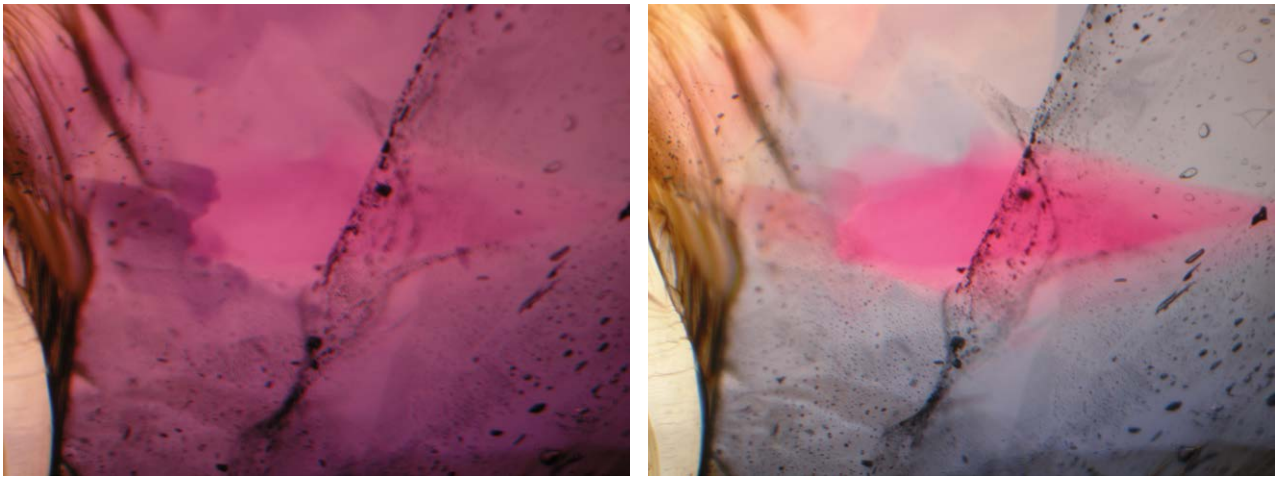

Figure 15: These two views of a Rwandan amethyst taken with different rotations of the polarizer show an irregularly shaped domain that displays a different coloration than the surrounding amethyst host. Photomicrographs by K. Schmetzer, in immersion; field of view 8.1 × 6.1 mm.

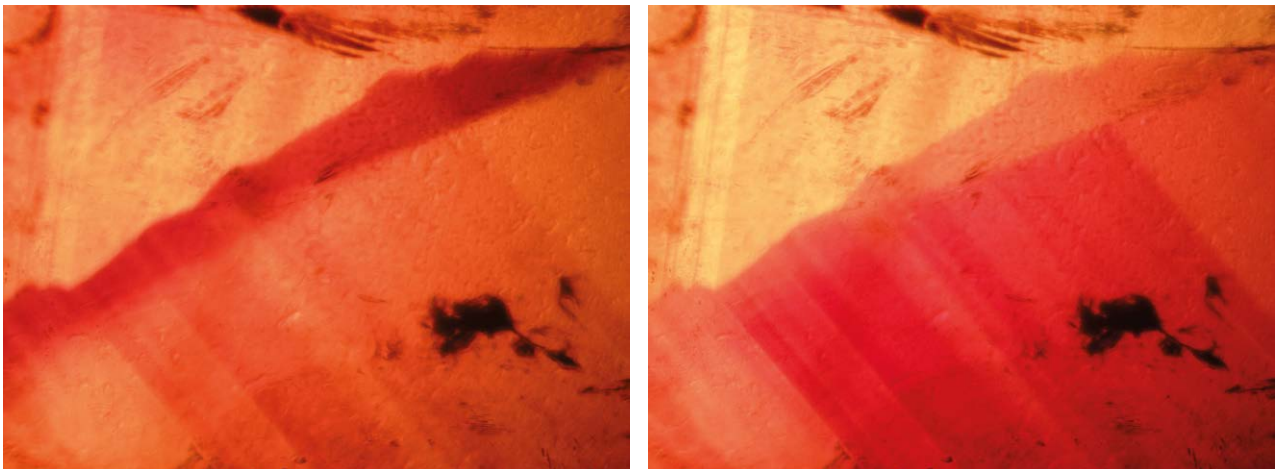

Figure 16: In this amethyst from Rwanda, a thin growth zone differing in colour and pleochroism from the two adjacent rhombohedral growth sectors is visible in a view inclined 42° to the c-axis. Its colour varies as the polarizer is rotated. Photomicrographs by K. Schmetzer, in immersion; field of view 7.6 × 5.7 mm.

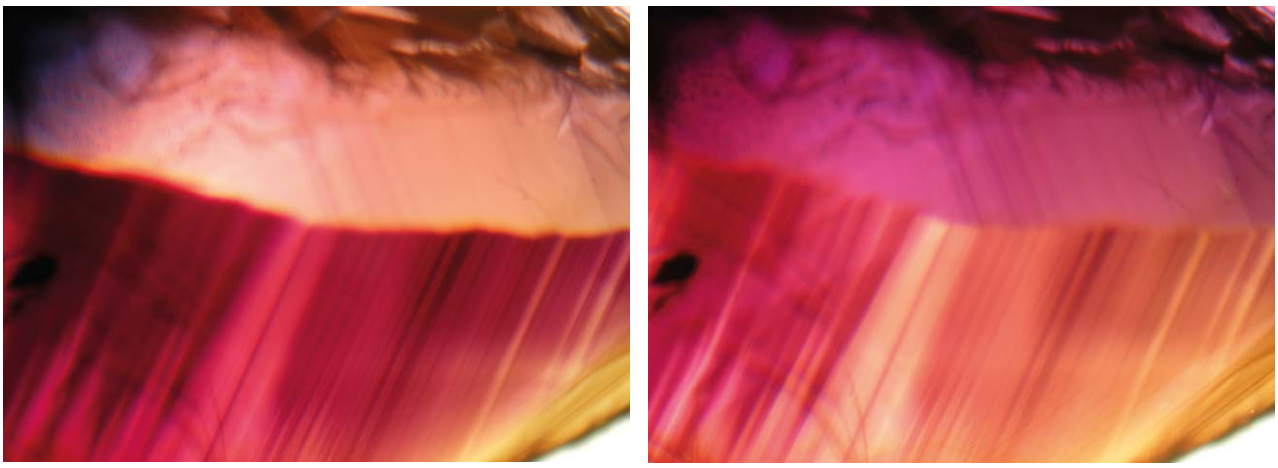

Figure 17: This Rwandan amethyst displays two rhombohedral growth sectors that, when using plane-polarized light and rotating the polarizer, exhibit both pleochroism and growth striations. In a view inclined 42° to the c-axis, the two series of striations form an angle of 133.7° with each other. Photomicrographs by K. Schmetzer, in immersion; field of view 8.1 × 6.1 mm.

Figure 18: If an amethyst is faceted from a single intense violet growth sector, no sectorial colour zoning is observed. Such samples may look homogeneous or may display a single series of rhombohedral growth striations in views toward both the table facet and the pavilion. The samples weigh 5.81 (left) and 8.26 ct (right). Photos by K. Schmetzer.

Figure 19: Faceted Rwandan amethyst consisting of a single growth sector will show only a single series of growth striations parallel to one rhombohedral face. Photomicrograph by K. Schmetzer, in immersion; field of view 8.7 × 7.1 mm.

Figure 20: A partially healed fracture with two-phase inclusions is seen in this rough sample of Rwandan amethyst. Photomicrograph by K. Schmetzer, in immersion; field of view 4.1 × 3.1 mm.

Samples Reportedly from Western Rwanda

Of the 14 samples (four faceted and 10 rough) reportedly from 'western Rwanda', 10 of them displayed the same characteristics and patterns described above for the samples from Ngororero. Four samples, however, were different (e.g. Figure 22). They consisted of one or two rhombohedral growth zones, and when two growth zones were present, they exhibited no or only very weak colour zoning between them. More specifically, both sectors were intense violet. In addition, Brewster fringes caused by Brazil-law twinning were seen in all sectors (Figure 23), as were rhombohedral growth striations. The striations formed angles of 94° with each other, thereby demonstrating symmetry-equivalent rhombohedral growth zones. Thus, to summarize, these four amethyst samples differ from the other Rwandan samples by being composed of two adjacent intense violet growth zones, both of which are twinned.

DISCUSSION AND CONCLUSIONS

Comparison of Amethyst Properties

Amethyst from multiple sources worldwide is generally characterized by sectorial growth zoning with somewhat more intense violet rhombohedral **r** growth sectors and somewhat lighter violet **z** growth sectors. In such amethyst, the more intense violet **r** growth zones show polysynthetic twinning on the Brazil law (see, e.g., Kiefert and Schmetzer, 1991; Lieber, 1994). Untwinned crystals of natural amethyst are rare, but limited examples have been mentioned (Lietz and Münchberg, 1958).

With respect to the Rwandan material examined for this study, the typical situation just described was largely reversed. The samples either were not polysynthetically twinned or, when polysynthetic twinning was present, the twinned sectors were related to the light violet or almost colourless areas. This was the case for all 28 of the rough stones reportedly from the Ngororero District. For the faceted amethysts, about one third of the samples were cut from a single intense violet rhombohedral growth sector and did not show Brewster fringes and polysynthetic twinning.

The literature reports few comparable examples, although amethyst from the Caxarai mine, Brazil, has similar optical properties (Kitawaki, 2002). That study designated the twinned sectors as **r** (light violet) and the untwinned sectors as **z** (intense violet). Such interpretation may be correct, but in the absence of more definitive data for the Rwandan material, the opposite also might apply. Therefore, for purposes of the present article, the authors have left this point open (i.e. the designation of twinned and untwinned growth sectors as **r** or **z**, respectively), simply because either interpretation might be accurate and a decision cannot be made on the basis of microscopic examination and the optical features observed.

Anomalous pleochroism in amethyst has been explained by variance in the uptake of trace elements, especially iron, at different lattice sites and/or in different rhombohedral **r** and **z** growth sectors (Cox, 1977; Adekeye and Cohen, 1986; Flörke et al., 2000). A detailed discussion of the various mechanisms that might apply is beyond the scope of this study.

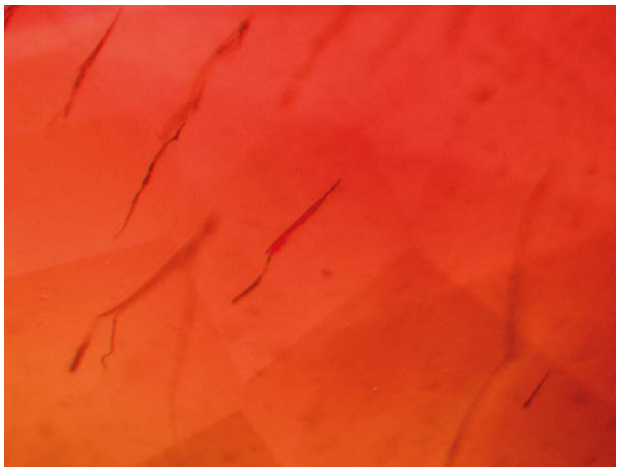

Figure 21: Some of the Rwandan amethyst samples display reddish brown solid inclusions. These are often referred to as 'beetle-legs' in the gemmological literature and have been attributed to platelets or fibres of hematite. Photomicrograph by K. Schmetzer, in immersion; field of view 4.6 × 3.5 mm.

Figure 22: These amethysts, reportedly from 'western Rwanda', proved to contain intense violet growth zones twinned on the Brazil law. The samples weigh 19.72, 11.99 and 5.20 ct. Photo by K. Schmetzer.

In contrast to the distinctive nature of the larger group of Ngororero material, only four of the investigated samples reportedly from 'western Rwanda' exhibited the properties typical for amethyst from many other sources throughout the world (see, e.g., Kiefert and Schmetzer, 1991). Their presence suggests that the amethyst in these two groups might have originated from two (or even more) different Rwandan localities.

The two potential mining areas in the Ngororero and Ruhango Districts mentioned in the Introduction are approximately 40–50 km from each other (Figure 2), so it would be easy for traders to include in parcels material from both localities. It is unknown if the two localities involve different host rocks and/or different modes of amethyst formation. Such factors could explain the contrasting properties of the two types of Rwandan samples. Geological fieldwork at both locations would be necessary to clarify this point.

Distinction from Synthetic Amethyst

If a faceted Rwandan amethyst consists of several growth sectors, the gem can be distinguished from synthetic material by optical examination. Such natural samples show sectorial growth zoning, in most cases also associated with polysynthetic twinning and, occasionally, with other forms of growth zoning or twinning (e.g. Dauphiné twinning). These patterns are absent from synthetic amethyst.

However, if a Rwandan amethyst has been faceted from only a single untwinned growth sector, the microscopic pattern would show only rhombohedral growth zoning parallel to a single rhombohedral face and no twinning (and thus no Brewster fringes). An analogous pattern is common for synthetic amethyst. Thus, samples with these features would require additional examination, such as by infrared spectroscopy, to identify the nature of the material.

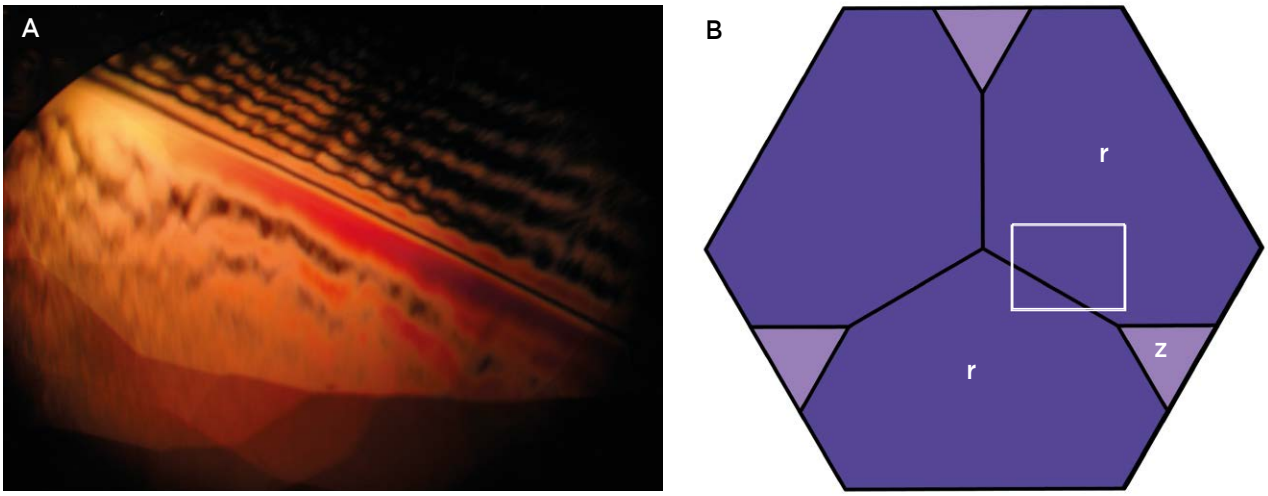

Figure 23: (A) Viewed parallel to the c-axis with crossed polarizers, this amethyst from 'western Rwanda' displays Brewster fringes due to Brazil-law twinning in two different, adjacent rhombohedral growth sectors. (B) The schematic diagram shows a crystal in the same view, highlighting the area in photo A. Photomicrograph by K. Schmetzer, in immersion; field of view 14.5 × 10.9 mm. Drawing by K. Schmetzer.

REFERENCES

Adekeye J.I.D. and Cohen A.J., 1986. Correlation of Fe^{4+} optical anisotropy, Brazil twinning and channels in the basal plane of amethyst quartz. *Applied Geochemistry*, **1**(1), 153–160, http://dx.doi.org/10.1016/0883-2927(86)90046-6.

Cox R.T., 1977. Optical absorption of the d^4 ion Fe^{4+} in pleochroic amethyst quartz. *Journal of Physics C: Solid State Physics*, **10**(22), 4631–4643, http://dx.doi.org/10.1088/0022-3719/10/22/032.

Flörke O.W., Röller K. and Siebers F., 2000. Amethyst: Farbzentren und Zwillingsgefüge. *Gemmologie: Zeitschrift der Deutschen Gemmologischen Gesellschaft*, **49**(2), 65–84.

Footprint to Africa, 2015. Rwanda discovers potential raw precious stones, http://footprint2africa.com/general-news/rwanda-discovers-potential-raw-precious-stones, accessed 2017.

Hope Magazine, 2017. Ngororero man arrested for smuggling minerals, www.hope-mag.com/index.php?com=news&option=read&ca=1&a=3149, accessed 2017.

Kiefert L. and Schmetzer K., 1991. The microscopic determination of structural properties for the characterization of optical uniaxial natural and synthetic gemstones. Part 3: Examples for the applicability of structural features for the distinction of natural and synthetic sapphire, ruby, amethyst and citrine. *Journal of Gemmology*, **22**(8), 471–482, http://dx.doi.org/10.15506/JoG.1991.22.8.471.

Kigali Today, 2015. Rwanda discovers new precious stone, http://ktpress.rw/2015/08/rwanda-discovers-new-precious-stone, accessed 2017.

Kitawaki H., 2002. Natural amethyst from the Caxarai mine, Brazil, with a spectrum containing an absorption peak at 3543 cm^{-1}. *Journal of Gemmology*, **28**(2), 101–108, http://dx.doi.org/10.15506/JoG.2002.28.2.101.

Lieber W., 1994. *Amethyst: Geschichte, Eigenschaften, Fundorte*. Christian Weise Verlag, Munich, Germany, 188 pp.

Lietz J. and Münchberg W., 1956. Über Symmetrie und Pleochroismus von Amethyst. *Neues Jahrbuch für Mineralogie, Monatshefte,* **1956**(10), 217–231.

Lietz J. and Münchberg W., 1958. Über unverzwillingte Amethystkristalle. *Neues Jahrbuch für Mineralogie, Monatshefte*, **1958**(1), 17–20.

National Institute of Statistics of Rwanda, 2010. Ngororero District Map, www.ngororero.gov.rw/fileadmin/user_upload/map_map.pdf, accessed 2017.

Pancharatnam S., 1954. On the pleochroism of amethyst quartz and its absorption spectra. *Proceedings of the Indian Academy of Sciences, Section A*, **40**, 196–210.

Rwanda News Agency, 2017. Ngororero: Illegal exploitation of amethyst on private property, http://rnanews.com/national/12814-ngororero-illegal-exploitation-of-amethyst-on-private-property, accessed 2017.

Stephan T. and Schmitz F., 2016. Amethyst of remarkable fine qualities from a reportedly new find in Rwanda. *Australian Gemmologist*, **26**(1–4), 45–47.

Stephan T. and Schmitz F., 2017. Amethyst aus Ruanda. *Gemmologie: Zeitschrift der Deutschen Gemmologischen Gesellschaft*, **66**(1/2), 54–58.

Troilo F., El Harfi A., Mouaddib S., Bittarello E. and Costa E., 2015. Amethyst from Boudi, Morocco. *Gems & Gemology*, **51**(1), 32–40, http://dx.doi.org/10.5741/gems.51.1.32.

Tuyisabe P., 2015. Rwanda: Administrative Division – Provinces and Districts, http://rwandadiasporagermany.com/rwanda-administrative-division-provinces-and-districts, accessed 2017.

White J.S., 2000. Strawberry quartz. *Gemmologie: Zeitschrift der Deutschen Gemmologischen Gesellschaft*, **49**(2), 95–102.

The Authors

Dr Karl Schmetzer
Taubenweg 16, D-85238 Petershausen, Germany
Email: SchmetzerKarl@hotmail.com

Bear Williams FGA
Stone Group Laboratories, PO Box 104504, Jefferson City, Missouri 65110, USA

Acknowledgements

The authors are grateful to the following companies or individuals for loaning rough or faceted amethyst from Rwanda and for providing, if available, information and photos concerning the origin of the samples: John E. Garsow (John E. Garsow Gems & Minerals, Murrieta, California, USA), Farooq Hashmi (Intimate Gems, Glen Cove, New York, USA), Jack Lowell (Colorado Gem & Mineral Co., Tempe, Arizona, USA), Ernst-Otto Sahm (Firma Hermann Thul, Kirschweiler, Germany) and Werner Radl (Mawingu Gems, Idar-Oberstein, Germany).

The authors also thank Prof. H. Albert Gilg (Technische Universität München, Germany) for X-ray powder diffraction analysis of the amethyst encrustations.

An innovator in gemstone reporting

• Identification of colored gemstones • Country of origin determination • Full quality and color grading analysis

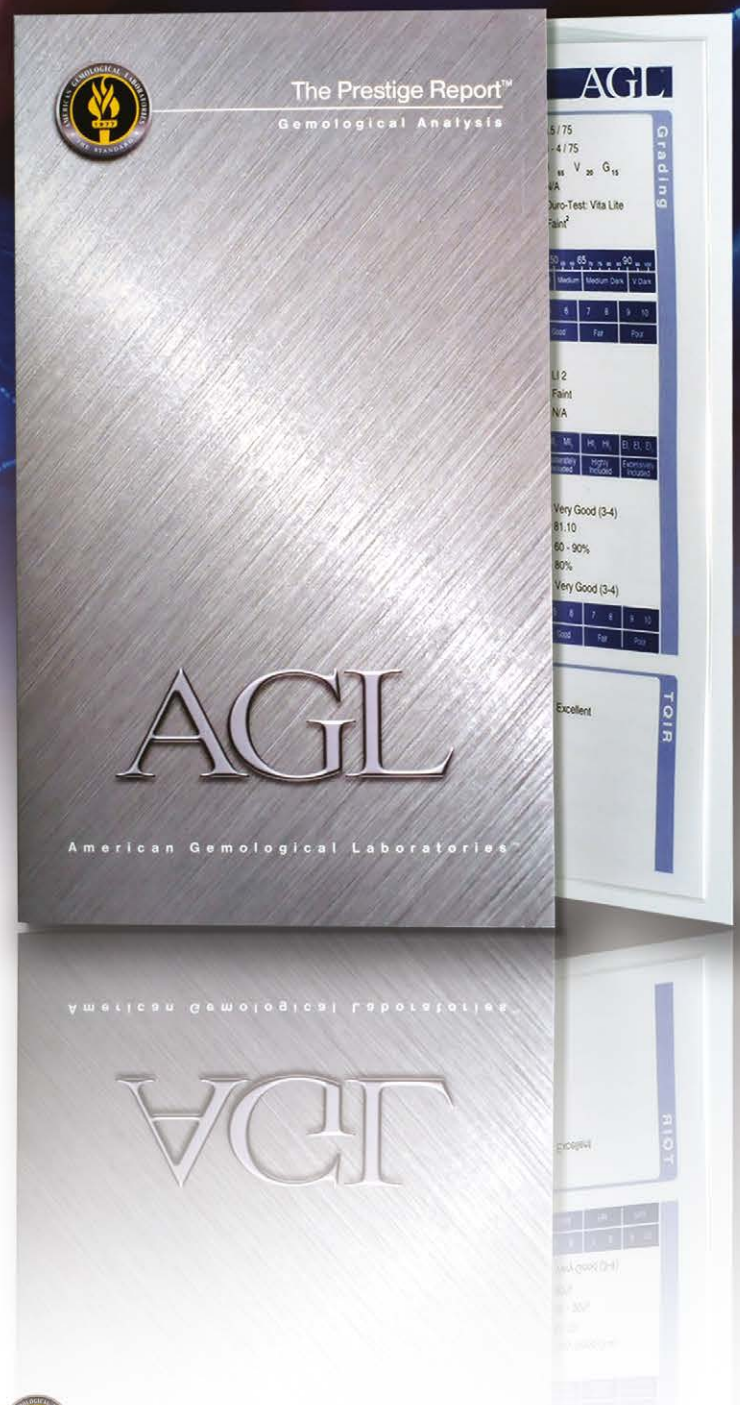

AMERICAN GEMOLOGICAL LABORATORIES AGL

580 5th Ave • Suite 706 • New York, NY 10036, USA
www.aglgemlab.com • +1 (212) 704 - 0727

A Preliminary SIMS Study Using Carbon Isotopes to Separate Natural from Synthetic Diamonds

Hao A. O. Wang, Laurent E. Cartier, Lukas P. Baumgartner, Anne-Sophie Bouvier, Florence Bégué, Jean-Pierre Chalain and Michael S. Krzemnicki

This preliminary study focuses on using secondary ion mass spectrometry (SIMS) to measure relative carbon isotope ratios for natural and synthetic diamonds (i.e. those grown by both chemical vapour deposition [CVD] and high-pressure, high-temperature [HPHT] techniques). The synthetic diamonds (of both CVD and HPHT origin) had significantly lower relative carbon isotope values than the natural diamonds. The lowest value was obtained for the CVD synthetic diamond sample, in agreement with results from other investigators. More research is desirable on the carbon isotope variation of synthetic diamonds.

The Journal of Gemmology, **36**(1), 2018, pp. 38–43, http://dx.doi.org/10.15506/JoG.2018.36.1.38

INTRODUCTION

Natural diamonds have been used in jewellery and for industrial purposes (e.g. abrasives) for centuries (Harlow, 1998). They constitute some of the most famous and valuable gems found worldwide. Diamonds form in the earth's mantle, and a number of different hypotheses for their specific geological formation continue to be discussed (Stachel and Harris, 2009; Stachel and Luth, 2015) and reviewed (Cartigny et al., 2014) in the literature. The chemical and physical properties of diamonds also are widely studied subjects (Clark et al., 1979; Shirey et al., 2013; Zaitsev, 2013).

However, openly available research on the identification and formation of synthetic diamonds is much scarcer. Synthetic diamonds were first produced in the 1950s in the USA and Sweden (Angus, 2002; Martineau et al., 2004). In recent years, advances in CVD and HPHT technology—the two methods used to synthesize diamonds—have made these synthetics much more widely available and of higher quality (Figure 1). The introduction of undisclosed synthetic diamonds into the market has become a critical issue for the diamond and jewellery industry at large (Even-Zohar, 2012; Kitawaki et al., 2013; Sheintal, 2015). Although various laboratory techniques involving spectroscopy (Fourier-transform infrared, ultraviolet-visible–near infrared and photoluminescence) and imaging (ultraviolet-wave UV and cathodoluminescence) can be used to distinguish natural from synthetic diamonds, further research is required to understand their formation mechanisms (Shigley et al., 1997; Wang et al., 2003).

Rapid developments in both CVD and HPHT technology require that research keep pace to ensure synthetic diamonds can be conclusively identified in the future, and to maintain consumer confidence in the diamond trade. Isotopic studies, such as those using SIMS instrumentation that are presented in this article, provide additional information for such efforts. Other studies that have applied SIMS to diamond research—for purposes of documenting chemical zoning and distinguishing different geological sources—include those by Hauri et al. (2002), Deines and Harris (2004), Cartigny (2005), Palot et al. (2012, 2014) and Stern et al. (2014). In addition,

Figure 1: Seven colourless and fancy-colour diamonds (weighing up to 3.03 ct) of various natural or synthetic origins are shown here. The top-right and bottom-left round brilliants are HPHT- and CVD-grown, respectively, and the other diamonds are natural. The confident separation of natural and synthetic diamonds is critical to maintaining consumer confidence in the trade. Composite photo by Luc Phan, SSEF.

Wang et al. (2014) used SIMS to investigate carbon isotopes in both natural and CVD synthetic diamonds. The current study includes HPHT synthetics along with CVD and natural samples.

SAMPLE SELECTION AND PREPARATION

Nine faceted samples were examined for this study: five natural diamonds, three colourless HPHT-grown synthetics and one colourless CVD synthetic diamond. The geological origin of the five natural diamonds and the exact manufacturing processes of the synthetic diamonds are not known. The samples were randomly chosen from different types of diamonds found in the market. Table I provides a summary of the samples.

Table I: Diamond samples analysed for this study.

Sample no.	Weight (ct)	Origin	Colour
1 (reference)	0.136	Natural	Brownish
2	0.088	Natural	Colourless
3	0.628	Natural	Grey
4	0.062	Natural	Green
5	0.028	Natural	Colourless
6	0.230	HPHT synthetic	Colourless
7	0.019	HPHT synthetic	Colourless
8	0.031	HPHT synthetic	Colourless
9	0.092	CVD synthetic	Colourless

To prepare them for analysis, the samples were pressed into indium metal in a sample holder. They were mounted with their table surface (or other large flat surface) facing upward. Last, the prepared holder was coated with gold before being inserted into the SIMS sample chamber.

METHODS

SIMS is an ion-beam microprobe technique used in surface analysis. The high sensitivity, high mass-resolving power and micrometre- to nanometre-scale spatial resolution of SIMS have made it a widely used technique in advanced materials research (Benninghoven et al., 1987; de Laeter, 2001). A primary ion beam is used to ionize elements on a sample's surface, thereby generating secondary ions that are analysed using a mass spectrometer. The SIMS method has a wide range of applications, including the analysis of carbon and nitrogen isotopes.

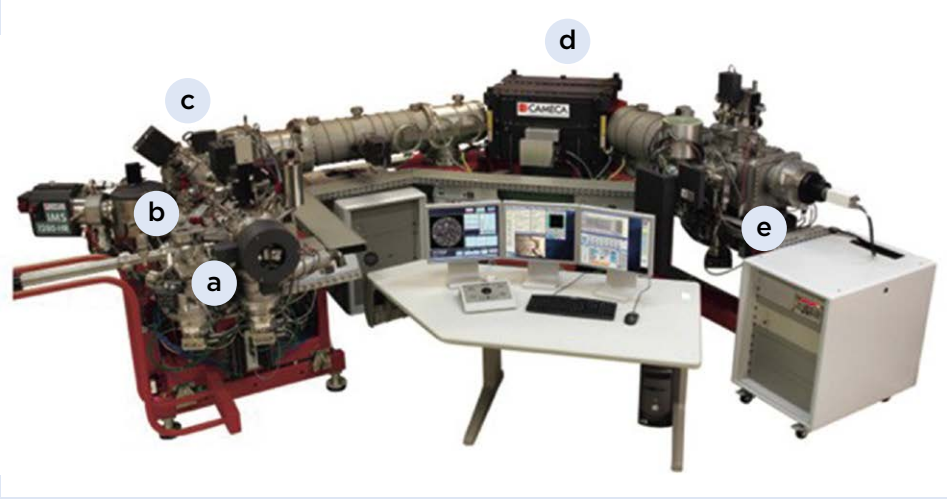

Figure 2: The SIMS instrument (Cameca IMS 1280-HR) at the SwissSIMS facility of the University of Lausanne consists of the following components: (a) sample chamber, (b) primary ion source, (c) electrostatic analyser, (d) magnet and (e) detection unit. Photo courtesy of SwissSIMS, University of Lausanne.

The carbon isotopes in our samples were measured using a Cameca IMS 1280-HR instrument (Figure 2) at the SwissSIMS facility of the Institute of Earth Sciences at the University of Lausanne, Switzerland (Seitz et al., 2017; Siron et al., 2017). We used a 10 kV Cs^+ primary beam and an ~0.6 nA current, resulting in an ~10 µm rastered beam size. An electron flood gun, with normal incidence, was used to compensate charges. We gathered $^{12}C^-$ and $^{13}C^-$ secondary ions, accelerated at 10 kV, in multi-collection mode using a Faraday cup (for $^{12}C^-$) and an electron multiplier (for $^{13}C^-$). A mass resolving power of ~6,000 was achieved, to overcome polyatomic interference of $^{13}C^-$ with $^{12}CH^-$, for example (Fitzsimons et al., 1999). The Faraday cup was calibrated at the beginning of the session. Each spot analysis took ~7 minutes, including pre-sputtering (60 seconds) and automated centring of secondary ions. The results of the analyses were expressed as the isotopic signature $\delta^{13}C$, which is a measure of the ratio of the isotopes $^{13}C/^{12}C$, reported in parts per thousand (per mil, ‰).

Since no standard reference diamond of known isotopic composition was available for this work, accurate $\delta^{13}C$ values were not obtainable. Nevertheless, the analyses were precise, and differences were meaningful. Natural diamond sample 1 was found to yield relatively homogeneous $^{13}C/^{12}C$ ratios (2σ = 0.21‰, 18 analyses). Therefore, for the purpose of qualitative analysis in this study, sample 1 was used as an external reference diamond to which the carbon isotope ratios for all other samples were normalized. For samples 2–9, four or five separate cluster locations on their surfaces were measured to address possible sample heterogeneity. At each cluster location, three SIMS analyses were carried out. The distance between these three replicates was much smaller compared to that between different cluster locations on a sample. After every six measurements of samples 2–9, two analyses were carried out on sample 1. Instrument drift over time was corrected in post-data evaluation using third-order polynomial fitting of the $^{13}C/^{12}C$ signal of sample 1. In addition, a homogeneity test was conducted on the surface of sample 2, in which two orthogonal directions across the table were scanned by lines of spots. Each SIMS analysis spot measured 10 µm in diameter and had a depth of less than a few hundred nanometres, which is not visible to the unaided eye. To remove the thin gold coating required for SIMS analysis, the samples were immersed in aqua regia that was heated to 40°C.

Ideally, $\delta^{15}N$ also would be a candidate to distinguish synthetic from natural diamonds. There are numerous studies investigating $\delta^{15}N$ in natural diamonds (Cartigny et al., 2001; Cartigny, 2005; Hogberg et al., 2016). However, the nitrogen concentrations in the synthetic samples randomly selected for this study were below the detection limit of the SIMS instrument. Natural type II diamonds also contain amounts of nitrogen that cannot be detected by SIMS. Therefore, using nitrogen isotope ratios to determine natural or synthetic origin is not applicable to general cases and was not pursued in this study.

The present research thus focused on using SIMS to determine normalized carbon isotope ratios, which could be measured on a relative basis without the use of a standard. To obtain quantitative data, it would be imperative to have bulk $\delta^{13}C$ results on a reference sample. This was not pursued in the context of this preliminary study, as the aim was to investigate only the possible separation of natural from synthetic diamonds.

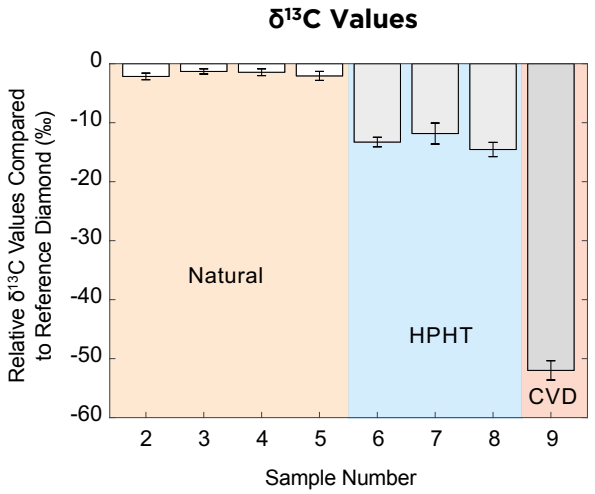

Figure 3: Relative $\delta^{13}C$ values are presented here for the four natural diamonds and the four of synthetic (HPHT and CVD) diamonds.

RESULTS

A summary of the carbon isotopic values is shown in Figure 3. Relative $\delta^{13}C$ for the four measured natural diamonds (samples 2–5) varied from –2.16 ± 0.56‰ (2σ) to –1.31 ± 0.43‰ (2σ). The three HPHT synthetic diamonds (samples 6–8) had lower relative $\delta^{13}C$ values ranging between –14.55 ± 1.21‰ (2σ) and –11.84 ± 1.78‰ (2σ). The CVD synthetic diamond (sample 9) had the lowest relative $\delta^{13}C$ value of –51.99 ± 1.63‰ (2σ), which is consistent with the work of Wang et al. (2014), who found that there was no overlap of $\delta^{13}C$ values for the natural and CVD synthetic diamonds they analysed. The low $^{13}C/^{12}C$ ratio for the CVD synthetic diamond might be explained by the ^{13}C-depleted methane used as a synthetic precursor to obtain good crystal quality and a flat surface on the CVD plates (Fiori et al., 2013). For HPHT-grown synthetic diamonds, the carbon source is different (commonly graphite), and fractionation in these crystals was investigated in detail by Reutsky et al. (2008). According to Cartigny (2005), there are three commonly hypothesized explanations for the different $\delta^{13}C$ values found in natural diamonds: (1) distinct carbon sources (i.e. different geological origins), (2) primordial isotopic variability and (3) fractionation of stable isotopes at mantle temperatures.

For the purpose of evaluating synthetic vs. natural origin, we observed no significant differences in relative carbon isotope ratios in the different areas analysed on the surfaces of the individual samples (both natural and synthetic). Nevertheless, other studies have shown that growth orientation and sectorization in natural and synthetic diamonds can have an influence on $\delta^{13}C$ and $\delta^{15}N$ ratios (Boyd et al., 1992; Bulanova et al., 2002, Reutsky et al., 2008; Fiori et al., 2013). Figure 4 shows the minor variability of relative $\delta^{13}C$ values in both of the line scans across the table facet of sample 2.

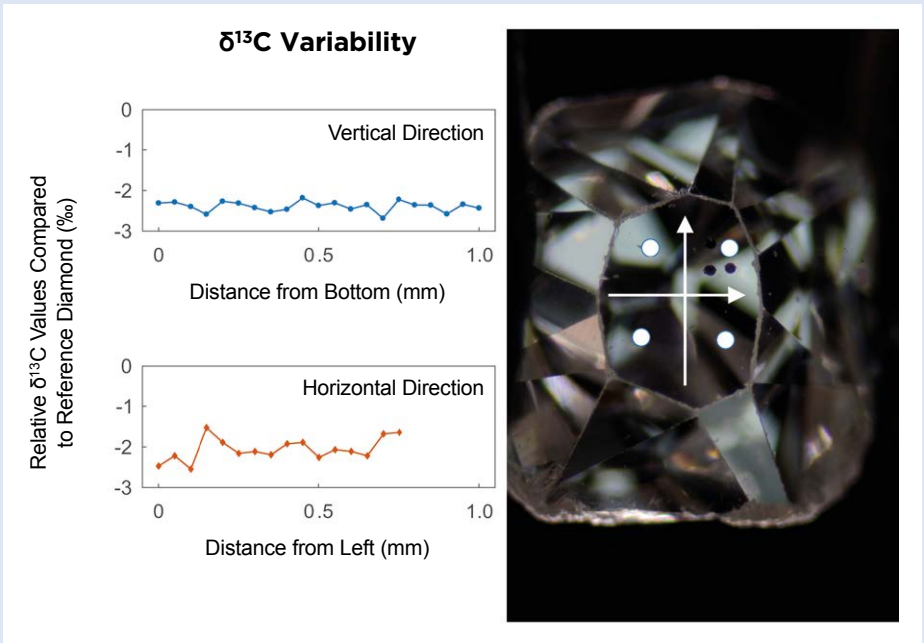

Figure 4: Sample 2, a colourless old-mine cut natural diamond of 0.088 ct (2.53 × 2.35 × 2.13 mm), exhibits only minor variability of relative $\delta^{13}C$ values in both directions across the surface of the table facet. The four white spots indicate cluster locations (three data points each) of SIMS analyses, and the arrows show the locations of the SIMS analytical traverses. Near the top-right cluster are three black spots resulting from laser ablation inductively coupled plasma mass spectrometry (performed for a separate study). Photo by SSEF.

CONCLUSIONS

Among the samples analysed in this SIMS study, the synthetic diamonds had distinctly lower relative $^{13}C/^{12}C$ values than the randomly selected natural samples. The data also showed that HPHT and CVD synthetic diamonds potentially can be distinguished from one another on the basis of their relative carbon-isotope ratios. More research is required to understand $\delta^{13}C$ variability and fractionation in synthetic diamonds. In addition, this preliminary study has shown the need for a carbon-isotope standard to obtain quantitative data for comparison with other diamond carbon-isotope studies. Future research using the SIMS technique will continue to provide a deeper understanding of diamond growth, and as such is complementary to other methods being used to separate natural from synthetic diamonds.

REFERENCES

Angus J.C., 2002. A short history of diamond synthesis. In J. Asmussen and D.K. Reinhard, Eds., *Diamond Films Handbook*, Marcel Dekker Inc., New York, New York, USA, 14–22.

Benninghoven A., Rudenauer F.G. and Werner H.W., 1987. *Secondary Ion Mass Spectrometry: Basic Concepts, Instrumental Aspects, Applications and Trends.* Wiley-Interscience, New York, New York, USA, 1,264 pp.

Boyd S.R., Pillinger C.T., Milledge H.J., Mendelssohn M.J. and Seal M., 1992. C and N isotopic composition and the infrared absorption spectra of coated diamonds: Evidence for the regional uniformity of CO_2–H_2O rich fluids in lithospheric mantle. *Earth and Planetary Science Letters*, **109**(3–4), 633–644, http://dx.doi.org/10.1016/0012-821x(92)90121-b.

Bulanova G.P., Pearson D.G., Hauri E.H. and Griffin B.J., 2002. Carbon and nitrogen isotope systematics within a sector-growth diamond from the Mir kimberlite, Yakutia. *Chemical Geology*, **188**(1–2), 105–123, http://dx.doi.org/10.1016/s0009-2541(02)00075-x.

Cartigny P., 2005. Stable isotopes and the origin of diamond. *Elements*, **1**(2), 79–84, http://dx.doi.org/10.2113/gselements.1.2.79.

Cartigny P., Harris J.W. and Javoy M., 2001. Diamond genesis, mantle fractionations and mantle nitrogen content: A study of $\delta^{13}C$–N concentrations in diamonds. *Earth and Planetary Science Letters*, **185**(1–2), 85–98, http://dx.doi.org/10.1016/s0012-821x(00)00357-5.

Cartigny P., Palot M., Thomassot E. and Harris J.W., 2014. Diamond formation: A stable isotope perspective. *Annual Review of Earth and Planetary Sciences*, **42**(1), 699–732, http://dx.doi.org/10.1146/annurev-earth-042711-105259.

Clark C.D., Mitchell E.W. and Parsons B.J., 1979. Colour centres and optical properties. In J.E. Field, Ed., *The Properties of Diamond*, Academic Press, London, 23–77.

de Laeter J.R., 2001. *Applications of Inorganic Mass Spectrometry*. John Wiley & Sons Inc., New York, New York, USA, 474 pp.

Deines P. and Harris J.W., 2004. New insights into the occurrence of ^{13}C-depleted carbon in the mantle from two closely associated kimberlites: Letlhakane and Orapa, Botswana. *Lithos*, **77**(1–4), 125–142, http://dx.doi.org/10.1016/j.lithos.2004.04.015.

Even-Zohar C., 2012. Synthetics specifically 'made to defraud'. *Diamond Intelligence Briefs*, **27**(709), 7281–7290.

Fiori A., Jomard F., Teraji T., Koizumi S., Isoya J., Gheeraert E. and Bustarret E., 2013. Synchronized B and ^{13}C diamond delta structures for an ultimate in-depth chemical characterization. *Applied Physics Express*, **6**(4), article 045801, 4 pp., http://dx.doi.org/10.7567/apex.6.045801.

Fitzsimons I.C.W., Harte B., Chinn I.L., Gurney J.J. and Taylor W.R., 1999. Extreme chemical variation in complex diamonds from George Creek, Colorado: A SIMS study of carbon isotope composition and nitrogen abundance. *Mineralogical Magazine*, **63**(6), 857–878, http://dx.doi.org/10.1180/002646199548970.

Harlow G.E., Ed. 1998. *The Nature of Diamonds*. Cambridge University Press, Cambridge, 278 pp.

Hauri E., Wang J., Pearson D.G. and Bulanova G.P., 2002. Microanalysis of $\delta^{13}C$, $\delta^{15}N$, and N abundances in diamonds by secondary ion mass spectrometry. *Chemical Geology*, **185**(1–2), 149–163, http://dx.doi.org/10.1016/s0009-2541(01)00400-4.

Hogberg K., Stachel T. and Stern R.A., 2016. Carbon and nitrogen isotope systematics in diamond: Different sensitivities to isotopic fractionation or a decoupled origin? *Lithos*, **265**, 16–30, http://dx.doi.org/10.1016/j.lithos.2016.06.020.

Kitawaki H., Yamamoto M., Hisanaga M., Okano M. and Emori K., 2013. Gem News International: Undisclosed samples of large CVD synthetic diamond. *Gems & Gemology*, **49**(1), 60–61.

Martineau P.M., Lawson S.C., Taylor A.J., Quinn S.J., Evans D.J.F. and Crowder M.J., 2004. Identification

of synthetic diamond grown using chemical vapor deposition (CVD). *Gems & Gemology*, **40**(1), 2–25, http://dx.doi.org/10.5741/gems.40.1.2.

Palot M., Cartigny P., Harris J.W., Kaminsky F.V. and Stachel T., 2012. Evidence for deep mantle convection and primordial heterogeneity from nitrogen and carbon stable isotopes in diamond. *Earth and Planetary Science Letters*, **357–358**, 179–193, http://dx.doi.org/10.1016/j.epsl.2012.09.015.

Palot M., Pearson D.G., Stern R.A., Stachel T. and Harris J.W., 2014. Isotopic constraints on the nature and circulation of deep mantle C–H–O–N fluids: Carbon and nitrogen systematics within ultra-deep diamonds from Kankan (Guinea). *Geochimica et Cosmochimica Acta*, **139**, 26–46, http://dx.doi.org/10.1016/j.gca.2014.04.027.

Reutsky V.N., Borzdov Y.M. and Palyanov Y.N., 2008. Carbon isotope fractionation associated with HPHT crystallization of diamond. *Diamond and Related Materials*, **17**(11), 1986–1989, http://dx.doi.org/10.1016/j.diamond.2008.06.003.

Seitz S., Baumgartner L.P., Bouvier A.-S., Putlitz B. and Vennemann T., 2017. Quartz reference materials for oxygen isotope analysis by SIMS. *Geostandards and Geoanalytical Research*, **41**(1), 69–75, http://dx.doi.org/10.1111/ggr.12133.

Sheintal U., 2015. CIBJO Diamond Commission Special Report: Threat of Synthetics and Corrupting of Diamond Grading Continues to Trouble International Diamond Sector. CIBJO, The World Jewellery Confederation, 4 pp., http://congress2015.cibjo.org/CIBJO%20Special%20Report%202015%20(Diamond).pdf.

Shigley J.E., Moses T.M., Reinitz I., Elen S., McClure S.F. and Fritsch E., 1997. Gemological properties of near-colorless synthetic diamonds. *Gems & Gemology*, **33**(1), 42–53, http://dx.doi.org/10.5741/gems.33.1.42.

Shirey S.B., Cartigny P., Frost D.J., Keshav S., Nestola F., Nimis P., Pearson D.G., Sobolev N.V. and Walter M.J., 2013. Diamonds and the geology of mantle carbon. *Reviews in Mineralogy and Geochemistry*, **75**, 355–421, http://dx.doi.org/10.2138/rmg.2013.75.12.

Siron G., Baumgartner L., Bouvier A.-S., Putlitz B. and Vennemann T., 2017. Biotite reference materials for secondary ion mass spectrometry $^{18}O/^{16}O$ measurements. *Geostandards and Geoanalytical Research*, **41**(2), 243–253, http://dx.doi.org/10.1111/ggr.12148.

Stachel T. and Harris J.W., 2009. Formation of diamond in the earth's mantle. *Journal of Physics: Condensed Matter*, **21**(36), article 364206, 10 pp., http://dx.doi.org/10.1088/0953-8984/21/36/364206.

Stachel T. and Luth R.W., 2015. Diamond formation — Where, when and how? *Lithos*, **220–223**, 200–220, http://dx.doi.org/10.1016/j.lithos.2015.01.028.

Stern R.A., Stachel T., Pearson G., Palot M., Cartigny P., Howell D. and Oh A., 2014. *Methods and Reference Materials for SIMS Diamond C- and N-Isotope Analysis*. CCIM Research Report 14-01, Canadian Centre for Isotopic Microanalysis, Department of Earth and Atmospheric Sciences, University of Alberta, Canada, 87 pp.

Wang W., Moses T., Linares R.C., Shigley J.E., Hall M. and Butler J.E., 2003. Gem-quality synthetic diamonds grown by a chemical vapor deposition (CVD) method. *Gems & Gemology*, **39**(4), 268–283, http://dx.doi.org/10.5741/gems.39.4.268.

Wang W., D'Haenens-Johansson U., Smit K., Breeding C.M. and Stern R., 2014. Carbon isotope analysis of CVD synthetic diamonds. *Geological Society of America Abstracts with Programs*, **46**(6), 268.

Zaitsev A.M., 2001. *Optical Properties of Diamond: A Data Handbook*. Springer-Verlag, Berlin and Heidelberg, Germany, 502 pp., http://dx.doi.org/10.1007/978-3-662-04548-0.

The Authors

Dr Hao A. O. Wang[1]
Dr Laurent E. Cartier FGA[1,2]
Prof. Dr Lukas P. Baumgartner[2]
Dr Anne-Sophie Bouvier[2]
Dr Florence Bégué[2]
Jean-Pierre Chalain[1]
Dr Michael S. Krzemnicki FGA[1]

[1] Swiss Gemmological Institute SSEF, Aeschengraben 26, 4051 Basel, Switzerland
Email: gemlab@ssef.ch

[2] Institute of Earth Sciences, SwissSIMS, University of Lausanne, 1015 Lausanne, Switzerland

Figure 1: Rainbow lattice sunstone displays conspicuous colourful patterns that are produced by light reflecting at a specific angle from inclusions. The gold ring on the left contains a 6.17 ct sunstone and the polished fragment on the right weighs 15.00 ct. Courtesy of Rainbow Lattice; photo by Jeff Scovil.

Revisiting Rainbow Lattice Sunstone from the Harts Range, Australia

Jia Liu, Andy H. Shen, Zhiqing Zhang, Chengsi Wang and Tian Shao

Rainbow lattice sunstone from the Harts Range, Northern Territory, Australia, shows a rare combination of phenomena including aventurescence, adularescence and a distinctive lattice pattern caused by oriented inclusions. Electron microprobe and X-ray diffraction (XRD) analysis, combined with laser Raman spectroscopy, indicate the host mineral is orthoclase ($Or_{96}Ab_4$), as previously reported in the literature. The inclusions causing the aventurescence were identified as hematite, while lattice patterns were found to consist of orangey brown platelets of hematite and black platelets of magnetite (rather than ilmenite, as previously reported). Scanning electron microscopy-energy dispersive spectroscopy (SEM-EDS) analysis of the magnetite showed that it is composed of very thin plates containing only Fe and O, without any Ti. The presence of magnetite is consistent with the black inclusions' attraction to a magnet, as well as testing with a vibrating sample magnetometer, which provided a ferromagnetic response.

The Journal of Gemmology, **36**(1), 2018, pp. 44–52, http://dx.doi.org/10.15506/JoG.2018.36.1.44

INTRODUCTION

Feldspar-group minerals are framework aluminosilicates (among the most common rock-forming minerals) that contain variable amounts of Na, K and Ca. Isomorphic substitution in feldspars is well developed, resulting in two solid-solution series: alkali feldspar (orthoclase–albite) and plagioclase (albite–anorthite). These can form an array of gem varieties—including sunstone, moonstone, etc.—which can differ widely in appearance.

In the gem trade, *sunstone* typically refers to aventurescent feldspar, and is known from various localities, mainly Tanzania and India (i.e. oligoclase with hematite inclusions) and Oregon, USA (i.e. labradorite with copper inclusions), although other occurrences have been reported (O'Donoghue, 2006). Viewed with pinpoint lighting from certain directions, sunstone exhibits a spangled appearance with interesting optical and physical properties that can include not only aventurescence, but also various body colours and strong pleochroism (Johnston et al., 1991; Choudhary and Huang, 2008). Aventurescence in sunstone typically arises from thin, platy hematite inclusions (Akizuki, 1976).

A rare gem feldspar known as *rainbow lattice sunstone* (e.g. Figures 1 and 2) exhibits both aventurescence (as seen in sunstone) and adularescence (as displayed by moonstone), with the added presence of oriented elongate and triangular mineral platelets. The material was discovered in the mid-1980s and was briefly described as a new gem variety by Koivula and Kammerling (1989). Since it has not been characterized in detail, the present authors examined this sunstone using microscopy, electron microprobe and XRD analysis, magnetic measurements, and SEM-EDS and Raman spectroscopy. We confirmed some of the results of previous studies but also report some unexpected new findings.

LOCATION AND GEOLOGY

Rainbow lattice sunstone is found in a localized remote area of desert named the Mud Tank Zircon Field (Faulkner and Shigley, 1989) in the Harts Range north-east of Alice Springs, Northern Territory, Australia. This area is comprised of dry plains with rocky outcrops. The sunstone was first discovered in late 1985 by Darren Arthur and Sonny Mason, who happened upon it while scouting the area near an abandoned mica mine. The mineralized area measures 500 × 600 m and is covered by a single mining claim. (Another rainbow lattice sunstone occurrence is located ~7 km away, but produces lower-quality material.) The sunstone is mined by Asterism Gems Australia Pty Ltd and marketed through Rainbow Lattice (www.rainbowlattice.com). Miners gather the rough material using only hand tools. The stones are then washed and sorted to separate the occasional pieces of rainbow lattice sunstone from the non-phenomenal feldspar. Over the years only a few kilograms of good-quality rough material has been produced, and the sunstone is sold as both partially polished rough pieces and cabochons. Some is stabilized with resin to make it saleable, and it also may be waxed or oiled as per standard processes used in the gem trade.

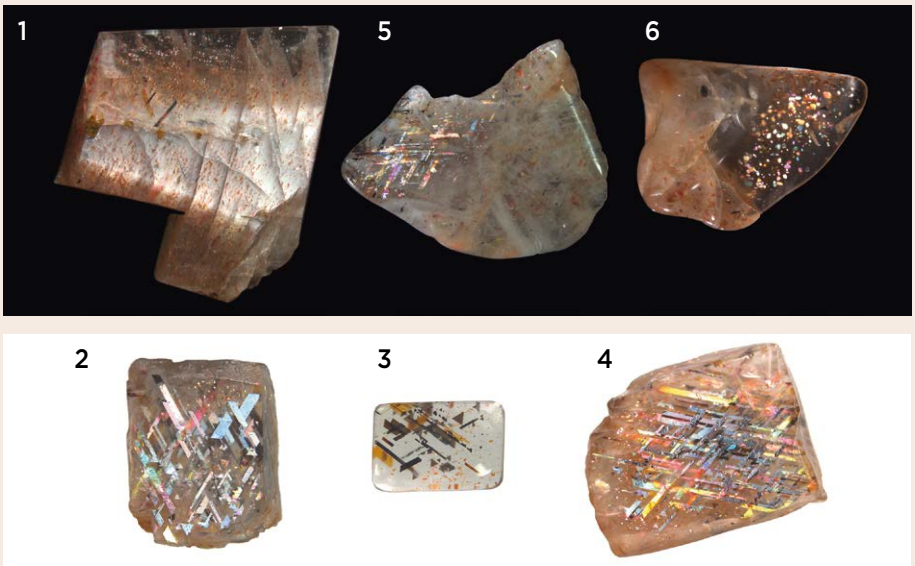

Figure 2: The six samples of rainbow lattice sunstone obtained for this study display a combination of optical effects, including adularescence (e.g. sample 1), aventurescence (see samples 1 and 6, in particular) and a rainbow lattice effect, which can be seen using different lighting conditions and directions. The samples weigh 0.29–3.57 g. Composite photos by J. Liu.

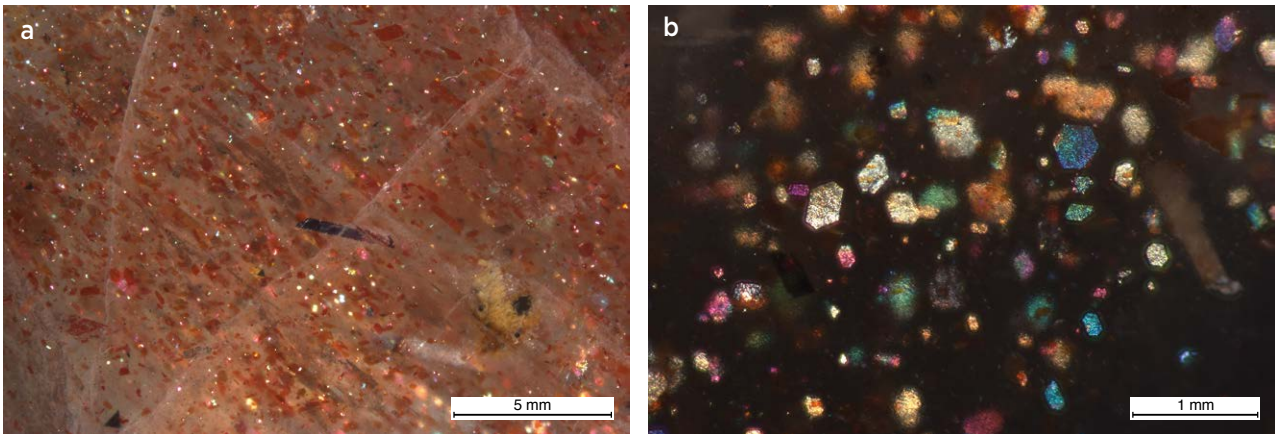

Figure 3: The aventurescence phenomenon in the sunstone is produced by pseudohexagonal reddish brown platelets of hematite (a) that exhibit a sparkling appearance with diverse colours in reflected light (b). The images are taken from sample 1 (a) and sample 6 (b). Photomicrographs by J. Liu.

The Harts Range comprises a complex assemblage of granite gneiss, marble, calc-silicate, amphibolite, psammite and pelite that have been metamorphosed to upper amphibolite to granulite facies (Huston et al., 2006). The metamorphosed sedimentary rocks are intruded mainly by granite, granodiorite and metamorphosed mafic rocks of uncertain origin. The igneous rocks are generally associated with widespread metasomatic granitization (Joklik, 1955; Daly and Dyson, 1956). The granodiorite in the Bruna gneiss unit contains pegmatites in which K-feldspar occurs, and the mining area is crosscut by quartz veins and pegmatite outcrops.

MATERIALS AND METHODS

Six study samples of rainbow lattice sunstone from the Harts Range were obtained at the 2017 gem shows in Tucson, Arizona, USA (Figure 2). From these, we chose two representative specimens (samples 1 and 2) for detailed examination.

Photomicrographs of all six samples were taken with a Leica M205A microscope at the Gemological Institute, China University of Geosciences (Wuhan). Refractive indices of all samples were measured with a refractometer, and specific gravity was determined hydrostatically.

Quantitative chemical analysis of the host feldspar was performed at the Earth Sciences Institute at China University of Geosciences (Wuhan) with a JEOL JXA-8230 electron microprobe operating with an accelerating voltage of 15 keV and a beam diameter of 3 µm. Structural analysis of the host feldspar was performed at the Gemological Institute, China University of Geosciences (Wuhan), with a Bruker AXS D8 Focus X-ray diffractometer equipped with a LynxEye X-ray detector (Cu$K\alpha$ X-ray source, Ni filter, accelerating voltage of 40 kV, current of 40 mA, scanning range of 15–90° and λ = 1.540598 Å).

SEM-EDS compositional data for a black lattice-forming inclusion in one of the sunstones were collected using an Oxford Instruments X-Max^N energy-dispersive spectroscopic system on a Zeiss Sigma 300 field emission scanning electron microscope in the State Key Laboratory of Geological Processes and Mineral Resources of China University of Geosciences (Wuhan), using a magnification of 284×, working distance of 8.5 mm, accelerating voltage of 20 kV and aperture size of 120 µm. The magnetic properties of the black inclusions were tested with a Lake Shore Cryotronics 7400 Series vibrating sample magnetometer (VSM) at the School of Materials Sciences and Engineering, Northeastern University, Shenyang, China.

Raman spectroscopy of the feldspar and the inclusions in all six samples was performed with a Bruker Senterra R200-L Raman spectrometer (laser wavelength 532 nm, resolution ~3–5 cm^{-1}, spectral range 45–3600 cm^{-1}, integration time 5 s, aperture 50 × 1000 µm, laser power 20 mW and 20 × objective lens). The inclusions were analysed with a lower laser power (5 mW) and a higher magnification (100 ×) in order to prevent phase transition from the laser's energy.

RESULTS AND DISCUSSION

Gemmological Properties

Observed with magnification, the typical aventurescence of the sunstone can be seen in Figure 3. The scattered reddish brown platelets showed pseudohexagonal and rhomb-shaped morphology. As illustrated in Figure 4, the lattice-forming inclusions in

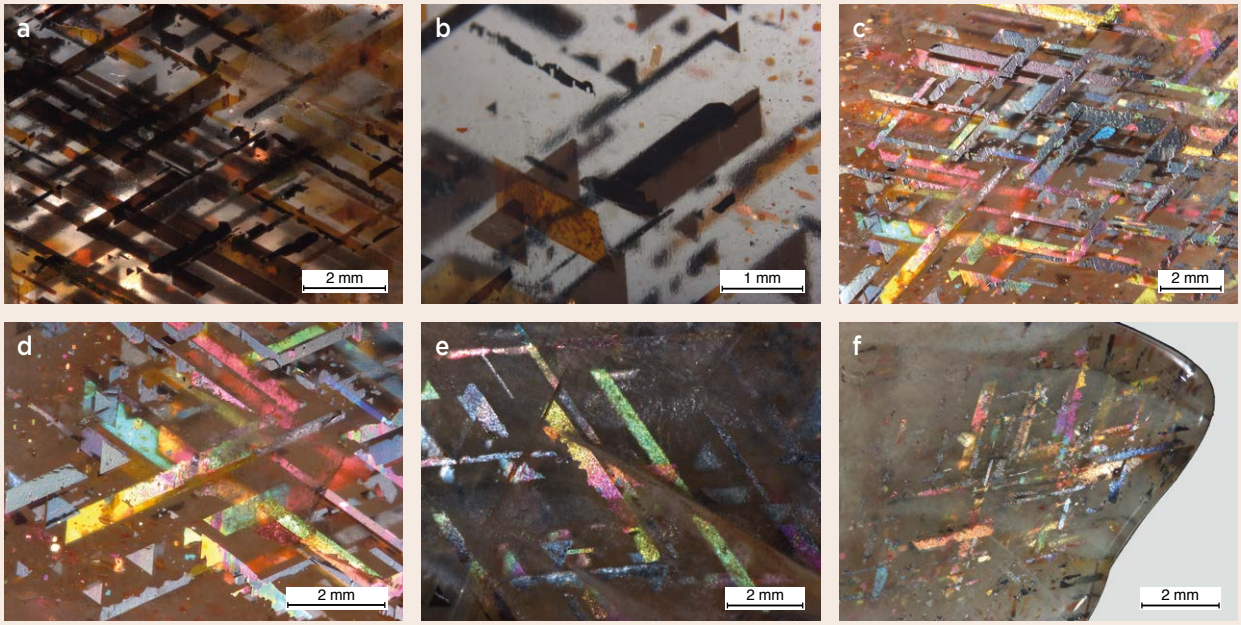

Figure 4: The black to orangey brown, platy, elongate and triangular inclusions that produce the rainbow lattice effect are shown in both transmitted (a, b) and reflected (c–f) light. The specimens include the following: sample 3 (b), sample 4 (a, c, d) and sample 5 (e, f). Photomicrographs by J. Liu.

the sunstone consisted of orangey brown to black elongate and triangular plates. The orangey brown ones displayed colourful reflections when viewed with oblique pinpoint lighting. Some of the samples displayed obvious adularescence when observed using various incident light angles (Figure 5).

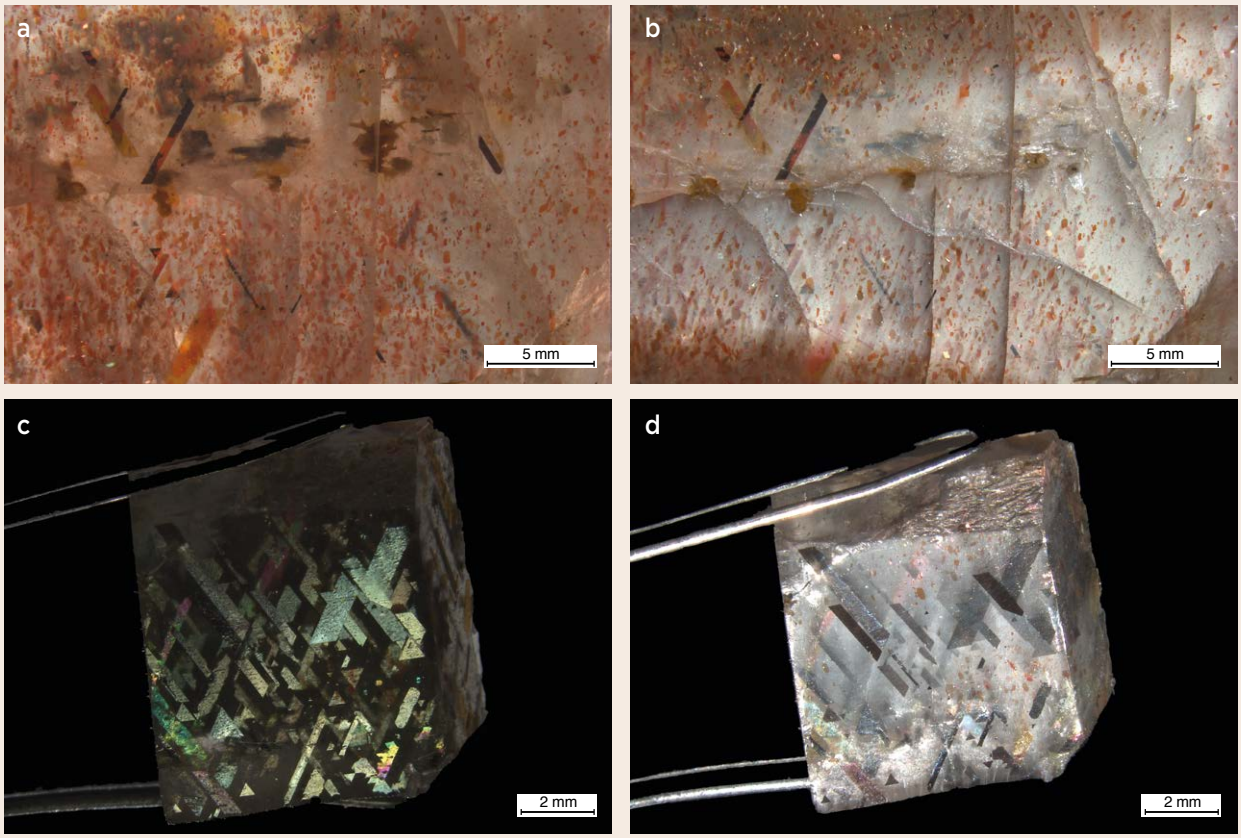

Figure 5: Rainbow lattice sunstone sample 1 displays abundant reddish brown hematite inclusions and also shows obvious adularescence when viewed with the lighting positioned at certain angles (a, b). Sample 2 reveals adularescence upon a slight tilting of the specimen with respect to the incident light (c, d). Photos by J. Liu.

Table I: Electron microprobe analyses of orthoclase constituting rainbow lattice sunstone samples 1 and 2.

Analysis no.	1	2	3	4	5
Oxides (wt.%)					
SiO_2	65.26	65.90	65.85	65.80	65.95
TiO_2	nd*	0.02	nd	nd	0.02
Al_2O_3	18.79	18.94	18.82	18.87	18.76
FeO	nd	0.02	nd	0.09	0.06
MnO	0.01	nd	nd	nd	0.02
MgO	nd	0.01	nd	nd	nd
CaO	0.10	0.05	0.09	0.03	0.04
Na_2O	0.64	0.65	0.66	0.68	0.59
K_2O	15.37	15.54	15.32	15.55	15.84
Total	100.17	101.13	100.74	101.02	101.28
Ions on the basis of 8 oxygens					
Si	2.605	2.607	2.614	2.605	2.604
Al	1.000	0.999	0.996	0.996	0.988
Ti	nd	0.001	nd	nd	0.001
Fe	nd	0.002	nd	0.007	0.005
Mn	0.001	nd	nd	nd	0.002
Mg	nd	0.001	nd	nd	nd
Ca	0.008	0.004	0.007	0.002	0.003
Na	0.102	0.103	0.105	0.108	0.093
K	2.455	2.459	2.433	2.463	2.502
Mol.% end members					
Or	95.70	95.84	95.60	95.72	96.29
Ab	3.99	4.01	4.12	4.19	3.59
An	0.31	0.15	0.28	0.09	0.12

* Abbreviation: nd = not detected.

Gemmological testing of the rainbow lattice sunstone revealed average RIs of 1.518 to 1.540, and an SG of 2.58, which are consistent with those of orthoclase (cf. RIs of 1.518–1.536 and SG values of 2.54–2.61; Lazarelli, 2010).

Chemical Composition, XRD Analysis and Magnetic Testing

Composition of the Host Feldspar. The quantitative chemical compositions and end-member components of the host feldspar are given in Table I. Our analyses showed 96% orthoclase and 4% albite.

Rochow (1962) reported the feldspar in the Harts Range as being microcline that has the same composition as the orthoclase. XRD analysis of the rainbow lattice sunstone (Figure 6) yielded a pattern that matched orthoclase in the Powder Diffraction File (PDF2 database, sample 00-019-0931).

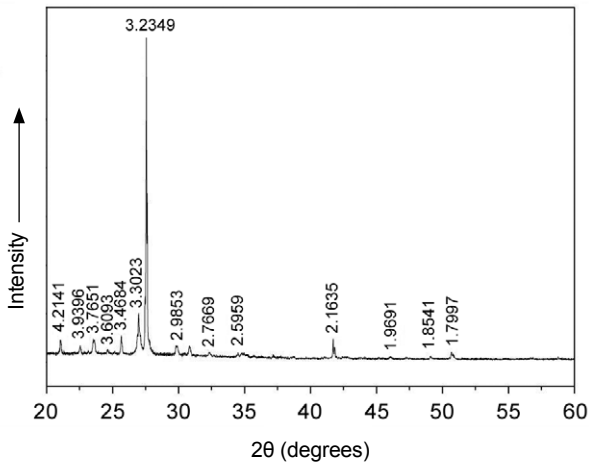

Figure 6: The XRD pattern of the host feldspar identified it as orthoclase rather than microcline. The diffraction peaks are labelled with the corresponding d-spacings (in angstroms).

Most gem feldspar that displays aventurescence is oligoclase (sodic plagioclase), although the effect is sometimes seen in orthoclase (K-feldspar). Hence two kinds of this gem material can be distinguished: 'oligoclase sunstone' and 'orthoclase sunstone' (Choudhary and Huang, 2008; Freeman et al., 2008). Rainbow lattice sunstone is of the latter variety.

Composition of the Black Lattice-Forming Inclusions. The black platy, elongate or triangular inclusions consisted of thin sheets with nanometre-scale thickness (Figure 7). Observations made with the SEM after the samples had been ground and polished showed that the inclusions were very brittle and easily removed by mechanical force. Qualitative SEM-EDS analysis revealed that these inclusions contained Fe and O. Although a previous report (Koivula and Kammerling, 1989) mentioned the black inclusions were ilmenite, no Ti was detected in the present study.

Suspecting that these inclusions were magnetite, we performed a simple magnet test on the sunstone, but this proved challenging because of the minute volume of the black platelets relative to the feldspar. Directly using a magnet to test the bulk sample did not show any magnetic behaviour. However, we found that a tiny fragment of the sunstone containing only one black inclusion was strongly attracted to a Nd-Fe-B magnet (Figure 8). This simple test proved

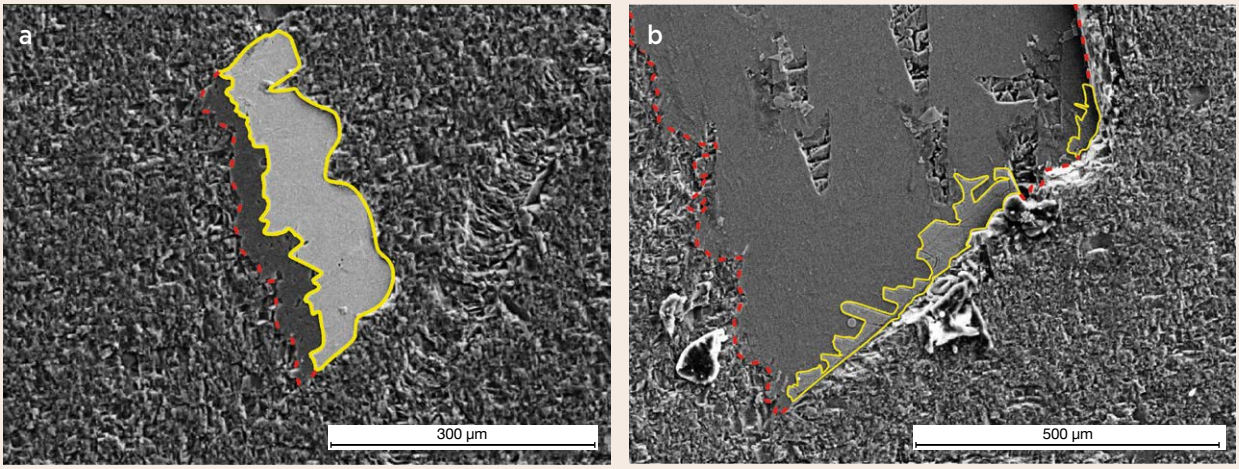

Figure 7: These SEM images of the black inclusions of magnetite in rainbow lattice feldspar reveal the brittle nature that resulted in their being partially removed by the grinding and polishing process used to prepare the samples. The yellow line designates the remaining areas of magnetite, while the dashed red lines show the inferred outline of the original platelets. Images by J. Liu.

that the black inclusion consisted of an oxide of iron that possessed strong magnetism.

Further VSM testing of the fragment mentioned above yielded a magnetic hysteresis loop (Figure 9) that showed the closed magnetization curve of a ferromagnetic substance with the hysteresis phenomenon. The hysteresis loop is an important feature of ferromagnetism; paramagnetic and diamagnetic substances do not show this phenomenon. The presence of magnetite

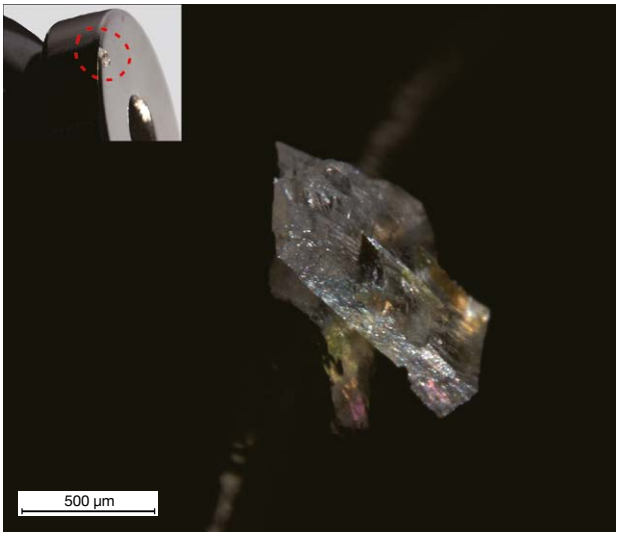

Figure 8: Magnetic testing of the black inclusions in the rainbow lattice sunstone was performed by placing this tiny piece of feldspar containing a single black platelet next to a Nd-Fe-B magnet. It was readily attracted to the magnet, as shown in the inset. Photomicrographs by J. Liu.

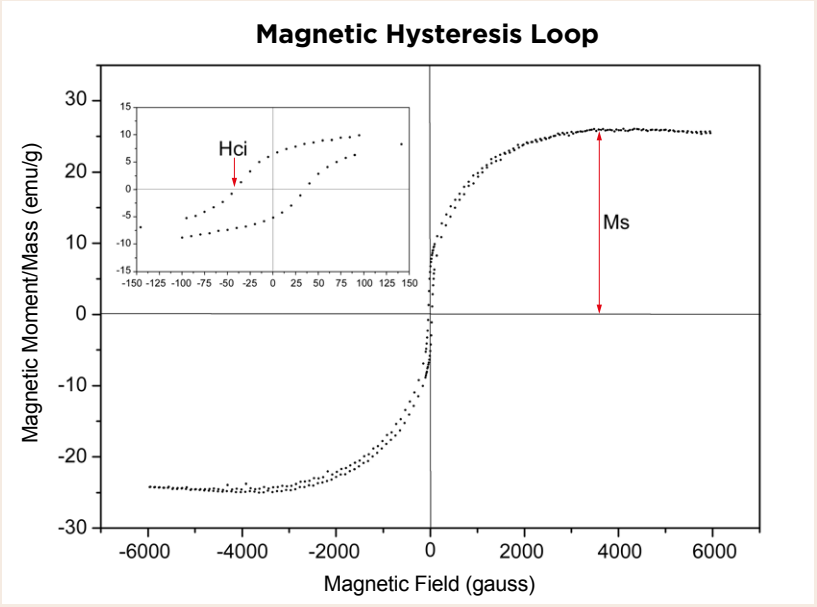

Figure 9: The magnetic hysteresis loop obtained with VSM analysis of the tiny feldspar fragment with a black inclusion in Figure 8 shows a coercivity (Hci) of 38.348 gauss and a mass magnetization (Ms) of 25.527 × 10^{-3} electromagnetic units/gram.

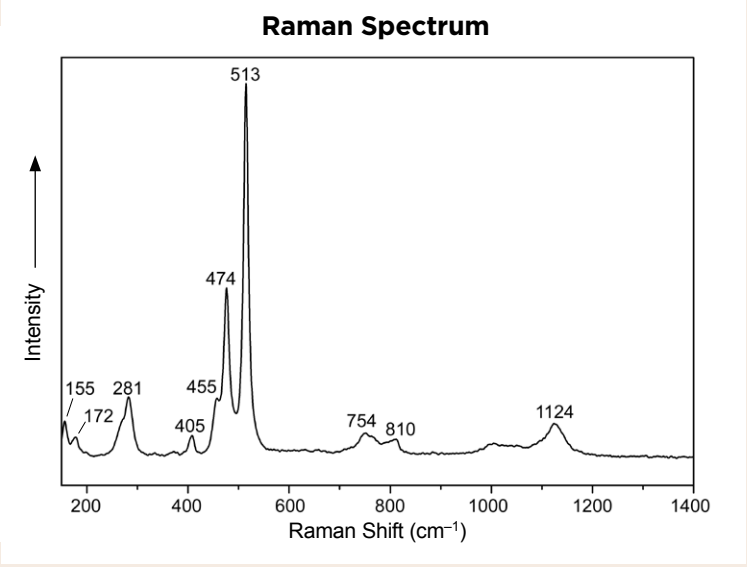

Figure 10: This representative Raman spectrum of the host feldspar shows peaks at 455, 474 and 513 cm^{-1} that prove its identity as orthoclase.

as the ferromagnetic material is consistent with the SEM-EDS analysis. The total mass of the fragment was 0.0254 g, the coercivity was 38.348 gauss and the mass magnetization (magnetic saturation state) was 25.527 × 10^{-3} electromagnetic units/gram. The low saturation of the magnetization is due to the trace amount of magnetite present in the fragment.

Raman Spectroscopy

Raman analysis of the feldspar (Figure 10) showed the strongest bands in the 450–520 cm^{-1} spectral region (455, 474 and 513 cm^{-1}) belonging to the vibrational modes of the four-membered rings of tetrahedra. The Raman peaks below 400 cm^{-1} (155, 172 and 281 cm^{-1}) corresponded to rotation-translation modes of the four-membered rings and cage-shear modes. The weaker Raman peaks in the 900–1200 cm^{-1} region (e.g. 1124 cm^{-1}) were assigned to the vibrational stretching modes of the tetrahedron. The moderate-to-weak peaks in the 700–900 cm^{-1} region (754 and 810 cm^{-1}) belonged to the deformation modes of the tetrahedron (McKeown, 2005). All of the Raman shifts provided a good fit with orthoclase.

The main Raman shifts (Figure 11) of the reddish brown platelets causing the aventurescence and the orangey brown lattice-forming inclusions were 226, 245, 297, 411, 500, 612 and 1319 cm^{-1}, which match hematite. The peaks at 226 and 500 cm^{-1} correspond to A_{1g} vibration modes, while the 245, 297 and 411 cm^{-1} features belong to E_g modes (León et al., 2004). The presence of the 655 cm^{-1} peak indicates an imperfect hematite crystal, and is called a 'disorder band' (Bersani et al., 1999). The 1319 cm^{-1} feature is assigned to a second harmonic vibration (Zoppi et al., 2005).

The main Raman shifts (Figure 12) of the black lattice-forming inclusions were 303, 538 and 664 cm^{-1}, which fit nicely with magnetite. The feature at 538 cm^{-1} is the T_{2g} symmetry mode, while the peaks at 303 and 664 cm^{-1} belong to the E_g and A_{1g} vibration modes (Shebanova and Lazor, 2003a,b). Combined with the SEM-EDS and VSM results, this confirmed that the black inclusions were magnetite.

Inclusions Producing the Aventurescence and Rainbow Lattice Effects

Sunstone inclusions may be composed of hematite, ilmenite, magnetite, native copper or goethite (Andersen, 1915; Sobolev, 1990). The appearance of the aventurescence phenomenon depends on the size of the inclusions. Small particles produce a reddish or golden sheen, while larger inclusions create an attractive, glittery appearance.

According to our study, the lattice appearance displayed by rainbow lattice sunstone is created by inclusions of hematite and magnetite. These minerals form very thin blades that occur within planes of a single orientation at different levels in the feldspar (like pages in a book). Platelets of hematite also produce aventurescence. Viewed with reflected light, the aventurescence is illuminated from one direction, while the colourful lattice effect appears when the lighting is shifted to a different angle.

The magnetite and hematite predominantly form triangular shapes or elongate blades with terminations that are parallel to the triangular directions. The magnetite inclusions in many cases have oxidized to hematite, corresponding to the iridescence or rainbow effect across the lattice patterning. In contrast, the unaltered magnetite is black with a metallic sheen.

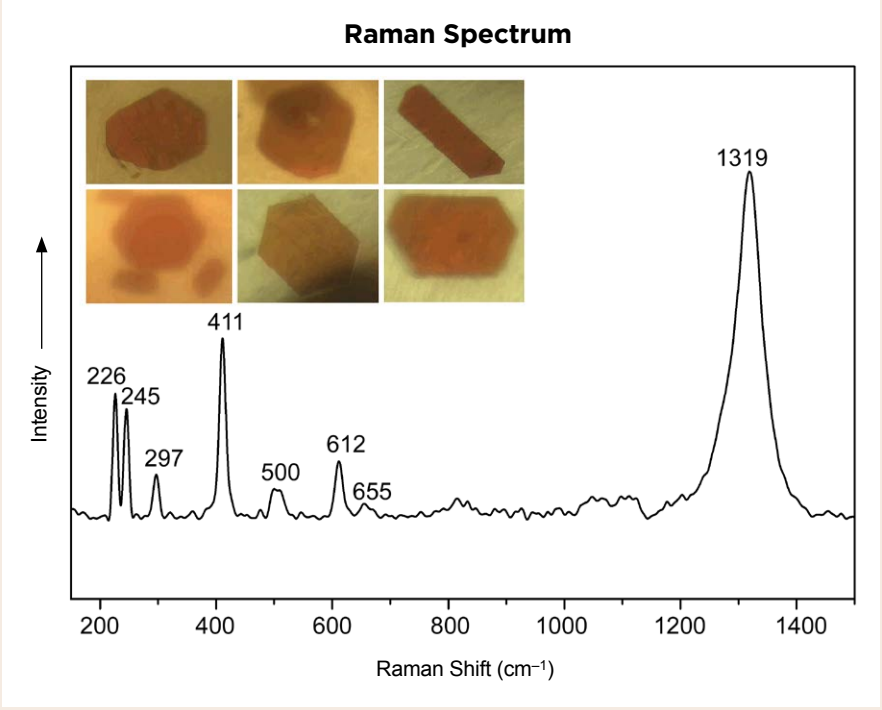

Figure 11: A representative Raman spectrum is shown for the reddish brown platelets (50–200 µm in dimension) in all six samples of rainbow lattice sunstone, confirming the inclusions are hematite. Inset photomicrographs by J. Liu.

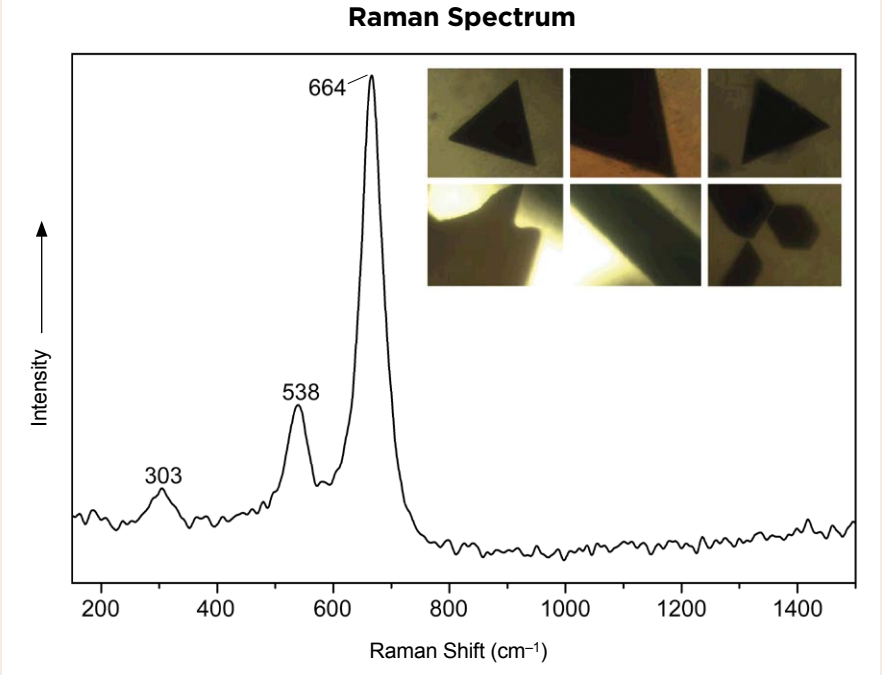

Figure 12: The black inclusions (50–200 µm in dimension) forming the lattice pattern in all six samples of rainbow lattice sunstone were identified as magnetite, as shown in this representative Raman spectrum. Inset photomicrographs by J. Liu.

CONCLUSIONS

Sunstone from the Harts Range, Australia, can show different optical effects including aventurescence, a colourful lattice pattern and adularescence. Electron microprobe data, XRD analyses and Raman spectroscopy revealed that the host feldspar is orthoclase with the composition $Or_{96}Ab_4$. The reddish brown platelets that cause the aventurescence were identified as hematite. The lattice pattern is created by black, elongate and triangular, platy inclusions that were previously believed to be ilmenite, but our investigations confirmed are magnetite. Some of these have altered into orangey brown hematite.

It is rare for aventurescence (as seen in sunstone) to occur together with adularescence (as exhibited by moonstone), and the added presence of a colourful lattice pattern that displays perfect parallel lines and equilateral triangles promotes further interest in this attractive feldspar.

REFERENCES

Akizuki M., 1976. Gemstones with optical effect – 3. *Journal of the Gemmological Society of Japan*, **3**(2), 51–56 (in Japanese with English abstract).

Andersen O., 1915. On aventurine feldspar. *American Journal of Science*, **4**(40), 351–399, http://dx.doi.org/10.2475/ajs.s4-40.238.351.

Bersani D., Lottici P.P. and Montenero A., 1999. Micro-Raman investigation of iron oxide films and powders produced by sol-gel syntheses. *Journal of Raman Spectroscopy*, **30**(5), 355–360, http://dx.doi.org/10.1002/(sici)1097-4555(199905)30:5%3C355::aid-jrs398%3E3.0.co;2-c.

Choudhary G. and Huang Y., 2008. Aventurine K-feldspar. *Journal of Gems & Gemmology*, **10**(3), 20–22 (in Chinese with English abstract).

Daly J. and Dyson D.F., 1956. *Geophysical Investigations for Radioactivity in the Harts Range Area, Northern Territory*. Report No. 32, Commonwealth of Australia Department of National Development, Bureau of Mineral Resources, Geology and Geophysics, Melbourne, Australia, 20 pp.

Faulkner M.J. and Shigley J.E., 1989. Zircon from the Harts Range, Northern Territory, Australia. *Gems & Gemology*, **25**(4), 207–215, http://dx.doi.org/10.5741/gems.25.4.207.

Freeman J.J., Wang A., Kuebler K.E., Jolliff B.L. and Haskin L.A., 2008. Characterization of natural feldspars by Raman spectroscopy for future planetary exploration. *Canadian Mineralogist*, **46**(6), 1477–1500, http://dx.doi.org/10.3749/canmin.46.6.1477.

Lazarelli H.N., 2010. Gemstones Identification Blue Chart. Self-published, www.gembluechart.com.

Huston D.L., Maidment D. and Hussey K., 2006. *Regional Geology and Metallogeny of the Eastern Aileron and Irindina Provinces: A Field Guide*. Geoscience Australia, Canberra, Australia, 44 pp.

Johnston C.L., Gunter M.E. and Knowles C.R., 1991. Sunstone labradorite from the Ponderosa mine, Oregon. *Gems & Gemology*, **27**(4), 220–233, http://dx.doi.org/10.5741/gems.27.4.220.

Joklik G.F., 1955. The mica-bearing pegmatites of the Harts Range, central Australia. *Economic Geology*, **50**(6), 625–649, http://dx.doi.org/10.2113/gsecongeo.50.6.625.

Koivula J.I. and Kammerling R.C., 1989. Gem News: A beautiful new form of orthoclase. *Gems & Gemology*, **25**(1), 47.

León C.P., Kador L., Zhang M. and Müller A.H.E., 2004. *In situ* laser-induced formation of α-Fe_2O_3 from Fe^{3+} ions in a cylindrical core-shell polymer brush. *Journal of Raman Spectroscopy*, **35**(2), 165–169, http://dx.doi.org/10.1002/jrs.1125.

McKeown D.A., 2005. Raman spectroscopy and vibrational analyses of albite: From 25°C through the melting temperature. *American Mineralogist*, **90**(10), 1506–1517, http://dx.doi.org/10.2138/am.2005.1726.

O'Donoghue M., Ed., 2006. *Gems*, 6th edn. Butterworth-Heinemann, Oxford, 277–281.

Rochow K., 1962. *An Investigation of the Harts Range and Plenty River Mica Mines*. Report No. 32, Commonwealth of Australia Department of National Development, Bureau of Mineral Resources, Geology and Geophysics, Melbourne, Australia, 16 pp.

Shebanova O.N. and Lazor P., 2003a. Raman spectroscopic study of magnetite ($FeFe_2O_4$): A new assignment for the vibrational spectrum. *Journal of Solid State Chemistry*, **174**(2), 424–430, http://dx.doi.org/10.1016/s0022-4596(03)00294-9.

Shebanova O.N. and Lazor P., 2003b. Raman study of magnetite (Fe_3O_4): Laser-induced thermal effects and oxidation. *Journal of Raman Spectroscopy*, **34**(11), 845-852, http://dx.doi.org/10.1002/jrs.1056.

Sobolev P.O., 1990. Orientation of acicular iron-ore mineral inclusions in plagioclase. *International Geology Review*, **32**(6), 616–628, http://dx.doi.org/10.1080/00206819009465804.

Zoppi A., Lofrumento C., Castellucci E.M. and Migliorini M.G., 2005. The Raman spectrum of hematite: Possible indicator for a compositional or firing distinction among *Terra Sigillata* wares. *Annali di Chimica*, **95**(3–4), 239–246, http://dx.doi.org/10.1002/adic.200590026.

The Authors

Jia Liu, Prof. Andy H. Shen, Dr Zhiqing Zhang, Dr Chengsi Wang and Dr Tian Shao

Gemmological Institute and Center for Innovative Gem Testing Technology, China University of Geosciences, Wuhan, 430074, China

Email: ahshen1@live.com

Acknowledgments

The authors thank Prof. Fei Huang of Northeastern University for his support of the VSM experiments. Funding was provided by the Center for Innovative Gem Testing Technology, Gemmological Institute, China University of Geosciences (Wuhan), CIGTWZ-2018002.

PAUL WILD

EXCELLENCE IN
GEMSTONE INNOVATION

SPINEL

Found in the most famous crown jewels of the world, the treasured spinel rivals ruby's vibrant colour, is singly refractive and highly transparent.

MINING • CUTTING • CREATION

PAUL WILD OHG • AUF DER LAY 2 • 55743 KIRSCHWEILER • GERMANY
T: +49.(0)67 81.93 43-0 • F: +49.(0)67 81.93 43-43 • E-MAIL: INFO@PAUL-WILD.DE • WWW.PAUL-WILD.DE

VISIT US AT

CARAT+
The world's premier diamond event

MAY 06 – 08, 2018 BOOTH 4L – 24

Neutron Radiography and Tomography: A New Approach to Visualize the Internal Structures of Pearls

Carina S. Hanser, Michael S. Krzemnicki, Christian Grünzweig, Ralph P. Harti, Benedikt Betz and David Mannes

Non-destructive imaging of the internal structures of pearls has so far been mainly based on X-ray imaging methods. As organic matter is almost transparent to X-rays, the identification of some structures can be difficult. This study shows that neutron imaging can be a helpful complementary method to visualize structures inside pearls beyond standard X-ray radiography and tomography, as neutrons are highly attenuated by hydrogen-bearing (organic) matter within pearls. The use of neutron radiography and tomography is shown for selected natural and cultured pearls (beaded and non-beaded). In addition, we present neutron phase contrast and darkfield images of a beaded cultured pearl, in analogy to X-ray phase contrast and darkfield imaging described in a previous study. While neutron imaging of pearls is particularly useful for understanding material inhomogeneities and void structures, this methodology is currently only available at large-scale facilities that are equipped to deal with nuclear reactions.

The Journal of Gemmology, **36**(1), 2018, pp. 54–63, http://dx.doi.org/10.15506/JoG.2018.36.1.54

INTRODUCTION

For about a century, the identification of pearls (i.e. differentiating between their natural or cultured formation; Figure 1) has been a crucial task for gemmologists, given the enormous differences in their rarity and price. Pearl identification is mostly based on the interpretation of internal structures, traditionally visualized by imaging methods such as X-ray radiography (Anderson, 1932; Scarratt et al., 2000; Strack, 2006; Sturman, 2009) and, more recently, X-ray computed microtomography (Wehrmeister et al., 2008; Karampelas et al., 2010; Krzemnicki et al., 2010; Otter et al., 2014) and X-ray phase contrast and darkfield imaging (Revol et al., 2016; Krzemnicki et al., 2017).

With this article, the authors present neutron imaging as a new and complementary method to visualize internal pearl structures. This paper is part of a larger joint research study between author CSH, the SSEF Swiss Gemmological Institute and the Paul Scherrer Institute, in which a total of 32 samples (13 natural and 19 cultured pearls) were investigated with the aim of comparing various imaging methods for pearl testing (Hanser, 2015). It is a follow-up to the article about X-ray phase contrast and darkfield imaging that was recently published in *The Journal* (Krzemnicki et al., 2017).

Similar to X-rays, neutrons can be applied for imaging purposes because of their selective attenuation via absorption and scattering by certain materials. But unlike X-rays, neutrons interact with the atomic nuclei only. Thus, even some lighter elements such as hydrogen strongly attenuate neutrons, whereas X-rays (which interact with the electrons of atoms) are very weakly attenuated by light elements and are increasingly affected by heavier elements (directly related to the element's atomic number). Generally speaking, neutron radiography images are inverse to

X-ray radiographs in many aspects, and in the case of pearls can reveal complementary information to the gemmologist. Calcium carbonate, which forms the pearl, absorbs neutrons rather weakly (and thus appears dark grey in neutron radiographs) in contrast to X-rays, which are strongly absorbed (appearing bright grey in X-ray radiographs). In contrast to this, zones rich in organic matter (and hydrogen) appear bright grey in neutron radiographs (i.e. they are strongly attenuated), whereas they are dark grey in X-ray radiographs (weakly attenuated). Empty cavities, drill holes and fissures remain dark in both methods, as both neutrons and X-rays are well transmitted and not absorbed.

The fact that neutrons are strongly attenuated by some lighter elements such as hydrogen makes them particularly interesting for imaging purposes in which organic matter is involved, such as in materials science (Lehmann and Wagner, 2010; Kardjilov et al., 2011), archaeology and cultural heritage studies (Lehmann et al., 2005; Mannes et al., 2015), including historic jewellery (Rehren et al., 2013; Saprykina et al., 2017), gemstones and pearls (Okamoto et al., 1983; Vontobel and Lehmann, 2010; Hanser, 2015; Mannes et al., 2017; Vitucci et al., 2018).

Pearls commonly contain macroscopic organic matter and void/cavity/fissure features within their calcium-carbonate matrix. As calcium, carbon and oxygen do not interact strongly with neutrons, high contrast between the hydrogen-containing organic matter and the calcium-carbonate polymorphs in pearls can be achieved with neutron imaging methods, as shown in this article.

MATERIALS AND METHODS

For this article we selected two natural and four cultured pearls (see Table I) from the 32 previously investigated samples in order to represent the full range of types (freshwater and saltwater, natural as well as beaded and non-beaded cultured) and display the most telling internal features. All of them had been identified and fully characterized using X-ray radiography and tomography, X-ray phase contrast and darkfield imaging, and energy-dispersive X-ray fluorescence spectroscopy for assessing freshwater vs. saltwater origin.

Figure 1: These pearls (0.7–9.3 ct) were submitted to SSEF for identification and differentiation into natural or cultured origin. Neutron imaging can complement the use of X-rays for difficult cases of identification that might be encountered in a group of pearls such as this. Photo by Luc Phan, © SSEF.

Table I: Natural and cultured pearls analysed for this study.

Sample no.	Type	Bead Nucleus	Origin	Species	Source	Weight (ct)	Diameter (mm)
NP-2e	Natural	–	Saltwater	*Pinctada radiata*	Bahrain	6.49	10.3
NP-2i	Natural	–	Saltwater	*Strombus gigas*	Caribbean Sea	1.86	7.3
CP-1b	Cultured	Non-beaded	Freshwater	*Hyriopsis cumingii*	China	9.92	13.0
CP-2m	Cultured	Non-beaded	Saltwater	*Pinctada margaritifera*	Polynesia	8.14	13.8
CP-2a	Cultured	Beaded	Saltwater	*Pinctada fucata*	Asia	3.89	8.3
CP-2g	Cultured	Beaded	Saltwater	*Pinctada margaritifera*	Polynesia	12.14	16.6

Neutron imaging was performed using the ICON beamline (Kaestner et al., 2011) of the Paul Scherrer Institute (PSI) in Villigen, Switzerland (Figure 2), using a cold neutron spectrum. Since neutrons (i.e. the uncharged particles of an atom's core) can be generated only by nuclear reactions, obtaining access to neutrons is limited to large-scale facilities. The two nuclear reactions that are commonly applied for this purpose are fission and spallation (see Glossary). At PSI, the neutrons were generated with a SINQ continuous spallation source (Blau et al., 2009), and were then passed into a moderator tank filled with heavy water at ambient conditions (to produce a thermal neutron spectrum) and a cold moderator filled with liquid deuterium at 25 K (for a cold neutron spectrum).

For neutron radiography, the pearls were placed on a sample holder using double-sided tape and affixed to an aluminium bar. To keep them in position, some of the pearls were wrapped in aluminium foil, as aluminium is practically transparent to neutrons. For neutron tomography, the samples were wrapped in aluminium foil and placed inside a thin-walled aluminium cylinder, which was placed close to the detector. The acquisition time was 90 s for each radiograph, recorded with a proton current of 1.42 mA by a scintillator-CCD camera system with a field of view of 27 × 27 mm (2048 × 2048 pixels) and a corresponding pixel size of 13.5 µm/pixel (Lehmann et al., 2007). The scintillator was a gadolinium oxysulfide screen with a coating thickness of 20 µm. For neutron

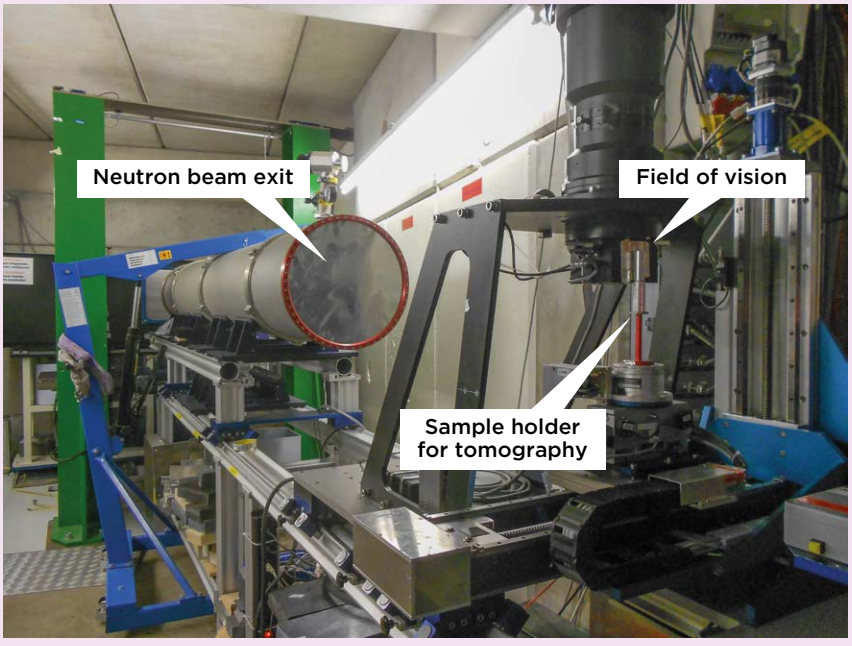

Figure 2: Shown here is a portion of the ICON beamline at the Paul Scherrer Institute that provides a cold neutron spectrum. The neutron beam passes through the exit and the field of vision and then strikes the sample. The signal produced is then recorded by a scintillator-CCD camera system (not visible in this image). Photo by C. Hanser.

Glossary

Nuclear fission: Highly energetic radioactive decay process by which an atomic core (nucleus) is split into smaller/lighter nuclei (e.g. in a chain reaction), often accompanied by the production of free neutrons and gamma radiation.

Nuclear spallation: Using a particle accelerator, a heavy nucleus (atom) emits a large number of neutrons each time it is hit by a high-energy particle. These highly energetic neutrons have to be slowed down to be usable for analysis purposes by a process known as moderation.

tomography the same setup was used, with each tomograph consisting of 626 radiographs over 360°, summing up to an overall acquisition time of approximately 22 hours.

None of the analysed pearls showed any change in colour after exposure to the neutrons. However, they did become temporarily radioactive due to the long time necessary for neutron tomography, and had to remain at the facility until reaching a threshold level below 0.1 µSv/h (as tested by a radiation protection officer using an officially calibrated dosimeter), a process which took several hours to a few days for the various pearls.

Neutron phase contrast and darkfield imaging were performed with the samples fixed on double-sided tape and using a lower acquisition time of 45 s for each image. No residual radioactivity was detected in the samples after this type of imaging. A detailed description of the setup and neutron interferometer gratings is given by Grünzweig et al. (2008) and Mannes et al. (2017).

RESULTS AND DISCUSSION

X-ray and neutron imaging were done independently on two completely different instrumental setups, and although we attempted to fix the samples in a consistent orientation, we were unable to obtain images with a perfectly matching sample position. All radiographs were edited (contrast sharpening and homogenizing of the black background around the samples) using built-in filters in Adobe Photoshop software. A comparison of X-ray radiography and neutron radiography images immediately reveals the complementary nature of these two methods.

Examples of Natural Pearls

Figure 3 shows natural pearl sample NP-2e (*Pinctada radiata*), which is characterized by an organic-rich core of radially arranged calcite prisms and multiple radial fissures overgrown by a nacre layer about 3 mm thick with weak onion-like structures. In the X-ray radiograph (Figure 3b) the nacre is distinctly brighter (higher X-ray attenuation) compared to the organic-enriched core (lower X-ray attenuation). Fissures appear dark, as they are voids with no attenuation effect on X-rays. (Note: Readers wishing to see X-ray phase contrast and darkfield images of this pearl are directed to Figure 6 in Krzemnicki et al., 2017.)

Neutron radiography of this pearl (Figure 3c) shows the inverse to X-radiography, with a brighter core owing to the enrichment of organic matter (i.e. strong neutron attenuation by hydrogen) compared to the dark grey nacre (distinctly lower neutron attenuation by calcium carbonate). Similar to the X-ray radiograph, the void fissures (mainly visible in the core) are dark, indicating no neutron attenuation; it can therefore be postulated that they contain no organic matter. However, compared to the image

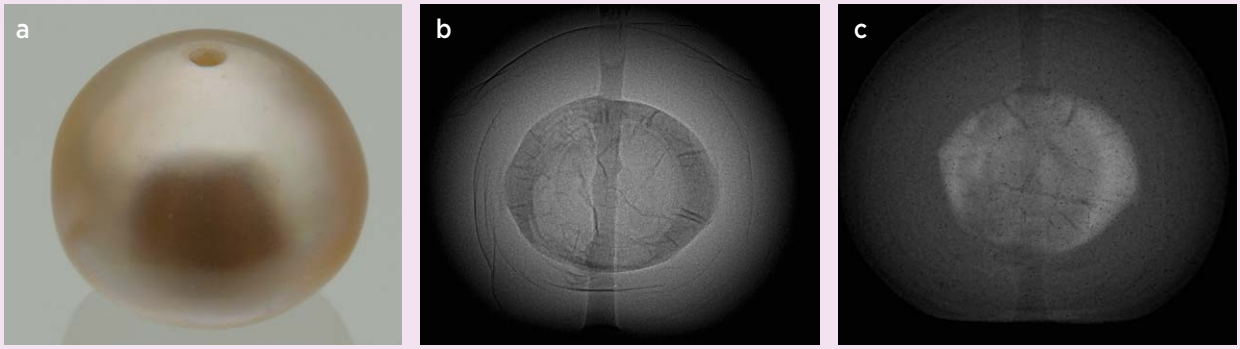

Figure 3: (a) Saltwater natural pearl NP-2e (*Pinctada radiata*, 10.3 mm in diameter) is shown here with its X-ray radiograph (b) and neutron radiograph (c). The inverse attenuation of the organic-rich core (dark grey in X-rays and light grey in neutrons) and the dense surrounding nacre layer (light grey in X-rays and dark grey in neutrons) is obvious.

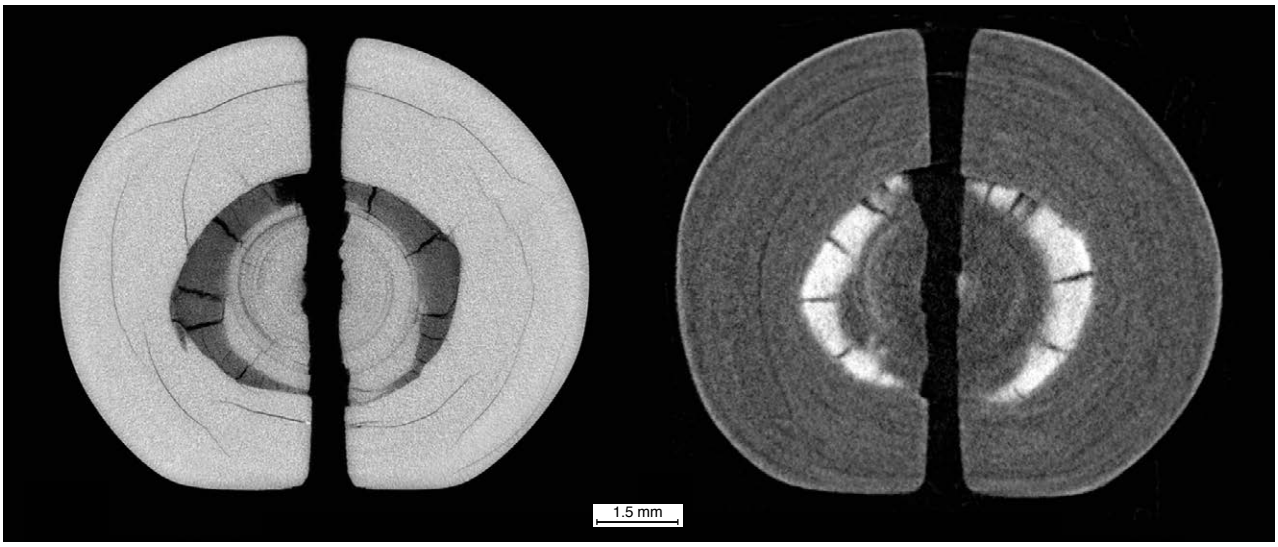

Figure 4: X-ray tomography (left) and neutron tomography (right) of the natural pearl shown in Figure 3 also illustrates the inverse attenuation of X-rays and neutrons in pearls. The organic-rich outer core layer with numerous radiating desiccation fissures appears dark grey in X-rays and bright grey in neutrons.

obtained with state-of-the-art digital X-ray radiography, the neutron radiograph appears less sharp using the current analytical setup.

Better contrast and resolution are shown by image slices of the same sample obtained by X-ray and neutron tomography (Figure 4). These images reveal that this saltwater natural pearl in fact contains an irregularly shaped core consisting of two phases: (1) an inner core portion dominated by calcium carbonate that appears bright grey in the X-ray tomograph and dark grey in the neutron tomograph (and also contains tiny radial calcite columns, of the type pictured in Figure 3b of Gutmannsbauer and Hänni [1994], together with fine onion-like structures), and (2) an outer core layer of calcium carbonate that is heavily enriched in organic matter and appears dark grey in the X-ray tomograph and bright grey in the neutron tomograph (along with pronounced desiccation fissures). The reason for such a distinct enrichment of organic matter in the outer core is not known, but might be the result of a haemorrhage event within the pearl sac during formation of this natural pearl. These tomographic slices allow a much more detailed interpretation of internal structures because they are not blurred by condensing a three-dimensional pearl on to a two-dimensional image, as with radiography.

Figure 5 shows a comparison of image slices obtained by X-ray and neutron tomography of non-nacreous natural pearl sample NP-2i, reportedly from *Strombus gigas* (Sue Hendrickson, pers. comm., 2015). This pearl is characterized by a large irregular-shaped internal cavity that is partially filled with numerous small spherules. X-ray tomography (Figure 5b) shows a rather strong attenuation of these spherules, resembling the bright appearance of the non-nacreous calcium carbonate surface layer (densely interwoven fibrous aragonite), thus indicating a rather calcareous nature of these spherules. However, the neutron tomograph (Figure 5c) clearly illustrates that these spherules also highly attenuate neutrons and are thus presumably rich in hydrogen. This indicates a distinctly different nature than the calcium carbonate (aragonite) of the pearl's surface. Similar tiny spherules have been documented previously (see Figure 4 in Krzemnicki et al., 2010), and research into their nature is ongoing.

Examples of Cultured Pearls

Figure 6 shows non-beaded freshwater cultured pearl CP-1b (*Hyriopsis cumingii*), imaged using X-ray and neutron radiography. Both images are dominated by a rather uniform attenuation as a result of the dense nacre of this cultured pearl. The irregular 'moustache' structure in the centre is clearly visible in the X-ray radiograph but also to some extent in the neutron image. (The slightly different shape of this structure in these two radiographs is due to variations in the sample's orientation.) Such tiny structures are highly characteristic of mantle-grown non-beaded cultured pearls (Scarratt et al., 2000; Strack, 2006). The fact that this structure is dark grey (i.e. has very low attenuation) in both types of radiographs indicates that it actually represents a tiny folded void and—at least in this case—is not filled with organic matter. The X-ray radiograph (Figure 6b) also shows a few very fine dark ring structures, which appear light grey in the neutron radiograph (Figure 6c), thus

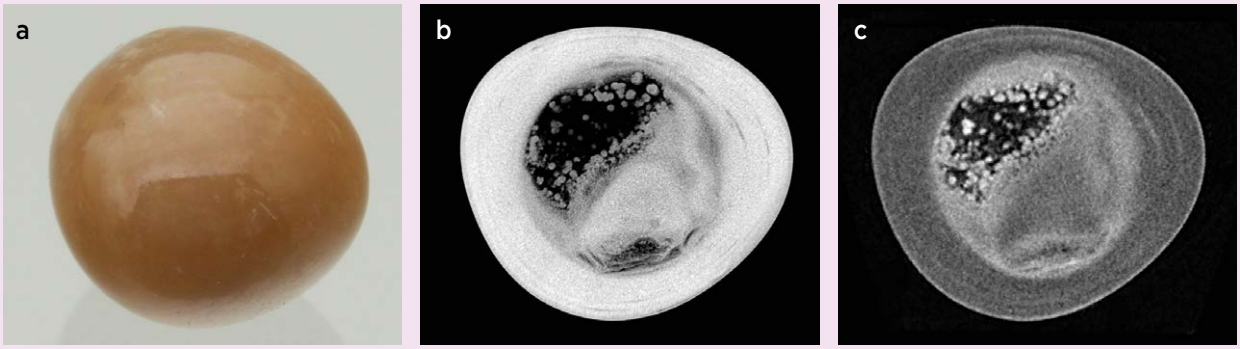

Figure 5: (a) Non-nacreous natural pearl NP-2i (*Strombus gigas*, 7.3 mm in diameter) is shown with its corresponding tomographic slices obtained using X-rays (b) and neutrons (c), which reveal a large cavity containing numerous small spherules.

implying that they represent onion-like growth features enriched in organic matter. However, the fuzzy appearance of the neutron radiograph obtained with the current analytical setup demonstrates that it is not the first choice for visualizing such fine internal features crucial for pearl identification. Much more detailed X-ray phase contrast and darkfield images of this same cultured pearl are presented in Figure 9 of Krzemnicki et al. (2017).

Figure 7 shows the complex external and internal structures of non-beaded saltwater cultured pearl CP-2m (*Pinctada margaritifera*; see also Figure 10 in Krzemnicki et al., 2017). The neutron radiograph (Figure 7b) highlights local concentrations of organic matter (containing hydrogen) as bright areas. The baroque shape, however, creates spurious overlay effects when condensed into a two-dimensional X-ray radiograph (which is therefore not shown here for comparison). As evident in the reconstructed image slices obtained by X-ray and neutron tomography (Figures 7c and 7d), the internal structures are much more discernible and displayed in great detail by both methods. The main feature is a large folded cavity structure (dark grey to black in the X-ray tomograph), accentuated by desiccation fissures. The neutron tomograph provides additional information that is different from what can be inferred from the X-ray tomography only. What seems to be an open void on the left side of the large folded cavity structure in the X-ray image proves to be filled with organic matter (bright grey in the neutron tomograph). The remaining part of the folded cavity is only coated by a thin layer of organic material resulting in a fine but pronounced light grey depiction of the cavity's outline. The smaller additional cultured pearl attached at the top, also known by the Japanese term *tokki*, is a common feature for gonad-grown cultured pearls (Krzemnicki et al., 2011; Gauthier et al., 2015). Interestingly, this tokki shows a small dark ring (with a tiny brighter spot in its centre) in both tomographic images. Based on X-ray tomography, this feature could be misinterpreted as having a local enrichment of organic matter in a small growth ring. The low neutron

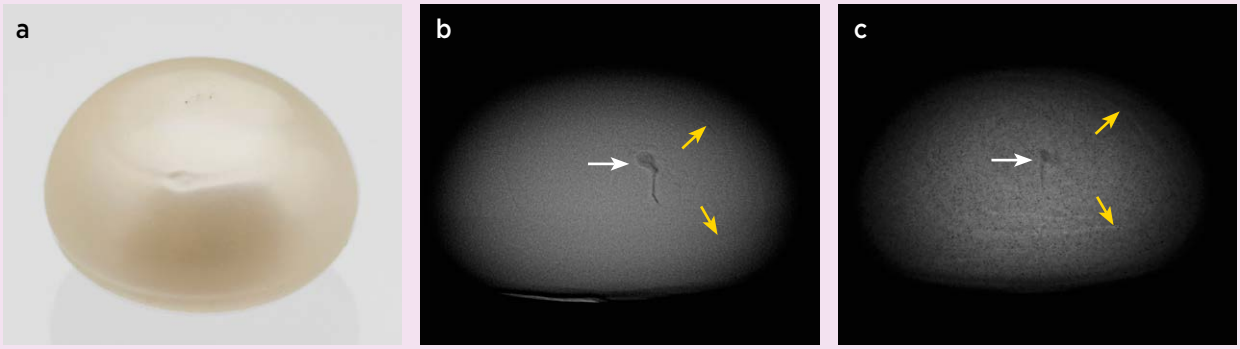

Figure 6: (a) Non-beaded freshwater cultured pearl CP-1b (*Hyriopsis cumingii*, 13.0 mm in diameter) is shown with its X-ray (b) and neutron (c) radiographs. The latter two images were not taken in exactly the same position, resulting in a slightly different appearance of the tiny 'moustache' void structure in the centre (white arrows). Fine growth rings (yellow arrows) appear light grey in the neutron radiograph, indicating that they are enriched in organic matter.

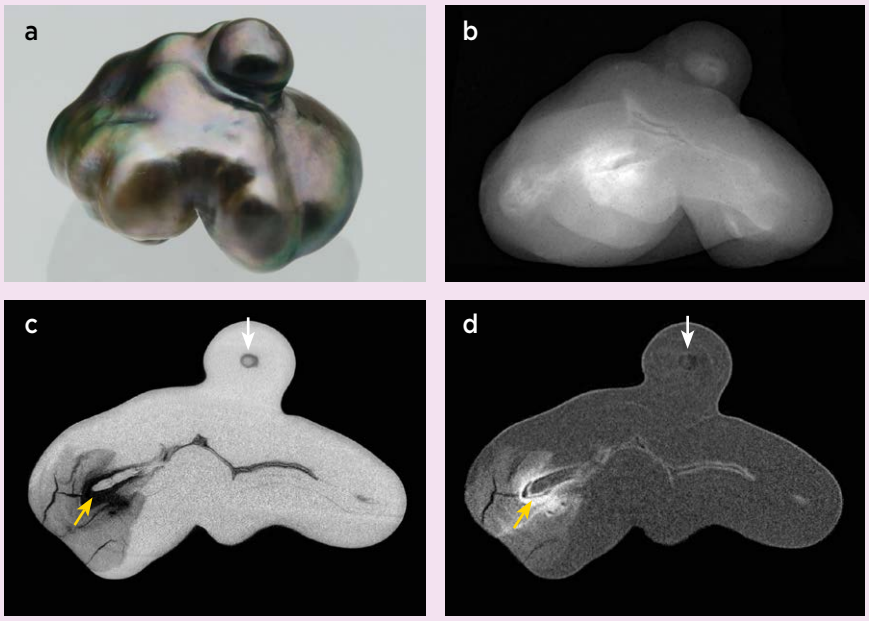

Figure 7: (a) Non-beaded saltwater cultured pearl CP-2m (*Pinctada margaritifera*, 13.8 mm in diameter) is imaged with neutron radiography (b), X-ray tomography (c) and neutron tomography (d). The tomographic sections display a large folded cavity structure (yellow arrows), with distinct enrichment of organic matter shown in the neutron tomograph. Attached to the top of the sample is a small additional cultured pearl (tokki), with a dark growth ring marked by white arrows.

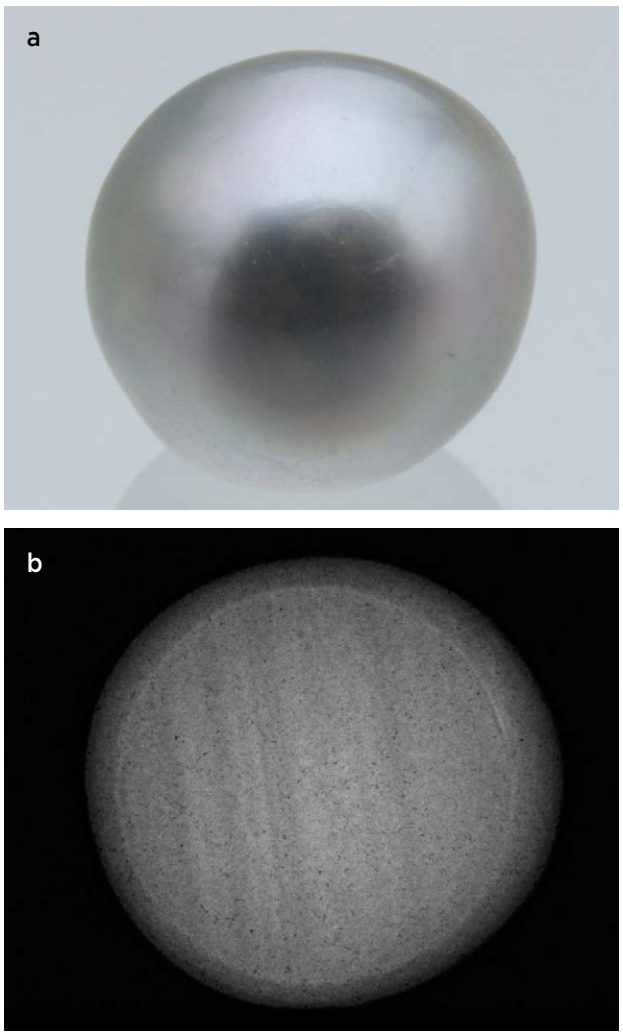

Figure 8: (a) Imaging of Akoya-type beaded saltwater cultured pearl CP-2a (*Pinctada fucata*, 8.3 mm in diameter) was performed with neutron radiography (b), which reveals a banded structure within the shell bead and a thin light grey circle resulting from a film of organic matter on the bead.

attenuation by this feature, however, indicates that the growth ring might be due to another reason, such as a distinctly lower nacre density.

Beaded cultured pearls are readily identified with both X-ray and neutron radiography. Figure 8 shows Akoya-type beaded cultured pearl CP-2a (*Pinctada fucata*) with distinct banding in the shell bead (a freshwater origin for this bead was confirmed by X-ray luminescence imaging; see Hänni et al., 2005). Inversely to X-ray radiography, the darker bands in the neutron radiograph are not inferred to represent layers showing variations in organic matter but rather zones of denser freshwater shell material, whereas the brighter bands might contain slightly higher amounts of organic matter. (An X-ray radiograph of this sample is not included here for comparison because it was taken in a slightly different position and therefore did not show the internal layering of the bead.) The bright thin layer between bead and nacre overgrowth represents a thin film of organic matter deposited on the bead in the newly formed pearl sac before the nacre overgrowth formed during pearl cultivation. The bead appears slightly brighter than the surrounding nacre because, as with all spherical objects, there is a gradual increase of attenuation with increasing transmission path through the sample. In addition, the thin layer of organic matter (seen here as the light grey circle between the bead and nacre overgrowth) also might contribute to the brighter overall appearance of the bead in this neutron radiograph.

A final example (Figure 9) is provided by beaded saltwater cultured pearl CP-2g (*Pinctada*

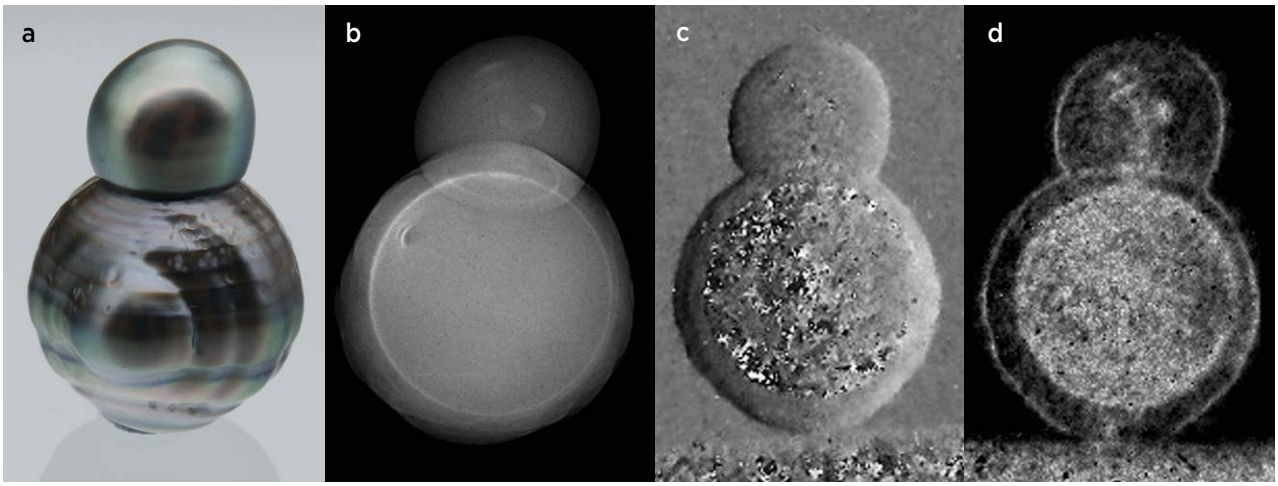

Figure 9: (a) Saltwater cultured pearl CP-2g (*Pinctada margaritifera*, 16.6 mm in diameter) is shown with its neutron radiograph (b), neutron phase contrast image (c) and neutron darkfield image (d). The bead is readily discernible by its organic coating, both with neutron radiography (bright grey circle) and neutron interferometry, which shows different appearances related to artefacts (in the neutron phase contrast image) and small-angle scattering (in the darkfield image).

margaritifera) with a relatively large additional cultured pearl (tokki) and distinct circling structures in two directions on its surface (cf. Gauthier et al., 2015). The bead is easily recognized in the neutron radiograph (Figure 9b) by a bright grey outline resulting from a distinct organic layer that surrounds it. For this sample (and all other samples studied by Hanser, 2015), we present additional neutron phase contrast and neutron darkfield images (Figures 9c and 9d, respectively). Using the current setup and analytical parameters, these images are, however, characterized by rather low resolution and noticeable artefacts, which limits their usefulness. The neutron phase contrast image reveals a noisy signal related to the bead, whereas in the neutron darkfield image the organic-rich coating on the bead and a few organic-rich spots in the tokki produce strong neutron small-angle scattering (i.e. a distinct bright reaction).

CONCLUSIONS

Most structures inside pearls can be visualized readily by X-ray imaging methods. However, neutron radiography and tomography can yield additional information that cannot be obtained by X-rays. Neutron imaging methods are especially useful to better understand material inhomogeneities and void structures, as well as filling substances (solid or liquid) in large hollow pearls (cf. Otter et al., 2014). Since access to neutron imaging techniques is, however, limited to large-scale facilities, their routine application to gemmological testing is impossible at this time. Still, in difficult cases of identifying the nature of a pearl, further analysis with neutrons can be helpful. It is important to note that activation of the samples as a result of neutron tomographic imaging will likely require that they be quarantined for up to several days after testing.

REFERENCES

Anderson B.W., 1932. The use of X rays in the study of pearls. *British Journal of Radiology*, **5**(49), 57–64, http://dx.doi.org/10.1259/0007-1285-5-49-57.

Blau B., Clausen K.N., Gvasaliya S., Janoschek M., Janssen S., Keller L., Roessli B., Schefer J., Tregenna-Piggott P., Wagner W. and Zaharko O., 2009. The Swiss spallation neutron source SINQ at Paul Scherrer Institut. *Neutron News*, **20**(3), 5–8, http://dx.doi.org/10.1080/10448630903120387.

Gauthier J.-P., Gutierrez G., Serrar M. and Bui T.N., 2015. Rares perles cerclées à double axe de rotation [Rare circled pearls with a double axis of rotation]. *Revue de Gemmologie A.F.G.*, No. 194, 4–7 (in French).

Grünzweig C., Pfeiffer F., Bunk O., Donath T., Kühne G., Frei G., Dierolf M. and David C., 2008. Design, fabrication, and characterization of diffraction gratings for neutron phase contrast imaging. *Review of Scientific Instruments*, **79**(5), article 053703, 6 pp., http://dx.doi.org/10.1063/1.2930866.

Gutmannsbauer W. and Hänni H.A., 1994. Structural and chemical investigations on shells and pearls of nacre forming salt- and freshwater bivalve molluscs. *Journal of Gemmology*, **24**(4), 241–252, http://dx.doi.org/10.15506/jog.1994.24.4.241.

Hänni H.A., Kiefert L. and Giese P., 2005. X-ray luminescence, a valuable test in pearl identification. *Journal of Gemmology*, **29**(5–6), 325–329, http://dx.doi.org/10.15506/JoG.2005.29.5.325.

Hanser C., 2015. *Comparison of Imaging Techniques for the Analysis of Internal Structures of Pearls*. Master's thesis, University of Freiburg, Germany, 137 pp.

Kaestner A.P., Hartmann S., Kühne G., Frei G., Grünzweig C., Josic L., Schmid F. and Lehmann E.H., 2011. The ICON beamline – A facility for cold neutron imaging at SINQ. *Nuclear Instruments and Methods in Physics Research Section A: Accelerators, Spectrometers, Detectors and Associated Equipment*, **659**(1), 387–393, http://dx.doi.org/10.1016/j.nima.2011.08.022.

Karampelas S., Michel J., Zheng-Cui M., Schwarz J.-O., Enzmann F., Fritsch E., Leu L. and Krzemnicki M.S., 2010. X-ray computed microtomography applied to pearls: Methodology, advantages, and limitations. *Gems & Gemology*, **46**(2), 122–127, http://dx.doi.org/10.5741/gems.46.2.122.

Kardjilov N., Manke I., Hilger A., Strobl M. and Banhart J., 2011. Neutron imaging in materials science. *Materials Today*, **14**(6), 248–256, http://dx.doi.org/10.1016/s1369-7021(11)70139-0.

Krzemnicki M.S., Friess S.D., Chalus P., Hänni H.A. and Karampelas S., 2010. X-ray computed microtomography: Distinguishing natural pearls from beaded and non-beaded cultured pearls. *Gems & Gemology*, **46**(2), 128–134, http://dx.doi.org/10.5741/gems.46.2.128.

Krzemnicki M.S., Mueller A., Hänni H.A., Gut H.-P. and Düggelin M., 2011. Tokki pearls: Additional cultured pearls formed during pearl cultivation: External and internal structures. *32nd International Gemmological Conference*, Interlaken, Switzerland, 13–17 July, 56–58.

Krzemnicki M.S., Hanser C.S. and Revol V., 2017. Simultaneous X-radiography, phase contrast and darkfield imaging to separate natural from cultured pearls. *Journal of Gemmology*, **35**(7), 628–638, http://dx.doi.org/10.15506/JoG.2017.35.7.628.

Lehmann E.H. and Wagner W., 2010. Neutron imaging at PSI: A promising tool in materials science and technology. *Applied Physics A*, **99**(3), 627–634, http://dx.doi.org/10.1007/s00339-010-5606-3.

Lehmann E.H., Vontobel P., Deschler-Erb E. and Soares M., 2005. Non-invasive studies of objects from cultural heritage. *Nuclear Instruments and Methods in Physics Research Section A: Accelerators, Spectrometers, Detectors and Associated Equipment*, **542**(1–3), 68–75, http://dx.doi.org/10.1016/j.nima.2005.01.013.

Lehmann E.H., Frei G., Kühne G. and Boillat P., 2007. The micro-setup for neutron imaging: A major step forward to improve the spatial resolution. *Nuclear Instruments and Methods in Physics Research Section A: Accelerators, Spectrometers, Detectors and Associated Equipment*, **576**(2–3), 389–396, http://dx.doi.org/10.1016/j.nima.2007.03.017.

Mannes D., Schmid F., Frey J., Schmidt-Ott K. and Lehmann E., 2015. Combined neutron and X-ray imaging for non-invasive investigations of cultural heritage objects. *Physics Procedia*, **69**, 653–660, http://dx.doi.org/10.1016/j.phpro.2015.07.092.

Mannes D., Hanser C., Krzemnicki M., Harti R.P., Jerjen I. and Lehmann E., 2017. Gemmological investigations on pearls and emeralds using neutron imaging. *Physics Procedia*, **88**, 134–139, http://dx.doi.org/10.1016/j.phpro.2017.06.018.

Okamoto S., Hiraoka E., Tsujii Y. and Furuta J., 1983. Neutron radiography of pearls. *Journal of the Gemmological Society of Japan*, **10**(3), 59–65, http://dx.doi.org/10.14915/gsjapan.10.3_59 (in Japanese with English abstract).

Otter L.M., Wehrmeister U., Enzmann F., Wolf M. and Jacob D.E., 2014. A look inside a remarkably large beaded South Sea cultured pearl. *Gems & Gemology*, **50**(1), 58–62, http://dx.doi.org/10.5741/gems.50.1.58.

Rehren T., Belgya T., Jambon A., Káli G., Kasztovszky Z., Kis Z., Kovács I., Maróti B., Martinón-Torres M., Miniaci G., Pigott V.C., Radivojević M., Rosta L., Szentmiklósi L. and Szőkefalvi-Nagy Z., 2013. 5,000 years old Egyptian iron beads made from hammered meteoritic iron. *Journal of Archaeological Science*, **40**(12), 4785–4792, http://dx.doi.org/10.1016/j.jas.2013.06.002.

Revol V., Hanser C. and Krzemnicki M., 2016. Characterization of pearls by X-ray phase contrast imaging with a grating interferometer. *Case Studies in Nondestructive Testing and Evaluation*, **6**, 1–7, http://dx.doi.org/10.1016/j.csndt.2016.06.001.

Saprykina I.A., Khokhlov A.N., Kichanov S.E. and Kozlenko D.P., 2017. Old Russian jewelries studies by means of neutron imaging method. *3D Imaging in Cultural Heritage*, British Museum, London, 9–10 November, 37–38.

Scarratt K., Moses T.M. and Akamatsu S., 2000. Characteristics of nuclei in Chinese freshwater cultured pearls. *Gems & Gemology*, **36**(2), 98–109, http://dx.doi.org/10.5741/gems.36.2.98.

Strack E., 2006. Pearls. Rühle-Diebener-Verlag, Stuttgart, Germany, 696 pp.

Sturman N., 2009. The Microradiographic Structures of Non-bead Cultured Pearls. Gemological Institute of America, Bangkok, Thailand, 20 August, 23 pp., www.gia.edu/gia-news-research-NR112009.

Vitucci G., Minniti T., Di Martino D., Musa M., Gori L., Micieli D., Kockelmann W., Watanabe K., Tremsin A.S. and Gorini G., 2018. Energy-resolved neutron tomography of an unconventional cultured pearl at a pulsed spallation source using a microchannel plate camera. *Microchemical Journal*, **137**, 473–479, http://dx.doi.org/10.1016/j.microc.2017.12.002.

Vontobel P. and Lehmann E., 2010. Results of tomography investigation of small samples at NEUTRA: Options for further improvements. Scientific and Technical Report 2000—Volume VI: Large Research Facilities. Paul Scherrer Institute, Villigen, Switzerland, 68.

Wehrmeister U., Goetz H., Jacob D.E., Soldati A., Xu W., Duschner H. and Hofmeister W., 2008. Visualization of the internal structures of cultured pearls by computerized X-ray microtomography. *Journal of Gemmology*, **31**(1), 15–21, http://dx.doi.org/10.15506/JoG.2008.31.1.15.

The Authors

Carina S. Hanser
Albert Ludwig University of Freiburg, Institute of Earth and Environmental Sciences, Albertstrasse 23b, Freiburg im Breisgau, Germany

Dr Michael S. Krzemnicki FGA
Swiss Gemmological Institute SSEF, Aeschengraben 26, 4051 Basel, Switzerland
Email: michael.krzemnicki@ssef.ch

Dr Christian Grünzweig, Ralph P. Harti, Dr Benedikt Betz and Dr David Mannes
Laboratory for Neutron Scattering and Imaging, Paul Scherrer Institut, CH-5232 Villigen, Switzerland

Acknowledgements

The authors thank the following for donating or loaning natural or cultured pearl samples for this research study: Sue Hendrickson (Chicago, Illinois, USA), Dr Wolf Bialoncyk (Vienna, Austria), Michael Bracher (Paspaley, Sydney, Australia), Andy Mueller (Hinata Trading, Kobe, Japan), Prof. Dr Henry A. Hänni (GemExpert, Basel, Switzerland), Isam Alezy (Natural Pacific Pearls, Sydney, Australia), Abdullah Al Suwaidi and Daiji Imura (RAK Pearls, Ras Al Khaimah, United Arab Emirates) and Patrick Flückiger (SwissPearls, Geneva, Switzerland). We also thank Judith Braun and Gina Brombach of SSEF Analytics for their valuable assistance.

Conferences

AGA TUCSON CONFERENCE

The 2018 Accredited Gemologists Association Conference in Tucson, Arizona, USA, took place 31 January and was attended by 142 people. The event was moderated by AGA president **Stuart Robertson** (Gemworld International Inc., Glenview, Illinois, USA) and featured six presentations.

Dr Thomas Hainschwang (GGTL-GEMLAB Laboratories, Balzers, Liechtenstein) provided an update on his ambitious project of characterizing treated-colour diamonds (Figure 1). He and his team have analysed a carefully pre-selected sample base of 105 natural untreated diamonds of various colours (colourless, yellow, brown, 'olive' green, grey and violet) using several spectroscopic techniques as well as fluorescence imaging. The stones are currently in the process of being treated by various methods (i.e. irradiating with neutrons, heating in small steps over a range of 100–1,300°C and annealing under high-pressure, high-temperature [HPHT] conditions). After each treatment step the samples are characterized again by the same techniques.

Shane McClure and **Andy Lucas** (Gemological Institute of America [GIA], Carlsbad, California, USA) described the geographic origin determination of emeralds, and started by differentiating two main types: high iron (from mica schist-type deposits such as Zambia and Brazil) and low iron (from localities such as Colombia and Afghanistan). They illustrated the inclusions, ultraviolet-visible (UV-Vis) spectral features and chemical composition of emeralds from various deposits in the context of the high- and low-iron categories.

Figure 1: During the AGA Tucson Conference, Dr Thomas Hainschwang presents a status report of his research project on characterizing treated-colour diamonds. Photo by B. M. Laurs.

Dr Çiğdem Lüle (Kybele LLC, Buffalo Grove, Illinois, USA) highlighted current challenges involving gemmological nomenclature and terminology, including the naming of newly discovered gem varieties, colour descriptions on laboratory reports, treatment disclosure and branded gems.

Nathan Renfro (GIA, Carlsbad) showed beautiful photomicrographs of internal features in ruby, emerald and sapphire, and provided useful examples of how certain features are characteristic of natural, treated or synthetic samples, and also can be indicative of specific geographic origins.

Richard and Billie Hughes (Lotus Gemology, Bangkok, Thailand) provided an overview of some gems from Madagascar, with examples of localities visited in 2005, 2010 and 2016. They also reviewed internal features seen in sapphires from various unspecified localities in Madagascar, and described experiments to investigate the effects of relatively low-temperature heat treatment (800–1,300°C) on the inclusions and UV-Vis spectra of Madagascar sapphires.

Sonny Pope (Suncrest Diamonds, Orem, Utah, USA) reviewed the colour enhancement of diamond using HPHT and irradiation treatments. The latest developments from his company include a new range of light 'baby' pink colours (derived from dark brown type IIa starting material) and 'sky' blue coloration produced by sequential HPHT and irradiation treatment of brown type IIa diamonds.

The conference also featured workshops by **Alan Hodgkinson** (Whinhurst, West Kilbride, Scotland) on visual optics, **Claire Mitchell** (JTV, Knoxville, Tennessee, USA) on testing gems with UV fluorescence and **Sarah Steele** (Ebor Jetworks Ltd, Whitby) on distinguishing black gem materials.

The AGA Gala took place that evening, where The Antonio C. Bonanno Award for Excellence in Gemology was presented to **William Hanneman** (Monterey, California, USA) in honour of his many contributions to gemmology that range from education to the development of innovative and affordable gem-testing instruments.

Brendan M. Laurs FGA

Figure 2: IGC participants and guests gather for a group photo in front of the Safari Hotel in Windhoek, Namibia. Photo courtesy of Tasnara Sripoonjan.

35TH INTERNATIONAL GEMMOLOGICAL CONFERENCE

The 35th biennial IGC took place at the Safari Hotel in Windhoek, Namibia, 11–15 October 2017. The conference was organized by **Dr Ulrich Henn** (German Gemmological Association, Idar-Oberstein), **Prof. Dr Henry Hänni** (GemExpert, Basel, Switzerland) and **Andreas Palfi** (Palfi, Holman and Associates, and Geo Tours Namibia, Windhoek). More than 80 delegates, observers and guests from 28 countries gathered for the conference (e.g. Figure 2), and some of them attended pre- and post-conference field trips. (For a report on the pre-conference excursion to a diamond mine on Namibia's coast, see pp. 16–18 of this issue of *The Journal*). A proceedings volume containing extended abstracts of the oral and poster presentations can be downloaded at www.igc-gemmology.org/igc-2017-programme.

The conference was opened by IGC Executive Committee secretary **Dr Jayshree Panjikar** (PANGEMTECH, Pune, India), followed by speeches from **Veston Malango** (Chamber of Mines, Windhoek) and The Honourable Deputy Minister **Kornelia Shilunga** (Ministry of Mines and Energy, Windhoek).

Gems of Namibia and South Africa were covered in the first conference session. **Dr Gabi Schneider** (Namibian Uranium Association, Swakopmund) reviewed the history of diamond mining in Namibia, from when they were discovered in 1908 to the present time. The coastal area from Oranjemund northward to Lüderitz has become one of the most important diamond-producing areas in the world. The initial rush spurred an industrial revolution to address the challenges of mining in the Namib Desert, a remote area that lacked nearby water and electricity. **Andreas Palfi** covered deposits for coloured stones and ornamental gems in Namibia, including tourmaline, garnet (demantoid and spessartine), aquamarine, topaz, quartz and other silica-based gems (pietersite and agates) and mineral specimens. He estimated that approximately 3,000 people are active in the industry, mostly as independent small-scale miners. **Dr Ulrich Henn** and co-authors from the German Gemmological Association reviewed the localities and gemmological properties of tourmaline from the Karibib and Usakos regions of Namibia. Henn reported that heating the tourmaline to 650°C for one hour can alter the colour from blue-green to green due to the conversion of Fe^{2+} to Fe^{3+}. **Edward Boehm** (RareSource, Chattanooga, Tennessee, USA) examined the geology, gemmology and market for spessartine from Namibia. Commonly sold as 'Mandarin garnet', Namibian spessartine commands relatively high prices (typically more than US$1,000/ct or ~£720/ct) compared to material from other localities (i.e. Nigeria, Mozambique, Brazil, Sri Lanka, Tanzania and Zambia). **Dr Harmony Musiyarira** and co-authors (Namibia University of Science and Technology, Windhoek) developed a growth strategy for the Namibian jewellery industry and coloured stone value chain. They collected information from small-scale miners by conducting interviews, distributing questionnaires and visiting mining areas, and determined that there is a need to move from a cost-based sector to a high-value-added and

competitive brand in the global market. At the end of the session, **this author** described recent mining of some alluvial diamond deposits in South Africa (for details, see Gem Note in *The Journal*, Vol. 35, No. 6, 2017, pp. 484–485).

The next session focused on gem corundum. **Terrence Coldham** (Sydney, Australia) presented convincing evidence that the Lava Plains deposit in northern Queensland is an *in situ* pyroclastic sapphire deposit. Since there are not enough sapphires found in alkali basalts to account for the grades of their associated alluvial deposits, he proposed that a large proportion of the world's BGY (blue, green, yellow)-type sapphires may have been brought to the surface during a pyroclastic phase of volcanism (rather than by eruptions of basaltic lava); in most cases the sapphires were then concentrated into economically significant deposits by weathering of the pyroclastics. **Dr Emmanuel Fritsch** (Institut des Matériaux Jean Rouxel and University of Nantes, France) and co-authors suggested that elongate crystallographically oriented inclusions in ruby and sapphire, which are commonly referred to as 'boehmite needles', are actually empty channels that form at the intersections of polysynthetic twin planes. **Shane McClure** (GIA, Carlsbad, California, USA) described recent sapphire mining at Gem Mountain (Rock Creek) and El Dorado Bar (Missouri River) in Montana, USA. Also he reported that another very active operation (Potentate Mining) recovered more than 40 kg of sapphires during the recent mining season at Wildcat Gulch in the Rock Creek area. **Wiliwan Atichat** and co-authors (The Gem and Jewelry Institute of Thailand [GIT], Bangkok) described GIT's system of colour grading padparadscha sapphires, which relies on the use of master stones consisting of three groups: orangey pink, orange-pink and pinkish orange.

In a session on diamonds, **Kentaro Emori** and co-authors (Central Gem Laboratory, Tokyo, Japan) documented two synthetic samples (1.03 ct brown CVD-grown and 0.07 ct yellow HPHT-grown synthetic diamonds) with features resembling natural stones. He reminded the audience that it is important to use comprehensive methodology for identifying challenging synthetics that are now present in the marketplace. **Roman Serov** and co-authors (Gemological Center, Lomonosov Moscow State University, Russia) reported on natural diamonds overgrown by a thick CVD synthetic layer to add weight. The latest generation of these 'hybrid diamonds' may contain jellyfish-like inclusions (Figure 3), and they generally lack a discernible natural/CVD boundary when viewed with a gemmological microscope (although this is readily seen with the DiamondView). **Dr Rainer Schultz Güttler** (University of São Paulo, Brazil) documented features of natural radiation staining on green diamonds from Brazil. In addition to the typical green spots on such diamonds, he showed how radioactive fluids may stain diamonds along cleavage fractures or may even 'dye' the surface of entire stones (though only to a depth of 25 µm). **Tay Thye Sun** (Far East Gemological Laboratory, Singapore) and co-authors examined the properties

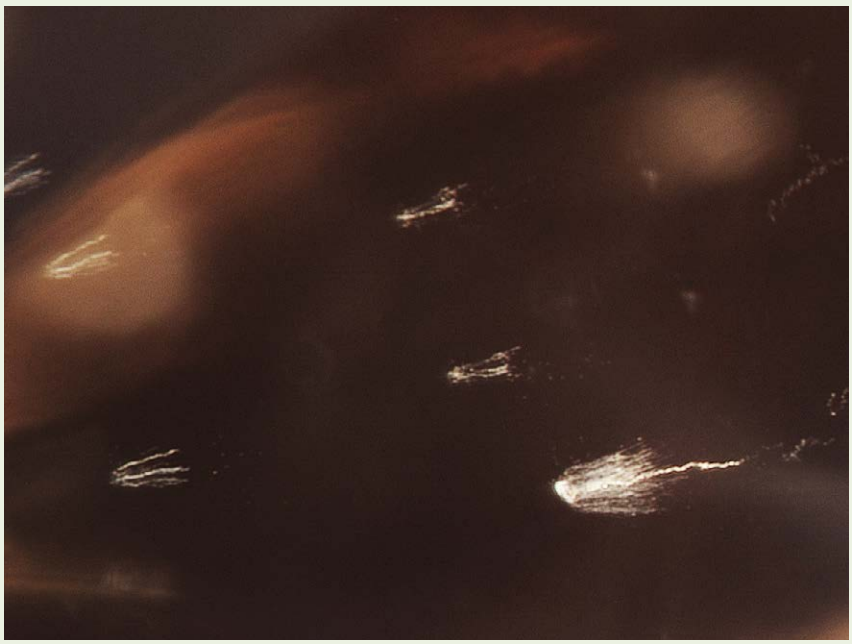

Figure 3: A 'hybrid' diamond contains jellyfish-like inclusions that nucleate at the boundary with the natural diamond and extend into the CVD synthetic diamond overgrowth. Photomicrograph by Roman Serov; image width 1.2 mm.

of diamonds from Landak River in West Kalimantan, Indonesia. They obtained samples during a visit to the mining area that ranged from colourless to yellow, brown, green and black, and most of them were type Ia (except for one that was type IIa). A photoluminescence (PL) peak of unknown origin was present in some of the diamonds at 612.4 nm.

Spinel, tourmaline and garnet were covered in the next session. **Dr Jayshree Panjikar** and **Aatish Panjikar** (PANGEMTECH, Pune, India) characterized spinel from Kermunda in Odisha State, India. The stones were mined from the soil by local villagers and tumbled into beads. They ranged from pale purplish red to dark orangey red, and UV-Vis spectroscopy revealed features related to Cr^{3+} and Fe^{2+}. Co-author **Dr Andy Shen** presented research of his PhD student **Cheng-Si Wang** (Gemmological Institute, China University of Geosciences, Wuhan, China) on reversible PL spectral features in Cr^{3+}-bearing spinel with heat treatment. Samples from Myanmar and Tanzania were heated from 200°C to 1,600°C for one hour in air, and then were quenched to room temperature, and finally were annealed to 700°C for several days (or under HPHT conditions for 45 minutes). Changes in the PL spectra that occurred during the initial heating could not be completely reversed by the annealing process, so the PL spectral criteria used to identify heated spinel were shown to be quite robust. **Dr Claudio Milisenda** and **Stefan Müller** (DSEF German Gem Lab, Idar-Oberstein) examined rare-earth element (REE) photoluminescence in Paraíba-type tourmaline from Maraca, Mozambique. Samples from this locality contain elevated Ca (and are thus liddicoatite), and PL spectroscopy showed REE features in the 850–920 nm range that were due to Nd^{3+}. By contrast, the Cu-bearing tourmaline from Mavuco (~20 km from Maraca) is elbaite and does not show REE-related PL features. **Dr Karl Schmetzer** (Petershausen, Germany) and co-authors reported on garnets from archaeological and presently known deposits in India (see article in *The Journal*, Vol. 35, No. 7, 2017, pp. 598–627).

Gem corundum was the topic of the next session. **Dr J. C. (Hanco) Zwaan** (Netherlands Gemmological Laboratory, Naturalis Biodiversity Center, Leiden) and co-authors studied the origin of sapphires from Sri Lanka (as reported in the FEEG conference report on p. 70 of this issue). **Dr Shang-i (Edward) Liu** (Gemmological Association of Hong Kong) and co-authors described the recent mining of some gem corundum deposits in Sri Lanka, including those at Kataragama, Rakwana, Hatton and Pohorabawa, and they also summarized the gemmological properties of sapphires from those localities. **Sutas Singbamroong** and co-authors (Gemstone and Precious Metal Laboratory, Dubai Central Laboratory, United Arab Emirates) documented lead-glass-filled padparadscha sapphires that appeared in December 2016 in Chanthaburi, Thailand. The stones showed typical features for this treatment, and the starting material was inferred to be fractured orangey pink corundum from East Africa. **Seung Kwon Lee** and **Kiran Kwon** (Wooshin Gemological Institute of Korea, Seoul, South Korea) performed a Raman spectroscopic study of heat-treated sapphires, and found inconclusive evidence about whether structural relaxation by impurities in the corundum is useful for identifying heat treatment.

A session on analytical techniques featured four presentations. Co-author **Walter Balmer** presented research by **Dr Michael Krzemnicki** and colleagues from the Swiss Gemmological Institute SSEF (Basel, Switzerland) on analysing trace elements and isotopes in gemstones and pearls using GemTOF (see article in *The Journal*, Vol. 35, No. 3, 2016, pp. 212–223). **Kentaro Emori** and **Dr Hiroshi Kitawaki** (Central Gem Laboratory, Tokyo, Japan) applied discriminant analysis and linear regression to trace-element data for natural and synthetic amethyst. Initial results showed that the multivariate analyses were more effective than comparing trace-element concentrations for differentiating between various geographic origins as well as natural vs. synthetic samples. **Masaki Furuya** (Japan Germany Gemmological Laboratory, Kofu, Japan) described procedures for screening synthetic diamonds from melee-sized parcels using phosphorescence imaging. In general, the parcels that Furuya encountered either contained a rather large amount of synthetics (which he inferred as intentional salting by suppliers) or had less than 1% synthetics (which were likely introduced by mistake). **Bahareh Shirdam** and **Dr Soheila Aslani** (University of Tehran, Iran) used inductively coupled plasma mass spectrometry (ICP-MS) and X-ray fluorescence spectroscopy to differentiate Persian turquoise from the historical Neyshabur area in Khorasan Province from a newer mining area at Meiduk in Kerman Province. Although certain trace elements (Cr, Fe, Zn, As and Sr) were found to be helpful in some cases for distinguishing between turquoise from the two localities, the samples' inclusions and gemmological characteristics also should be considered to make a reliable separation.

Organic gems—specifically pearls and amber—were covered in the next session. **Nick Sturman** and co-authors (GIA, Bangkok, Thailand) characterized *Pinctada maxima* non-bead cultured pearls obtained from Jewelmer's farms in Palawan, Philippines, and found six types of internal structures using real-time X-ray imaging: structure-free voids, voids containing partitions, voids surrounded by organic areas, linear voids, atypical features such as intermediate boundaries, and other features (including mixtures of these various types). **Dr Stefanos Karampelas** and co-authors (Bahrain Institute for Pearls & Gemstones [DANAT], Manama, Bahrain) examined natural pearls harvested from *Pinctada radiata* in the Kingdom of Bahrain, and found structures generally consisting of onion-skin-like layering with a darker-appearing centre; some samples also contained radial columnar structures in their core. **Elisabeth Strack** (Gemmologisches Institut Hamburg, Hamburg, Germany) described freshwater pearls from north-western Russia (see article in *The Journal*, Vol. 34, No. 7, 2015, pp. 580–592). **Dr Shang-i (Edward) Liu** studied feather and insect inclusions in Burmese amber. Biologists recently have discovered new species of ants that lived only during the Cretaceous Period, and their presence as inclusions in amber therefore provides evidence of Burmese origin.

The next session was devoted to miscellaneous gems. **Willow Wight** (Canadian Museum of Nature, Ottawa) reviewed the production and marketing of ammolite from Alberta, Canada. Korite Minerals is growing their presence in the Chinese market, and they recently expanded their mine to increase their annual production of ammolite gems from 6 million carats in 2016 to an estimated 8 million carats in 2017. **Anette Juul-Nielsen** and **Arent Heilmann** (Ministry of Mineral Resources, Nuuk, Greenland) are producing a gem occurrence map of Greenland. As part of a larger project to document mineral localities in that country, gem materials have been added since 2015 (focusing on central-western Greenland), with 300 data entries so far. **Stephen Kennedy** (Gem & Pearl Laboratory, London) and **Dr Jens Najorka** (Natural History Museum, London) studied imitations of Tianhuang and Shoushan stones. These carvings (e.g. seal stones) are highly valued in China and typically consist of compact yellow clay-mineral aggregates sourced from near Fuzhou, Fujian Province, China. X-ray powder diffraction analysis of recently encountered imitations revealed two types of chlorite, and the yellow colour of the carvings was due to dyeing. **Dr Çiğdem Lüle** (Kybele LLC, Buffalo Grove, Illinois, USA) described gemmological nomenclature and terminology challenges (as reported in the AGA conference report on p. 64 of this issue).

The final oral session was devoted to beryl, cordierite and jade. **Dr Lore Kiefert** and co-authors (Gübelin Gem Lab, Lucerne, Switzerland) described the mining and properties of emerald from Ethiopia. Local diggers began producing significant amounts of emerald in the Kenticha area of southern Ethiopia in May 2016, and numerous pits of 5–10 m depth have been dug in the sloped terrain. The emeralds are typically light coloured and have high clarity, and they exhibit gemmological and chemical properties that are consistent with stones derived from schist-hosted deposits. **Dr Karen Fox** and **Dr Chris Yakymchuk** (University of Waterloo, Canada) reviewed occurrences of gem-quality cordierite in Canada. Chemical analysis of samples from 15 localities using laser ablation ICP-MS and electron microprobe showed various amounts of overlap. **Dr Ahmadjan Abduriyim** (Tokyo Gem Science and GSTV Gemological Laboratory, Tokyo, Japan) and co-authors reviewed the history and gemmology of jadeite jade from Japan, and compared it with jadeite from other sources. Significant differences in the accessory mineral content and chemical composition (i.e. for the chromophores V, Co, Mn, Cr, Fe and Ti) were described for material from Japan (Itoigawa), Myanmar, Guatemala and Russia.

Poster presentations at the IGC covered a range of subjects related to coloured stones; those named below are the first authors (although some of them could not be in attendance and had co-authors present the research). **Dr Laurent Cartier** (Swiss Gemmological Institute SSEF) and colleagues reviewed possible strategies, opportunities and limitations of tracking gems from mine-to-market and from market-to-mine using various approaches. **Thanong Leelawatanasuk** and co-authors (GIT, Bangkok) described unusual fancy-colour sapphires from the Bo Phloi gem field in Kanchanaburi, Thailand. The samples were violet, purple, pink, green, yellow and parti-coloured, and the different colours related well to their trace-element contents. **Thanapong Lhuaamporn** and co-authors from GIT characterized high-quality untreated blue sapphires that reportedly were produced from Bo Phloi. Rather than the typical dark tone of sapphires produced from this basaltic deposit, many of the samples showed an attractive intense medium blue colour. **Dr Panjawan Thanasuthipitak** (Chiang Mai University, Thailand)

Figure 4: Namibian dealers display rough and cut gems as well as finished jewellery at the Namibian Coloured Gemstone & Jewellery Showcase, which took place in conjunction with the IGC. Photo by B. M. Laurs.

and co-authors highlighted various gem materials from northern Thailand with the potential for use in jewellery, including rock crystal, almandine, fluorite, serpentinite and silicified rhyolite. **Dr Arūnas Kleišmantas** (Vilnius University, Lithuania) and co-authors described the chemical composition (i.e. chromophores V, Cr, Fe and Co) and mineral inclusions in spinel from Sri Lanka and Vietnam. **Dr Michael Krzemnicki** and co-authors documented cobalt diffusion-treated spinel, including its coloration patterns, microscopic features, visible absorption spectra, and physical and chemical properties. **Dr Leander Franz** (University of Basel, Switzerland) and co-authors described kosmochlor-bearing jadeite rocks from Kenterlau-Itmurundy near Lake Balkhash, Kazakhstan. The samples were found to consist of jadeitites, omphacite jadeitites, phlogopite-analcime jadeitites, phlogopite-omphacite jadeitites and kosmochlor-analcime-albite-omphacite jadeitites. **Gagan Choudhary** (Gem Testing Laboratory, Jaipur, India) characterized 'Aquaprase' (blue to bluish green chalcedony) from Africa, which is coloured by Cr ± Ni impurities. **Prof. Dr Henry Hänni** described 'Sannan-Skarn', an ornamental stone from Balochistan, Pakistan, that mainly consists of calc-silicates. **Jian Mao** (Gemstone Testing Centre of ECUST, Shanghai, China) and **Elizabeth Su** (Gemsu Rona [Shanghai] Jewellery Co. Ltd, Shanghai, China) used Raman spectroscopy to identify inclusions of graphite and zircon in Myanmar jadeite. **Dr Andy Shen** and co-authors reported that the colour change exhibited by diaspore from Turkey is caused by Fe^{2+}–Ti^{4+} pairs located in adjacent edge-sharing octahedral sites in the crystal structure. **Dr John Saul** (ORYX, Paris, France) related the formation of different types of coloured stone deposits to collisional and extensional processes related to the amalgamation and breakup, respectively, of continents. **Daniel Barchewitz** (B&WTek, Lübeck, Germany) demonstrated how the GemRam portable Raman spectrometer can be used for gem identification. Both desktop and handheld models are available.

On 12–13 October, the Namibian Coloured Gemstone & Jewellery Showcase took place at the Safari Hotel in conjunction with the IGC (Figure 4). Approximately 20 dealers from throughout Namibia offered gem rough, mineral specimens, cut stones and finished jewellery. The event also featured a photo exposition, business matchmaking programme, live auction and jewellery competition.

The next IGC will take place in August 2019 in Nantes, France.

Brendan M. Laurs FGA

50TH IGE ANNIVERSARY AND 20TH FEEG SYMPOSIUM

The 50th Spanish Gemmological Institute (IGE) and 20th Federation for European Education in Gemmology (FEEG) joint conference took place on the weekend of 18–19 November 2017 in the Hall of the Gómez Pardo Foundation in Madrid, Spain. The event was attended by 125 people, and coincided with the second occurrence of ExpoGema, a Spanish gemmological fair and an exhibition of unique gems from some leading Spanish dealers and collectors. A highlight of the weekend was the FEEG Diploma Ceremony, which took place in the auditorium of the Madrid School of Mines.

Benjamin Calvo (IGE president, Madrid), **Dr Loredana Prosperi** (FEEG president, Madrid) and **Dr Egor Gavrilenko** (IGE Gem Testing Laboratory, Madrid) inaugurated the conference and workshops.

Mikko Åström and **Alberto Scarani** (Magilabs, Helsinki, Finland and Rome, Italy) reviewed the application of techniques such as Raman, photoluminescence, UV-Vis-NIR and Fourier-transform infrared spectroscopy in everyday gemmological practice.

Dr Thomas Hainschwang (GGTL-GEMLAB Laboratories, Balzers, Liechtenstein) gave an overview of the current status of diamond synthesis and treatments. He pointed out the many challenges that exist today in the distinction of natural and synthetic diamonds and in identifying the colour origin of natural diamonds.

Fabian Schmitz (German Gemmological Association, Idar-Oberstein) examined the tourmaline group, which is characterized by an extraordinary variety of colour. He discussed the different colour causes in tourmaline and explained the Usambara effect, which is a colour change (green/red) that depends on the path length of transmitted light. The longer the path length, the more red will be observed.

Dr Fernando Gervilla (Departamento de Mineralogía y Petrología e Instituto Andaluz de Ciencias de la Tierra, Universidad de Granada–Consejo Superior de Investigaciones Científicas, Granada, Spain) investigated the nature of Cr-rich inclusions in green nephrite jade, including chromian spinel with variable chemical composition, chlorite, Cr-rich zoisite and/or Cr-rich garnet. The results suggested that it might be possible to create a reference database for source-tracing studies of nephrite using specific mineralogical assemblages of 'black inclusions'.

Dr J. C. (Hanco) Zwaan (Netherlands Gemmological Laboratory, Naturalis Biodiversity Center, Leiden), explored sapphire formation in Sri Lanka. He visited a recently discovered locality for *in situ* sapphire where large corundum crystals were surrounded by plagioclase, K-feldspar and biotite. He concluded that gem-quality sapphire formation in Sri Lanka was essentially a metasomatic process, promoted by a sequence of events which included ultra-high-grade metamorphism priming the rocks, a tectonic contact that created space, and fluid/pegmatitic melt transfer from underthrusted gneisses.

Dr Ilaria Adamo (Italian Gemmological Institute, Milan) reviewed various gem localities in Italy. Val Malenco is the source of nephrite jade, gem-quality serpentine, demantoid, rhodonite and 'clinothulite' (a varietal name for the opaque pink variety of clinozoisite). Elba Island is the type locality for elbaite tourmaline. Other gems include Sardinian peridot, Sicilian simetite amber and red coral or *Corallium rubrum*, which is endemic to the Mediterranean Sea.

Geoffrey Domini (World Gem Foundation, Palma de Mallorca, Spain), explored the various instruments used in the past to identify gem materials and why they are as relevant today as they were 50 years ago.

Dr Egor Gavrilenko shared some experiences with using a coloured stone quality-grading system at the IGE Gem Testing Laboratory, and pointed out some aspects that seem problematic and need more elaboration in the future. Colour-quality grading at the laboratory is based on Gemewizard's system, clarity is evaluated by the unaided eye except for the 'Loupe clean' grade, and cut quality is mostly graded using the unaided eye as well. The most important cut parameters are light return, windowing, face-up symmetry and polish quality.

Dr Peter Lyckberg (European Commission, Brussels, Belgium) highlighted the importance of

Figure 5: Antoinette Matlins leads a workshop titled 'Gem Identification Made Easy'. Photo courtesy of IGE.

Figure 6: The diploma ceremony for new European Gemmologists was held in the auditorium of the Madrid School of Mines. Photo courtesy of IGE.

origin information for both minerals and gems. The exact origin is vital for understanding their genesis. He provided various examples, from very old deposits such as 1.7 billion-year-old Volodarsk pegmatites that yield heliodor and bicoloured topaz, to the youngest 4–23 million-year-old deposits of aquamarine and topaz in the Hindu Kush-Karakoram-Himalaya mountain ranges.

Antoinette Matlins (South Woodstock, Vermont, USA) never attends any gem or jewellery show without a Chelsea filter, a calcite dichroscope, a 10× loupe, a portable UV lamp, a flashlight and an SSEF Diamond Spotter. A trained gemmologist can identify more than 85% of gem materials with those instruments. She explained how to properly use them to avoid costly mistakes and recognize profitable opportunities.

Gail Brett Levine (National Association of Jewelry Appraisers, Rego Park, New York, USA) gave some guidelines for appraising antique-cut diamonds. Table- and point-cut diamonds are not valued individually, so one has to valuate the entire jewellery item as a whole. The same rule applies to rose cuts, although larger stones may command a premium. The past five years have seen an upsurge at auction of Old European-cut diamonds accompanied by recent GIA reports. A chipped girdle on such stones might have been repaired, which results in a modern-looking girdle, or these diamonds might have been repolished to remove abrasions. Pricing guides can be useful for tackling appraising issues.

Johann Leibbrandt (Bonhams, Madrid) presented information about his company. Bonhams was founded in London in 1793 and is today the sole international auction house that is privately owned and in British hands.

Five workshops were offered after the conference. **Mikko Åström** and **Alberto Scarani** offered hands-on experience with various spectroscopic techniques applied to gemmology. They also introduced a new tool in their line of equipment: the EXA spectrometer for identifying natural vs. synthetic diamonds. In advanced mode it is also very useful for coloured stone identification. **Dr Egor Gavrilenko** gave a workshop on basic and advanced techniques for identifying synthetic diamonds, focusing on the use of microscopic observation, anomalous birefringence, magnetism, fluorescence, phosphorescence, short-wave UV transparency and the application of various instruments (SSEF Diamond Spotter, D-Screen, DiamondSure, DiamondView and more). **Antoinette Matlins** explained the clues that portable and inexpensive gemmological tools can provide for gemstone identification (Figure 5), especially on field trips, at gem shows and in small labs. **María Milla** and **Mara Soriano** (IGE) showed the use of Macrorail equipment for the photomicrography of inclusions in gemstones. **José María Alonso Florentino**, **Benedicte Parnaudeau** and **Vicky Redondo** (IGE) offered a practical session in gem cutting and polishing.

FEEG celebrated 50 new graduates (e.g. Figure 6), bringing the total to 1,140 European Gemmologists since its start in 1996. There is a growing need to serve an expanding network of gem enthusiasts and jewellery professionals throughout the European continent, and these graduates are the future of gemmology.

The next FEEG Symposium will be held in Vicenza, Italy, in January 2019.

Dr Egor Gavrilenko and Guy Lalous
Spanish Gemmological Institute
Madrid, Spain

Gem-A Notices

Gifts to the Association

Gem-A is most grateful to the following for their generous donations which will support continued research and teaching:

Terrence Coldham, Intogems Pty Ltd, Normanhurst, New South Wales, Australia, for four imitation star stones (one blue and three red cabochons) and for a 1.13 ct faceted unheated tanzanite.

Anzor Douman, Arzawa Mineralogical lnc., Winchester, Virginia, USA, for seven demantoids from Kerman Province, Iran.

Mauro Pantò, Sassari, Italy, for a faceted yellow brucite from Pakistan and a faceted black plagioclase from Greenland.

Helen Serras-Herman FGA, Gem Art Center, Rio Rico, Arizona, USA, for a 24.38 ct pear-shaped cabochon consisting of chrysocolla, atacamite and malachite, from the Tiger mine, Arizona, USA.

Vanna Tea, Hope Gems LLC, San Jose, California, USA, for a 2.69 ct oval mixed-cut blue zircon from Cambodia.

Diploma Preparation

Gem-A has recently expanded our range of workshops and classes to includes a new Foundation-to-Diploma five-day transfer workshop. This is designed to support the transition from Foundation level to the more intense Diploma course, and includes a full review of all instruments as well as some of the science behind gemstones. This is especially valuable to those students who may have had to step away from their studies for a little while, and who consequently might feel less confident about returning to the classroom. It also may be taken by those who would just like a quick brush up of their practical and theoretical skills. Please contact education@gem-a.com for more information.

New Position at Gem-A: Head of Education

As part of our ongoing commitment to progress, Gem-A is now looking to appoint a new full time Head of Education at its headquarters in London. Located in the heart of London's historic jewellery district, this is an exciting opportunity to be an integral part of a successful and growing global organisation. As the world's longest established provider of gem and jewellery education, our prestigious and internationally recognised Gemmology and Diamond Diplomas are taught in seven different languages and 26 countries around the world. While this role will be primarily based in London, Gem-A forms an international community of gem professionals and enthusiasts, and this new position offers the opportunity for significant international and UK travel. Please visit www.gem-a.com/jobs for more information.

New Professorship in Gemmology at University of Arizona

The RealReal, a leading authenticated luxury consignment company, has recently announced a first-of-its-kind collaboration with the University of Arizona (Tucson, Arizona, USA) to create an endowed chair in gemmology. This now enables the creation of a long-awaited degree program in geosciences with a concentration in gemmology. Offering a full curriculum of undergraduate, master's and PhD programs, as well as scientific research, the University of Arizona and The RealReal also have partnered with Gem-A to offer students the opportunity to obtain Gem-A diploma certifications. The University is currently looking to appoint a professor to this prestigious position, and Gem-A will keep our members updated on how this ground-breaking venture is progressing.

Save the Date: Gem-A Conference 2018

This year's annual Gem-A Conference will take place from 3–4 November 2018, at etc.venues County Hall, Central London. The Gem-A Conference offers an amazing line-up of speakers from all corners of gemmology, exclusive workshops and trips including private viewings of museum collections, and the opportunity to network with some of the leaders in the field. Please visit www.gem-a.com/event/conference for video highlights from the 2017 Conference, and for future announcements on 2018 Conference registration.

Learning Opportunities

CONFERENCES AND SEMINARS

8th Annual International Gold Conference – Gold: Vortex, Virtues, and Values
12–13 April 2018
New York, New York, USA
https://iacgold2018.eventbrite.com

15th Annual Sinkankas Symposium – Tanzanite & Tsavorite
14 April 2018
Carlsbad, California, USA
www.sinkankassymposium.net

2nd International Conference and Expo on Diamond, Graphite & Carbon Materials
16–17 April 2018
Las Vegas, Nevada, USA
http://diamond-carbon.conferenceseries.com/symposium.php

45th Rochester Mineralogical Symposium
19–22 April 2018
Rochester, New York, USA
www.rasny.org/minsymp

American Gem Society Conclave
23–25 April 2018
Nashville, Tennessee, USA
www.americangemsociety.org/page/conclave2018

Scottish Gemmological Association Conference
4–6 May 2018
Cumbernauld, Scotland
www.scottishgemmology.org/conference

4th Mediterranean Gem and Jewellery Conference
18–20 May 2018
Budva, Montenegro
www.gemconference.com
Note: Will include workshops on ruby and sapphire, emerald, and diamond, as well as diamond identification with advanced instruments

32nd Annual Santa Fe Symposium
20–23 May 2018
Albuquerque, New Mexico, USA
www.santafesymposium.org

12th International New Diamond and Nano Carbons Conference
20–24 May 2018
Flagstaff, Arizona, USA
www.mrs.org/ndnc-2018

Society of North American Goldsmiths' 47th Annual Conference
23–26 May 2018
Portland, Oregon, USA
www.snagmetalsmith.org/conferences/made

AGA Las Vegas Conference
1 June 2018
Las Vegas, Nevada, USA
http://accreditedgemologists.org

JCK Las Vegas
1–4 June 2018
Las Vegas, Nevada, USA
http://lasvegas.jckonline.com/en/Events/Education
Note: Includes a seminar programme

17èmes Rendez Vous Gemmologiques de Paris
11 June 2018
Paris, France
www.afgems-paris.com/rdv-gemmologique
Note: Simultaneous English-French translation will be provided.

Diamonds – Source to Use 2018
11–14 June 2018
Johannesburg, South Africa
www.saimm.co.za/saimm-events/upcoming-events/saimm-diamonds-source-to-use-2018

14th Biennial Pan American Conference on Research on Fluid Inclusions (PACROFI XIV)
12–14 June 2018
Houston, Texas, USA
www.pacrofi.com

RFG2018 Resources for Future Generations: CIM-GAC-MAC Joint Meeting
16–21 June 2018
Vancouver, British Columbia, Canada
www.rfg2018.org
Session of interest: New Developments in Canadian Diamond Exploration – Finding the Next Generation of Diamond Deposits

Sainte-Marie-aux-Mines 55th Mineral & Gem Show
21–24 June 2018
Sainte-Marie-aux-Mines, France
www.sainte-marie-mineral.com/english/modules/cultural-activities
Note: Includes a seminar programme

Northwest Jewelry Conference
10–12 August 2018
Seattle, Washington, USA
www.northwestjewelryconference.com

22nd Meeting of the International Mineralogical Association
13–17 August 2018
Melbourne, Victoria, Australia
www.ima2018.com
Sessions of interest:
- Mantle Xenoliths, Kimberlites and Related Magmas: The Diamond Trilogy
- Pegmatite Mineralogy, Geochemistry, Classification and Origins
- Recent Advances in our Understanding of Gem Minerals
- Sciences Behind Gemstone Treatments

Dallas Mineral Collecting Symposium
24–26 August 2018
Dallas, Texas, USA
www.dallassymposium.org

IJL London
2–4 September 2018
London
www.jewellerylondon.com/Whats-On/Seminars
Note: Includes a seminar programme

29th International Conference on Diamond and Carbon Materials
2–6 September 2018
Dubrovnik, Croatia
www.elsevier.com/events/conferences/international-conference-on-diamond-and-carbon-materials

Hong Kong Jewellery & Gem Fair
12–18 September 2018
Hong Kong
http://exhibitions.jewellerynetasia.com/9jg/en-us/specialevents
Note: Includes a seminar programme

2018 GIA Symposium: New Challenges. Creating Opportunities
7–9 October 2018
Carlsbad, California, USA
http://discover.gia.edu/symposium

Munich Mineral Show
26–28 October 2018
Munich, Germany
https://munichshow.com/en
Note: Includes a seminar programme

Swiss Geoscience Meeting
30 November–1 December 2018
Bern, Switzerland
https://geoscience-meeting.ch
Note: Includes a gemmology session

EXHIBITIONS

Asia and Middle East

Art & Jewelry
Until 2 June 2018
Custot Gallery, Dubai, United Arab Emirates
www.custotgallerydubai.ae/copie-de-black-white

Australia and New Zealand

Cartier: The Exhibition
Until 22 July 2018
National Gallery of Australia, Canberra, Australia
https://nga.gov.au/cartier

Europe

Gold! Collected by Sophia Lopez Suasso
Until 2 April 2018
Cromhout Huis, Herengracht, Amsterdam, The Netherlands
www.cromhouthuis.nl/en/activities/gold-collected-sophia-lopez-suasso

Splendours of the Subcontinent: A Prince's Tour of India, 1875–6
Until 22 April 2018
The Queen's Gallery, Palace Holyroodhouse, Edinburgh, Scotland
www.royalcollection.org.uk/whatson/event/831418/Splendours-of-the-Subcontinent

Modernist Jewellery
Until 29 April 2018
National Museum of Scotland, Edinburgh
www.nms.ac.uk/national-museum-of-scotland/whats-on/modernist-jewellery

Fibulae
Until 3 June 2018
Rijksmuseum, Amsterdam, The Netherlands
www.rmo.nl/english/exhibitions/fibulae

Jewellery: Made By, Worn By
Until 3 June 2018
Museum Volkenkunde, Amsterdam, The Netherlands
https://volkenkunde.nl/en/exhibition-jewellery-madeby-wornby

Eva's Beauty Case & Adam's Necessaire. Schmuck und Styling im Spiegel der Zeiten
Until 12 August 2018
Braunschweigisches Landesmuseum, Braunschweig, Germany
www.3landesmuseen.de/Eva-s-Beauty-Case-Adam-s-Necessaire.1649.0.html

East Meets West – Exquisite Treasures from the Aga Khan Collection
5 May 2018–6 January 2019
Schmuckmuseum Pforzheim, Germany
www.schmuckmuseum.de/flash/SMP_en.html

The Splendour of Power
6 May–30 September 2018
Museet på Koldinghus, Kolding, Denmark
www.koldinghus.dk/uk/exhibitions-2017/the-splendour-of-power-2018.aspx

North America

Beads: A Universe of Meaning
Until 15 April 2018
The Wheelwright Museum of the American Indian, Santa Fe, New Mexico, USA
https://wheelwright.org/exhibitions/beads

Louis Comfort Tiffany: Treasures from the Driehaus Collection
Until 27 May 2018
Taft Museum, Cincinatti, Ohio, USA
www.taftmuseum.org/cur_exhib

Golden Kingdoms: Luxury and Legacy in the Ancient Americas
Until 28 May 2018
The Met Fifth Avenue, New York, New York, USA
www.metmuseum.org/exhibitions/listings/2018/golden-kingdoms

Jewelry of Ideas: Gifts from the Susan Grant Lewin Collection
Until 28 May 2018
Cooper Hewitt, Smithsonian Design Museum, New York, New York, USA
www.cooperhewitt.org/channel/jewelry-of-ideas

Fabergé and the Russian Crafts Tradition: An Empire's Legacy
Until 24 June 2018
The Walters Art Museum, Baltimore, Maryland, USA
https://thewalters.org/events/event.aspx?e=4769

'Modern Gem & Jewelry Collection' Presented by Somewhere in the Rainbow
Until July 2018
Flandrau Science Center & Planetarium, University of Arizona, Tucson, Arizona, USA
https://flandrau.org/exhibits/somewhere-rainbow

Peacock in the Desert: The Royal Arts of Jodhpur, India
Until 19 August 2018
The Museum of Fine Arts, Houston, Texas, USA
www.mfah.org/exhibitions/peacock-in-desert-royal-arts-jodhpur-india

Crowns of the Vajra Masters: Ritual Art of Nepal
Until 16 December 2018
The Met Fifth Avenue, New York, New York, USA
www.metmuseum.org/exhibitions/listings/2017/crowns-of-vajra-masters

Past is Present: Revival Jewelry
Until 19 August 2018
Museum of Fine Arts, Boston,
Massachusetts, USA
www.mfa.org/news/past-is-present-revival-jewelry

American Jewelry from New Mexico
2 June–14 October 2018
Albuquerque Museum, New Mexico, USA
www.cabq.gov/culturalservices/albuquerque-museum/exhibitions/american-jewelry

Fabergé Rediscovered
9 June 2018–13 January 2019
Hillwood Estate, Museum & Gardens,
Washington DC, USA
www.hillwoodmuseum.org/exhibitions/faberg%C3%A9-rediscovered

OTHER EDUCATIONAL OPPORTUNITIES

Gem-A Workshops and Courses
Gem-A, London
www.gem-a.com/education/courses/workshops

American Society of Appraisers Courses
- Jewelry Forensics for Appraisers
  7–8 May 2018
  Gemological Institute of America,
  Carlsbad, California, USA
  www.appraisers.org/Education/View-Course?CourseID=623

- Appraising Gems and Jewelry for Insurance Coverage
  9–11 May 2018
  Gemological Institute of America, Carlsbad,
  California, USA
  www.appraisers.org/Education/View-Course?CourseID=448

Jewelry and Decorative Arts Tour of Israel
21–30 April 2018
The Jewelry Center, New York,
New York, USA
www.92y.org/class/arts-tour-of-israel

Introduction to Gemstones
6 June, 15 August, 4 October or 13 December 2018
London Jewellery School, London
www.londonjewelleryschool.co.uk/taster-classes/introduction-to-gemstones

Lectures with Gem-A's Midlands Branch
Fellows Auctioneers, Birmingham
Email louiseludlam@hotmail.com
- 27 April 2018
  James Gosling—Cravat Pins & Tie Pins: The Chronological and Gemmological Development of these Beautiful and Almost Forgotten Items of Jewellery

Lectures with The Society of Jewellery Historians
Society of Antiquaries of London,
Burlington House, London
www.societyofjewelleryhistorians.ac.uk/current_lectures
- 24 April 2018
  Dr Zara Power Florio—All that Glitters: Jewellers and Gems in Georgian Ireland
- 26 June 2018
  Tara Kelly—Purchasing the Past: Consumers of Irish Facsimile Jewellery, 1840–1940
- 25 September 2018
  Christopher Thompson Royds—My Work as a Jeweller
- 23 October 2018
  Anna Tabakhova—Clasps: 4000 years of Fasteners in Jewellery
- 27 November 2018
  Helen Ritchie—Designers and Jewellery: Jewellery and Metalwork from the Fitzwilliam Museum, 1850–1950

Compiled by Sarah Salmon and Brendan Laurs

New Media

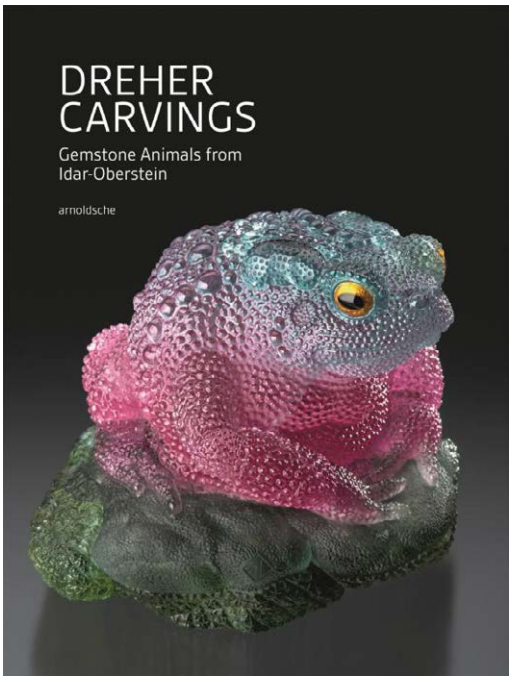

Dreher Carvings: Gemstone Animals from Idar-Oberstein

Ed. by Johanna Eberl, 2017. Arnoldsche Art Publishers, Stuttgart, Germany, www.arnoldsche.com/en/New-Books/dreher-carvings.html, 240 pages, illus., ISBN 978-3897905078. €48.00 hardcover.

This volume starts with the compilation of a number of relatively short passages by various authors, each of which gives a summary of a topic related to the gem carvings created by the Dreher family in Idar-Oberstein, Germany. Following a Foreword by Dieter Hahn and Jörg Lindemann of the German Gemstone Museum, Oleg Gerdt prepared the first contribution, 'Idar-Oberstein, a Gemstone of Europe'. He outlines the historical development of Idar-Oberstein and its gem industry, which was based on 400-million-year-old deposits of agate, jasper and amethyst. These were known to the ancient Romans, but first references to large-scale production date from the 14th century. The first water-driven lapidary mill was recorded in 1454, and the secrets of the gem cutters were closely guarded by their guild. The activities only declined with the depletion of the agate deposits and the arrival of Napoleon. Fortunately, the discovery of Brazilian agates and the development of their coloration techniques led to a revival, and Idar-Oberstein became the leading cutting and carving centre technologically and an important furnisher for luxury firms such as Fabergé.

In this line of tradition, Wilhelm Lindemann then describes 'Gerd and Patrick Dreher – The Art of Stonecutting Today'. While mainly cameos, seals, etc. have been engraved since antiquity, stone sculptures have been created since the Renaissance and Mannerist eras, mostly in France (Paris) and Idar-Oberstein. Stone carving no longer just meant copying templates but expressing oneself as an artist. Parallel to the development of Idar-Oberstein as a jewellery furnishing centre, carving artists appeared in the 19th century, but only after Fabergé's times were they recognized as such. The Dreher family is a good example of this development. Today, Gerd and Patrick are the first members of the family who sign their creations.

Will Larson and Gerd Dreher co-wrote the section titled 'Five Generations of Gemstone Carving: The Dreher Family'. They provide a portrait of the family history from simple stonecutters and carvers to outstanding artists, including their relation with Fabergé, their specialization in animal carvings and their international activities, such as various expositions.

In 'The Dreher Family Cultural Code', Mikhail Ovchinnikov focuses on the development and mutual influence of the Idar-Oberstein carvers and the Russian tradition of gem carving, especially in St Petersburg, as well as other influences visible in the Drehers' creations (e.g. Japanese netsuke).

Ekkehard Schneider then describes 'The Process of Carving a Gemstone'. This process has depended on the development of carving techniques and tools, always of great importance for the quality of the carvings. Thus, finer tools made much more precise carvings possible. Especially since the 1970s, fine diamond tools allowed great steps forward.

Robert Weldon contributed 'Photographers Delight: Capturing a "Living" Dreher Carving'. Taking photos means representing three-dimensional objects with a two-dimensional medium. This makes it difficult to capture the manifold forms, surfaces, movements, colours and expressions with the appropriate choice of background, lighting, perspective and detail.

The text part of the volume ends with a two-page spread titled 'Step by Step: A Gemstone Animal Comes to Life'. Several photos illustrate the five-step process of carving an obsidian hippopotamus, from

rough fashioning of the overall form with a diamond saw to finer and finer elaboration of details to the final polishing of the surface.

Elsewhere in the volume, various 'Homages' by Raquel Alonso-Perez, Anton Ananiev, Maxim Artsinovich, Galina Gabriel, Alan Hart, Johannes Keilmann, Bill Larson, Carl Larson, Will Larson, Robert Myers, and Rüdiger Pohl relate stories of their personal acquaintance and friendship with the Drehers. Finally, a list of selected exhibitions and television documentaries rounds off the book.

The remaining three quarters of the volume are dedicated to 'Wildlife in Gemstones', which is a fantastic gallery of some 200 colour photos showing the range of animal carvings created by Gerd and Patrick Dreher. They contain a complete zoo: snails and toads, starfish and sea horses, fish and otters, mice and mallards, cockatoos and bears, hippopotamuses and warthogs, horses, gorillas and chimpanzees. While some of them, such as the mallard, are composed of various stone species (like the Fabergé carvings), most are carved out of a single block of rough. For the latter pieces, the artist uses the potentialities of the stone in a precise manner so that the colours and structures of the rough form specific parts of the animal, as well as the base it is sitting on. What cannot be described adequately, but can be shown by the photos, is the way in which the typical movement and posture of the animals is captured in the carvings. A perfect example of this is the carving of two playing otters on p. 122.

Although quite a number of Dreher carvings are made from valuable gem materials—such as ruby in zoisite, various beryls and tourmaline—most of their works are executed in less expensive stones such as obsidian, jasper, agate, rock crystal and other quartzes. This gives the viewer a greater appreciation of how incredibly artfully the character of the animals is captured. A good example of this is a mouse on a mushroom that is carved in smoky quartz (pp. 84–85). But don't come too close! Maybe it will run away...

When I was asked about reviewing *Dreher Carvings*, I didn't know very much about them. Carved gems had never been the focus of my interest as a collector, but this has changed dramatically. Now I am an absolute fan, and as the book is so much more affordable than the actual carvings, I certainly recommend buying it.

Dr Rolf Tatje
Duisburg, Germany

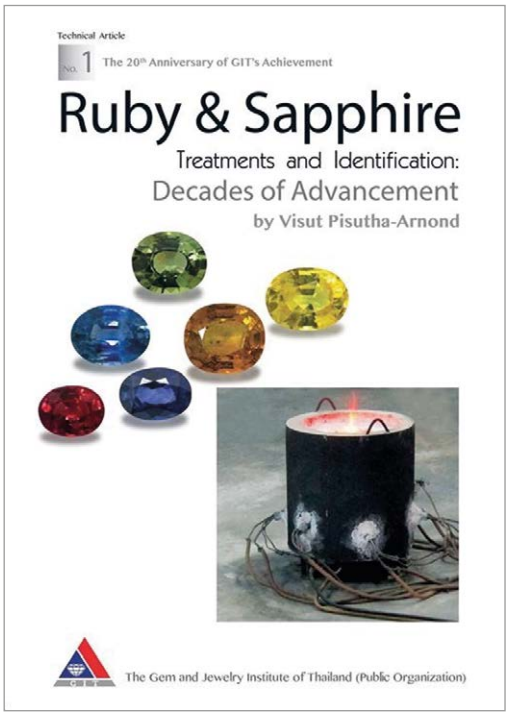

Ruby & Sapphire – Treatments and Identification: Decades of Advancement

Visut Pisutha-Arnond, 2017. Technical Article No. 1, Gem and Jewelry Institute of Thailand, Bangkok, www.git.or.th/bookstore/product_detail.aspx?lang=en&pid=80&ptype=book, 95 pp., illus., ISBN 978-6169145097. US$15.00 softcover.

Heat treatment of corundum is probably the most important and controversial treatment performed on coloured stones, and constant developments are reported. Because of this importance, a multitude of articles and books have been dedicated to this subject during the past few decades.

This booklet by Dr Pisutha-Arnond consists of 90 pages of text, plus an extensive reference list, and is the first in a series of special Technical Articles that the Gem and Jewelry Institute of Thailand plans to publish for their 20th anniversary. It describes classical heat treatment, high-temperature heating with and without flux, low-temperature heat treatment, heating with the addition of elements such as Ti, Cr, Be and Pb (with or without colorants), as well as a relatively new treatment that involves high-pressure and temperature conditions in the presence of water. It also briefly mentions other treatments used to enhance corundum.

The author gives a thorough overview of the

mechanisms taking place within corundum during the various types of heat treatment (using triangular diagrams to help explain the formation of certain colours), describes the heating processes themselves and shows images of microscopic features useful for detecting these treatments. This section also explains spectroscopic features and chemical properties associated with the various treatments, such as changes in FTIR and UV-Vis spectra, and the addition of chemical elements not intrinsic to corundum.

It is obvious from the text that the writer is not a native English speaker, which sometimes makes it difficult to read through the material. In addition, the illustrated UV-Vis spectra have varying wavelength ranges—with the narrowest range spanning 350–750 nm and the widest range covering 300–1500 nm, as well as other ranges in between—which makes it difficult to compare the spectra at first glance.

Overall, however, the booklet provides a good compilation of information on corundum treatments, including the newest developments, with relevant illustrations and graphs. I recommend it for the interested student as well as for practicing gemmologists. Hopefully some improvements could be made to the English and the graphs in a second edition.

Dr Lore Kiefert FGA
Gübelin Gem Lab, Lucerne, Switzerland

Other Book Titles

COLOURED STONES

Collector's Guide to Silicates: Di- and Ring Silicates
By Robert J. Lauf, 2017. Schiffer Publishing, Atglen, Pennsylvania, USA, 272 pages, ISBN 978-0764354366. US$45.00 hardcover.

DIAMOND

Carbon: The Black, the Gray and the Transparent
By Tapan Gupta, 2018. Springer, Cham, Switzerland, 319 pages, ISBN 978-3319664040. US$129.00 hardcover or $99.00 eBook.

GEM LOCALITIES

Lake Superior Agates
By James Magnuson, 2018. Adventure Publications, Cambridge, Minnesota, USA, 22 pages, ISBN 978-1591938088. US$9.95 spiral-bound.

GENERAL REFERENCE

Fleischer's Glossary of Mineral Species, 12th edn.
By Malcolm Back, 2018. Mineralogical Record Inc., Tucson, Arizona, USA, 424 pages. US$38.00 softcover.

Rock Explorer: Gems
By Claudia Martin, 2018. QED Publishing, London, 24 pages, ISBN 978-1784939632. £6.99 softcover.

JEWELLERY HISTORY

American Baroque: Pearls and the Nature of Empire, 1492–1700
By Molly A. Warsh, 2018. Omohundro Institute of Early American History and Culture and the University of North Carolina Press, Chapel Hill, North Carolina, USA, 304 pages, ISBN 978-1469638973. US$39.95 hardcover.

Bejewelled: Men and Jewellery in Tudor and Jacobean England
By Natasha Awais-Dean, 2017. The British Museum, London, 165 pages, ISBN 978-0861592098. £40.00 softcover.

Engraved Gems: From Antiquity to the Present
Ed. by Ben J. L. van den Bercken and Vivian C. P. Baan, 2017. *Papers on Archaeology of the Leiden Museum of Antiquities (PALMA)* 14, Sidestone Press, Leiden, The Netherlands, 184 pages, ISBN 978-9088905063. €120.00 hardcover, €39.95 softcover or €9.95 eBook.

Natter's Museum Britannicum: British Gem Collections and Collectors of the Mid-Eighteenth Century
By John Boardman, Julia Kagan and Claudia Wagner, 2018. Archaeopress Archaeology, Oxford, 316 pages, ISBN 978-1784917272. £55.00 hardcover.

Treasures of the Mughals and the Maharajas: The Al Thani Collection
By Amin Jaffir and Gian Carlo Claza, 2018. Skira Editore, Milan, Italy, 304 pages, ISBN 978-8857235943. €60.00 hardcover.

JEWELLERY AND *OBJETS D'ART*

1990s Jewellery: The Hans Schullin Collection
By Sophie Beer and Hans Schullin, 2018. Arnoldsche Art Publishers, Stuttgart, Germany, 128 pages, ISBN 978-3897904842. €28.00 hardcover.

Art as Jewellery: From Calder to Kapoor
By Louisa Guinness, 2018. ACC Art Books, Suffolk, 336 pages, ISBN 978-1851498703. £45.00 hardcover.

Bulgari: Treasures of Rome
By Vincent Meylan, 2018. ACC Art Books, Suffolk, 296 pages, ISBN 978-1851498796. £55.00 hardcover.

Chaumet: Arts, Photography, Fêtes
By Antoine de Baecque, Gabriel Bauret and Jerome Neutres, 2017. Assouline Publishing, New York, New York, USA, 80 pages, ISBN 978-1614286233. US$75.00 hardcover box set.

Ebbe Weis-Weingart: 70 Years of Jewellery
By Christianne Weber-Stöber, Sabine Runde, Peter Schmitt and Christoph Engel, 2018. Arnoldsche Art Publishers, Stuttgart, Germany, 208 pages, ISBN 978-3897905092. €44.00 hardcover.

Fabergé and the Russian Crafts Tradition: An Empire's Legacy
By Margaret Trombly, 2017. Thames & Hudson, London, 224 pages, ISBN 978-0500480229. £18.49 hardcover.

Gianfranco Ferré – Under Another Light: Jewels and Ornaments
By Francesca Alfano Miglietti, 2018. Skira Editore, Milan, Italy, 276 pages, ISBN 978-8857236698. €45.00 softcover.

Gianmaria Buccellati Foundation: A Century of Goldsmith's Art
By Gianmaria Buccellati, 2018. Skira Editore, Milan, Italy, 320 pages, ISBN 978-8857234366. €76.93 hardcover.

Gemologue: Street Jewellery Styles & Styling Tips
By Liza Urla, 2018. ACC Art Books, Suffolk, 354 pages, ISBN 978-1851498819. £25.00 softcover.

Jewellery Matters
By Marjan Unger, 2018. NAI Publishers, Rotterdam, The Netherlands, 520 pages, ISBN 978-9462083752. €39.95 hardcover.

Jewelry of Ideas: The Susan Grant Lewin Collection
By Ursula Ilse-Neuman, 2018. Arnoldsche Art Publishers, Stuttgart, Germany, 176 pages, ISBN 978-3897905122. €28.00 hardcover.

Peacock in the Desert: The Royal Arts of Jodhpur, India
By Karni Jasol, 2018. Museum of Fine Arts, Houston, Texas, USA, 288 pages, ISBN 978-0300232967. US$85.00 hardcover.

Stuart Devlin: Designer Goldsmith Silversmith
By Carole Devlin and Victoria Kate Simkin, 2018. ACC Art Books, Suffolk, 528 pages, ISBN 978-1851498727. £75.00 hardcover.

Traditional Indian Jewellery: The Golden Smile of India
By Bernadette van Gelder, 2017. ACC Art Books, Suffolk, 608 pages, ISBN 978-1851498536. £125.00 hardcover.

MISCELLANEOUS

The Denver Gem & Mineral Show: A Retrospective
By Mark Ivan Jacobson, 2017. Greater Denver Area Gem and Mineral Council Inc., Denver, Colorado, USA, 144 pages, ISBN 978-0692939918. US$14.00 softcover.

Compiled by Sarah Salmon and Brendan Laurs

Literature of Interest

COLOURED STONES

Accurate reporting of key trace elements in ruby and sapphire using matrix-matched standards. J. Stone-Sundberg, T. Thomas, Z. Sun, Y. Guan, Z. Cole, R. Equall and J.L. Emmett, *Gems & Gemology*, **53**(4), 2017, 438–451, http://dx.doi.org/10.5741/gems.53.4.438.*

The absorption- and luminescence spectra of Mn^{3+} in beryl and vesuvianite. M. Czaja, R. Lisiecki, A. Chrobak, R. Sitko and Z. Mazurak, *Physics and Chemistry of Minerals*, 2017, 14 pp., http://dx.doi.org/10.1007/s00269-017-0934-x.*

Colored gemstones. It's now time to sell cut. J. Dyer, *Rivista Italiana di Gemmologia/Italian Gemological Review*, No. 3, 2018, 49–56.

Gemmological characteristic comparison of aquamarines from four different origins. T. Wu and Z. Yin, *Journal of Gems & Gemmology*, **19**(3), 2017, 35–44 (in Chinese with English abstract).

Gemmological characteristic and identification of gem-quality benitoite. S. Xu and X. Shi, *Journal of Gems & Gemmology*, **19**(2), 2017, 49–56 (in Chinese with English abstract).

Inclusions in natural, synthetic, and treated ruby. N.D. Renfro, J.I. Koivula, J. Muyal, S.F. McClure, K. Schumacher and J.E. Shigley, *Gems & Gemology*, **53**(4), 2017, 457–458, http://dx.doi.org/10.5741/gems.53.4.457.*

LA-ICP-MS U–Pb dating of rutile inclusions within corundum (ruby and sapphire): New constraints on the formation of corundum deposits along the Mozambique Belt. E.S. Sorokina, D. Rösel, T. Häger, R. Mertz-Kraus and J.M. Saul, *Mineralium Deposita*, **52**(5), 2017, 641–649, http://dx.doi.org/10.1007/s00126-017-0732-x.

Silica colloid ordering in a dynamic sedimentary environment [Australian opal]. M. Liesegang and R. Milke, *Minerals*, **8**(1), 2018, 12 pp., http://dx.doi.org/10.3390/min8010012.*

Study on the spectral characteristics and the alexandrite effect of diaspore. D. Zhou, T. Lu, J. Ke, H. Chen, G. Shi and K. Li, *Spectroscopy and Spectral Analysis*, **37**(11), 2017, 3504–3509 (in Chinese with English abstract).

CULTURAL HERITAGE

Amber, beads and social interaction in the late prehistory of the Iberian Peninsula: An update. C.P. Odriozola, A.C. Sousa, R. Mataloto, R. Boaventura, M. Andrade, R. Villalobos García, J.Á. Garrido-Cordero, E. Rodríguez, J.M. Martínez-Blanes, M.Á. Avilés, J. Daura, M. Sanz and J.A. Riquelme, *Archaeological and Anthropological Sciences*, 2017, 29 pp., http://dx.doi.org/10.1007/s12520-017-0549-7.

Daryā-ye Nur: History and myth of a crown jewel of Iran. A. Malecka, *Iranian Studies*, **51**(1), 2017, 69–96, http://dx.doi.org/10.1080/00210862.2017.1362952.

Gemmes et sculptures anciennes du Proche-Orient (Ancient gems and sculptures from the Middle East). H.-J. Schubnel, *Revue de Gemmologie A.F.G.*, No. 201, 2018, 17–24 (in French).

Mechanical engineering in ancient Egypt, part 58: Semiprecious stones applications. G.A. Hassaan, *International Journal of Emerging Engineering Research and Technology*, **5**(9), 2017, 20–31, www.ijeert.org/papers/v5-i9/3.pdf.*

Preserving the heritage of gemstone regions and resources worldwide: Future directions. L. Cartier, *InColor*, No. 37, 2018, 74–78, www.incolormagazine.com/incolor/37/74.*

Restitution de «vingt des plus beaux diamants» de Tavernier vendus à Louis XIV. Partie 2 : Les nouvelles découvertes (Restitution of "twenty of the most beautiful diamonds" Tavernier sold to Louis XIV. Part 2: The new discoveries). F. Farges, P. Dubuc and M. Vallanetdelhom, *Revue de Gemmologie A.F.G.*, No. 201, 2018, 26–31 (in French).

DIAMONDS

Crystal morphological evolution of growth and dissolution of curve-faced cubic diamonds from placers of the Anabar diamondiferous region. A.D. Pavlushin, D.A. Zedgenizov and K.L. Pirogovskaya, *Geochemistry International*, **55**(12), 2017, 1193–1203, http://dx.doi.org/10.1134/s0016702917090051.

Diamond miners respond. S. Walker, *Engineering and Mining Journal*, **218**(9), 2017, 58–66, http://emj.epubxp.com/i/872627-sep-2017.*

Diamond with unusual Diamond View [*sic*] fluorescence pattern. M. Chauhan, *Rivista Italiana di Gemmologia/Italian Gemological Review*, No. 3, 2018, 30–31.

Discussion on diamond color grading system. Y. Cheng, H. Liu, C. Fan, C. Zhang, Y. Wang and Q. Jia, *Journal of Synthetic Crystals*, **46**(1), 2017, 174–177 (in Chinese with English abstract).

Evidence for large scale fractionation of carbon isotopes and of nitrogen impurity during crystallization of gem quality cubic diamonds from placers of north Yakutia. V.N. Reutsky, A.A. Shiryaev, S.V. Titkov, M. Wiedenbeck and N.N. Zudina, *Geochemistry International*, **55**(11), 2017, 988–999, http://dx.doi.org/10.1134/s001670291711009x.

Measurement and analysis of diamond fluorescent emission colour under 365 nm ultraviolet excitation. W. Wu, B. Shi and Z. Xu, *Journal of Gems & Gemmology*, **19**(1), 2017, 38–44 (in Chinese with English abstract).

Mineral inclusions in diamonds may be synchronous but not syngenetic. F. Nestola, H. Jung and L.A. Taylor, *Nature Communications*, **8**, article 14168, 2017, 6 pp., http://dx.doi.org/10.1038/ncomms14168.*

Nanosculptures on round surfaces of natural diamonds. A.A. Chepurov, S.S. Kosolobov, D.V. Shcheglov, V.M. Sonin, A.I. Chepurov and A.V. Latyshev, *Geology of Ore Deposits*, **59**(3), 2017, 256–264, http://dx.doi.org/10.1134/s1075701517030023.

Non-destructive in situ study of plastic deformations in diamonds: X-ray diffraction topography and μFTIR mapping of two super deep diamond crystals from São Luiz (Juina, Brazil). G. Agrosì, G. Tempesta, G. Della Ventura, M. Cestelli Guidi, M. Hutchison, P. Nimis and F. Nestola, *Crystals*, **7**(8), article 233, 2017, 11 pp., http://dx.doi.org/10.3390/cryst7080233.*

Spectral characteristics and concentration quantitative analysis of NV center ensembles in diamond. F. Wang, Z. Ma, M. Zhao, Z. Lin, S. Zhang, Z. Qu, J. Liu and Y. Li, *Spectroscopy and Spectral Analysis*, **37**(5), 2017, 1477–1481 (in Chinese with English abstract).

Study on the CL and FTIR spectra of the alluvial diamond from western Yangtze Craton and its significance in the growth rate analysis of the diamond. Z. Yang, W. Zhou, X. Zeng, S. Huang, X. Li and Y. Chen, *Spectroscopy and Spectral Analysis*, **37**(6), 2017, 1739–1744 (in Chinese with English abstract).

The very deep origin of the world's biggest diamonds. E.M. Smith, S.B. Shirey and W. Wang, *Gems & Gemology*, **53**(4), 2017, 388–403, http://dx.doi.org/10.5741/gems.53.4.388.*

GEM LOCALITIES

Characteristic of growth zone of emerald from Malipo, Yunnan Province. Y. Zou, W. Sun, X. Zhao and D. Wang, *Bulletin of the Chinese Ceramic Society*, **36**(2), 2017, 419–424 (in Chinese with English abstract).

Colour origin of dark green tourmaline from Zambia. P. Zhong and A.H. Shen, *Journal of Gems & Gemmology*, **19**(6), 2017, 7–14 (in Chinese with English abstract).

Colour origin of green chalcedony from Taiwan. Z. Zhou and L. Li, *Journal of Gems & Gemmology*, **19**(2), 2017, 34–40 (in Chinese with English abstract).

Corundum formation by metasomatic reactions in Archean metapelite, SW Greenland: Exploration vectors for ruby deposits within high-grade greenstone belts. C. Yakymchuk and K. Szilas, *Geoscience Frontiers*, 2017, 24 pp., http://dx.doi.org/10.1016/j.gsf.2017.07.008.*

Fluid inclusion studies on emeralds from Malipo area, Yunnan Province, China. W. Huang, T. Shui and P. Ni, *Acta Mineralogica Sinica*, **37**(1), 2017, 75–83 (in Chinese with English abstract).

Gem deposits of Myanmar. K. Thu and K. Zaw, in A.J. Barber, K. Zaw and M.J. Crow, Eds., *Myanmar: Geology, Resources and Tectonics*, Geological Society of London Memoir 48, Geological Society of London, 2017, 497–529, http://dx.doi.org/10.1144/m48.23.

Gemmological and spectral characteristic of ruby from Yen Bai, Vietnam. Q. Wang and J. Di, *Journal of Gems & Gemmology*, **19**(4), 2017, 1–10 (in Chinese with English abstract).

Gems of Italy [alabaster to beryl]. *Rivista Italiana di Gemmologia/Italian Gemological Review*, No. 3, 2018, 16–28.

Jadeitite and other high-pressure metamorphic rocks from the jade mines belt, Tawmaw area, Kachin State, northern Myanmar. Thet Tin Nyunt, H.-J. Massonne and Tay Thye Sun, in A.J. Barber, K. Zaw and M.J. Crow, Eds., *Myanmar: Geology, Resources and Tectonics*, Geological Society of London Memoir 48, Geological Society of London, 2017, 295–315, http://dx.doi.org/10.1144/m48.13.

Mining rubies in Greenland—The Aappaluttoq ruby mine. A. Lucas, A. Palke and W. Vertriest, *InColor*, No. 37, 2018, 42–52, www.incolormagazine.com/incolor/37/42.*

The Montepuez ruby deposits, what's next? C. Simonet, *InColor*, No. 37, 2018, 32–40, www.incolormagazine.com/incolor/37/32.*

A new occurrence of euclase in Western Australia. S.M. Stocklmayer, *Australian Journal of Mineralogy*, **18**(2), 2017, 39–44.

A study of texture and structure of turquoise from Luonan, Shaanxi Province. Y. Luo, X. Yu, Y. Zhou and X. Yang, *Acta Petrologica et Mineralogica*, **36**(1), 2017, 115–123 (in Chinese with English abstract).

Tectonic environments of sapphire and ruby revealed by a global oxygen isotope compilation. J. Wong and C. Verdel, *International Geology Review*, **60**(2), 2017, 188–195, http://dx.doi.org/10.1080/00206814.2017.1327373.

Tectonic and metamorphic evolution of the Mogok metamorphic and jade mines belts and ophiolitic terranes of Burma (Myanmar). M.P. Searle, C.K. Morley, D.J. Waters, N.J. Gardiner, U. Kyi Htun, Than Than Nu and L.J. Robb, in A.J. Barber, K. Zaw and M.J. Crow, Eds., *Myanmar: Geology, Resources and Tectonics*, Geological Society of London Memoir 48, Geological Society of London, 2017, 261–293, http://dx.doi.org/10.1144/m48.12.

Trace-element compositions of sapphire and ruby from the eastern Australian gemstone belt. J. Wong, C. Verdel and C.M. Allen, *Mineralogical Magazine*, **81**(6), 2017, 1551–1576, http://dx.doi.org/10.1180/minmag.2017.081.012.

Trésors d'Orient : la Jadéite du Japon – son histoire et sa gemmologie (Treasures of the East: Japan's jadeite – Its history and gemology). A. Abduriyim, *Revue de Gemmologie A.F.G.*, No. 201, 2018, 4–11 (in French).

XAFS study on the location of Cu and Mn in a greenish blue elbaite from Alto dos Quntos [*sic*] mine, Brazil. K. Sugiyama, H. Arima, H. Konno and T. Mikouchi, *Journal of Mineralogical and Petrological Sciences*, **112**(4), 2017, 139–146, http://dx.doi.org/10.2465/jmps.161011.*

INSTRUMENTATION

Basic elements of photoluminescence spectroscopy in gemology. A. Scarani and M. Åström, *Rivista Italiana di Gemmologia/Italian Gemological Review*, No. 3, 2018, 44–47.

Computer colour grading of green jadeite jade based on HSL chroma parameter. L. Zhang and X. Yuan, *Journal of Gems & Gemmology*, **19**(3), 2017, 45–51 (in Chinese with English abstract).

Real-time microradiography of pearls: A comparison between detectors. S. Karampelas, A.T. Al-Alawi and A. Al-Attawi, *Gems & Gemology*, **53**(4), 2017, 452–456, http://dx.doi.org/10.5741/gems.53.4.452.*

Thermal inertia – What is it and why should we care? K. Feral, *Gemmology Today*, February 2018, 74–77, www.worldgemfoundation.com/GTFEB2018DV4/html5forpc.html?page=0.*

The value of simple, portable instruments – Part 2. My favorite gem-testing tool: The calcite dichroscope. A. Matlins, *Gemmology Today*, February 2018, 42–43, 46–48, www.worldgemfoundation.com/GTFEB2018DV4/html5forpc.html?page=0.*

MISCELLANEOUS

2019 forecast color palette as seen through the lens of the gem & jewelry industry. K. Champion, *GemGuide*, **37**(1), 2018, 10–12.

Les dislocations dissoutes : des inclusions pas toujours faciles à identifier - 2nd partie (Dissolved dislocations: Inclusions not always easy to identify – Part 2). M. Philippe and E. Fritsch, *Revue de Gemmologie A.F.G.*, No. 201, 2018, l2–16 (in French with English abstract).

Forensic gemmology. What legally constitutes a gem? M. Calabrò, *Rivista Italiana di Gemmologia/ Italian Gemological Review*, No. 3, 2018, 32–35.

Gem virtuosos: The Drehers and their extraordinary carvings. R. Weldon, C. Jonathan and R. Tozer, *Gems & Gemology*, **53**(4), 2017, 404–422, http://dx.doi.org/10.5741/gems.53.4.404.*

From gemstones to stamps: A colourful issue. G.B. Sutherland and F.L. Sutherland, *Australian Journal of Mineralogy*, **18**(2), 2017, 23–28.

A study on problems faced by exporters of gems and jewellery industry [in India]. P. Agarwal, R. Devgun and J.S. Bhatnagar, *IOSR Journal of Business and Management*, **19**(4), 2017, 1–7, http://dx.doi.org/10.9790/487x-1904040107.*

NEWS PRESS

A battle over diamonds: Made by nature or in a lab? P. Sullivan, *New York Times*, 9 February 2018, www.nytimes.com/2018/02/09/your-money/synthetic-diamond-jewelry.html.*

Multinationals move in to Colombia's emerald mountains. *The Economist*, 6 January 2018, http://tinyurl.com/y8xqs3nf.*

The mystery of the Mont Blanc treasure chest and the Frenchman who claims it. *The Local*, 12 February 2018, www.thelocal.fr/20180212/frenchman-still-waiting-to-know-if-mont-blanc-treasure-will-be-his.*

Precious gems bear messages from Earth's molten heart. N. Angier, *New York Times*, 11 December 2017, www.nytimes.com/2017/12/11/science/gemstones-diamonds-sapphires-rubies.html.*

Secrets to Earth's interior found trapped in diamonds. I. Semeniuk, *The Globe and Mail*, 8 March 2018, www.theglobeandmail.com/technology/science/earths-innermost-secrets-trapped-in-diamonds/article38257647.*

Top jewellery brands warned on ethics behind supply chains. H. Sanderson, *Financial Times*, 8 February 2018, www.ft.com/content/a7f19c58-0c35-11e8-8eb7-42f857ea9f09.

Why diamonds and gems are catching the eye of serious investors. J. Newman, *Robb Report*, 29 November 2017, http://robbreport.com/style/jewelry/serious-investors-turn-diamonds-gems-e17-2763388.*

ORGANIC GEMS

Application of GC-MS and FTIR in identification of amber and copal resin. J. Li, Y. Lan, C. Hu and X. Li, *Journal of Gems & Gemmology*, **19**(2), 2017, 9–19 (in Chinese with English abstract).

Fluorescence spectral characteristic of blue amber from Dominican Republic, Mexico and Myanmar. W. Jiang, S. Nie and Y. Wang, *Journal of Gems & Gemmology*, **19**(2), 2017, 1–8 (in Chinese with English abstract).

Gemmological characteristic of hydrothermally treated amber. W. Jiang, Y. Wang, S. Nie and F. Liu, *Journal of Gems & Gemmology*, **19**(1), 2017, 9–16 (in Chinese with English abstract).

Identification characteristic of a new ivory imitation material. L. Yu, *Journal of Gems & Gemmology*, **19**(3), 2017, 24–34 (in Chinese with English abstract).

Identification of the repaired amber. H. Zhu, B. Sun and F. Yan, *Superhard Material Engineering*, **29**(2), 2017, 65–67 (in Chinese with English abstract).

Representation of functional group and thermal variation behavior of jet in Fushun Liaoning. Y. Xing, *Spectroscopy and Spectral Analysis*, **37**(6), 2017, 1819–1825 (in Chinese with English abstract).

Type of amber from Myanmar and its gemmological characteristic. X. Xie, J. Di and X. Wu, *Journal of Gems & Gemmology*, **19**(5), 2017, 48–59 (in Chinese with English abstract).

PEARLS

Akoya cultured pearl farming in eastern Australia. L.M. Otter, O.B.A. Agbaje, L.T.-T. Huong, T. Hager and D.E. Jacob, *Gems & Gemology*, **53**(4), 2017, 423–437, http://dx.doi.org/10.5741/gems.53.4.423.*

Mono- and polychromatic inner shell phenotype diversity in *Pinctada margaritifera* donor pearl oysters and its relation with cultured pearl colour. C. Ky, C. Lo and S. Planes, *Aquaculture*, **468**(1), 2017, 199–205, http://dx.doi.org/10.1016/j.aquaculture.2016.10.017.

Spectral characteristics and coloration mechanism of silver-gray color seawater cultured pearls produced by *Pinctada martensii*. Y. Song, Y. Zhang, Y. Wu and Z. Lu, *Acta Mineralogica Sinica*, **37**(6), 2017, 712–716 (in Chinese with English abstract).

The transition of pearl trade and the Mikimoto's strategy for constructing reciprocal relationship. N. Sato, *Journal of North-east Asian Cultures*, **1**(50), 2017, 419–435, http://dx.doi.org/10.17949/jneac.1.50.201703.024 (in Korean with English abstract).

SIMULANTS

Gemmological characteristic of imitated turquoise. L. Zhu, C. He, M. Yang, J. Di, R. Lu and A.H. Shen, *Journal of Gems & Gemmology*, **19**(6), 2017, 15–20 (in Chinese with English abstract).

Gemmological characteristic of turquoise imitation: Gorceixite. Y. Qu, *Journal of Gems & Gemmology*, **19**(4), 2017, 25–30 (in Chinese with English abstract).

Gemological and mineralogical characteristics of an imitation of Dushan jade. K. Meng, Y. Luo, F. Jiang, X. Du, Z. Wang, M. Gu and J. Luo, *Acta Mineralogica Sinica*, **37**(3), 2017, 342–346 (in Chinese with English abstract).

The identification features of lapis lazuli imitation and the optimally processed lapis lazuli. S. Zhu and F. Deng, *Superhard Material Engineering*, **29**(1), 2017, 55–58 (in Chinese with English abstract).

Identification of the reconstituted blood stone. H. Zhu, T. Li, F. Yan, P. Wang and X. Zhao, *Superhard Material Engineering*, **29**(5), 2017, 65–68 (in Chinese with English abstract).

Structure and identification method of various composite gemstones. L. Yu, *Superhard Material Engineering*, **29**(5), 2017, 61–64 (in Chinese with English abstract).

SYNTHETICS

Analysis of type IIb synthetic diamond using FTIR spectrometry. I.V. Klepikov, A.V. Koliadin and E.A. Vasilev, *IOP Conference Series: Materials Science and Engineering*, **286**(1), 2017, article 012035, 5 pp., http://dx.doi.org/10.1088/1757-899x/286/1/012035.*

Measurements of natural and synthetic diamond samples using kelvin probe, surface photovoltage and ambient pressure photoemission techniques. S. Challinger, I. Baikie and A.G. Birdwell, *MRS Advances*, **2**(41), 2017, 2229–2234, http://dx.doi.org/10.1557/adv.2017.143.

Progress of high quality diamond single crystal prepared by CVD method. X. Liu, H. Guo, X. An, Y. Li and L. Jiang, *Journal of Synthetic Crystals*, **46**(10), 2017, 1897–1901 (in Chinese with English abstract).

Spectroscopic study of synthetic hydrothermal Fe^{3+}-bearing beryl. M.N. Taran, M.D. Dyar and V.M. Khomenko, *Physics and Chemistry of Minerals*, 2017, 8 pp., http://dx.doi.org/10.1007/s00269-017-0936-8.

TREATMENTS

Colour change of colourless-yellowish scapolite by electron irradiation and heat treatment. J. Jiang, M. Chen and Q. Ren, *Journal of Gems & Gemmology*, **19**(1), 2017, 22–29 (in Chinese with English abstract).

Enhanced lapidary materials: Phantoms of the opera. H. Serras-Herman, *GemGuide*, **37**(1), 2018, 4–9.

Gemmological characteristic and heat treatment of gem-quality zircon from Muling, Heilongjiang Province. H. Ai and X. Zhai, *Journal of Gems & Gemmology*, **19**(6), 2017, 1–6 (in Chinese with English abstract).

Gemmological characteristic of Zachery electrolytic treated turquoise and natural turquoise. X. Xu, H. Song, C. Yang, J. Liao, Y. Yu, S. Chen and X. Chen, *Journal of Gems & Gemmology*, **19**(5), 2017, 14–24 (in Chinese with English abstract).

Influence of water on turquoise quality characterized by spectroscopy under variable temperatures. Z. Dai, X. Lyu, Y. Gong and J. Ni, *Journal of Gems & Gemmology*, **19**(3), 2017, 12–23 (in Chinese with English abstract).

Mechanism analysis of the color enhancement of the brown tinted diamonds with HPHT. H. Jin and Y. Jin, *Acta Petrologica et Mineralogica*, **36**(1), 2017, 124–128 (in Chinese with English abstract).

The optical characteristic of electron irradiated beryl by UV-visible and mid-IR spectroscopic analyses. A. Ittipongse, *SNRU Journal of Science and Technology*, **9**(3), 2017, 568–573, www.tci-thaijo.org/index.php/snru_journal/article/view/102446.*

An overview of technology for heating processing for gemstone color improvement in recent years. X. Yan and J. Luo, *Superhard Material Engineering*, **29**(2), 2017, 61–64 (in Chinese with English abstract).

Preparation of "natural" diamonds by HPHT annealing of synthetic diamonds. C. Fang, Y. Zhang, Z. Zhang, C. Shan, W. Shen and X. Jia, *CrystEngComm*, **20**(4), 2017, 505–511, http://dx.doi.org/10.1039/c7ce02013a.

Research on the identification of filled tourmaline and its filling grade. S. Dai, W. Qu, Y. Xia, H. Chen, D. Chen, Q. Luo and S. Xu, *Journal of Mineralogy and Petrology*, **37**(3), 2017, 6–15 (in Chinese with English abstract).

Residual radioactivity of treated green diamonds. P. Cassette, F. Notari, M.-C. Lépy, C. Caplan, S. Pierre, T. Hainschwang and E. Fritsch, *Applied Radiation and Isotopes*, **126**, 2017, 66–72, http://dx.doi.org/10.1016/j.apradiso.2017.01.026.

COMPILATIONS

***G&G* Micro-World.** Aragonite spheres in Ethiopian opal • Twinned calcite inclusion in Burmese ruby • K-feldspar with iridescent inclusions • Yellow fluid inclusions in Burmese spinel • Dravite crystals on Burmese ruby • Vesuvianite in Burmese ruby • Wollastonite in manufactured glass beads • Shattuckite in quartz. *Gems & Gemology*, **53**(4), 2017, 466–471, www.gia.edu/gg-issue-search?ggissueid=1495258047309&articlesubtype=microworld.*

Gem News International. Facet-grade ruby from Longido, Tanzania • 50th anniversary of tsavorite discovery • Azurite-malachite from Peru • Type IIa diamonds with strong phosphorescence • Unusual growth structure in black diamond • More on the Foxfire diamond • Coated beryl imitating emerald • Filled freshwater cultured pearl • Update on dyed hydrophane opal • Conference reports • Peter J. Dunn (1942–2017). *Gems & Gemology*, **53**(4), 2017, 472–490, www.gia.edu/gg-issue-search?ggissueid=1495258047309&articlesubtype=gni.*

Lab Notes. Cat's-eye alexandrite with unique inclusion pattern • 'Lizard skin' pattern on deformed diamond • *Gota de aceite* in a Zambian emerald • Dyed quartzite imitation of ruby-in-zoisite • Synthetic moissanite imitating rough diamond • Natural sapphires with synthetic ruby overgrowth. *Gems & Gemology*, **53**(4), 2017, 459–464, www.gia.edu/gg-issue-search?ggissueid=1495258047309&articlesubtype=labnotes.*

CONFERENCE PROCEEDINGS

44th Rochester Mineralogical Symposium. Rochester, New York, USA, 20–23 April 2017, 46 pages, www.rasny.org/minsymp/Program Notes 44 RMS.pdf.*

**Article freely available for download, as of press time*

Save the Date!

The Gem-A Conference 2018

November 3-4, 2018

etc. venues County Hall, London, UK

- Discover an amazing line-up of **speakers** from all corners of gemmology
- Network with **industry leaders** during the Conference and at the Saturday evening dinner
- Learn from speakers and **fellow delegates**
- Attend **exclusive workshops** and enjoy guided trips including private viewings
- Be part of our **global community** of gemstone and diamond enthusiasts and professionals
- The Conference concludes with the **Gem-A Graduation** and Presentation of Awards!

Contact Us

21 Ely Place, London, EC1N 6TD,
United Kingdom
+44 (0)207 404 3334
information@gem-a.com
education@gem-a.com
membership@gem-a.com
www.gem-a.com

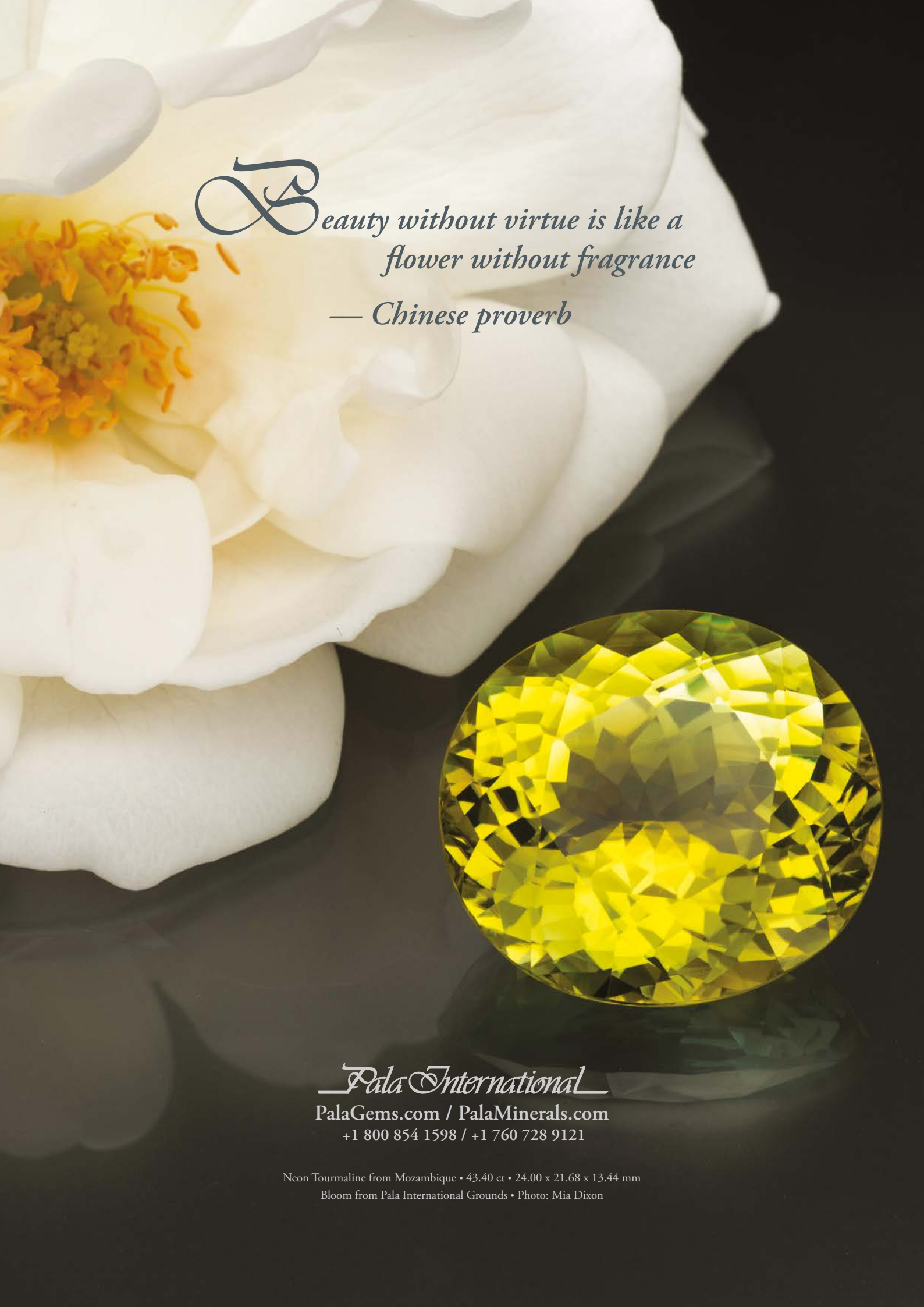

Pala International

PalaGems.com / PalaMinerals.com

+1 800 854 1598 / +1 760 728 9121

Neon Tourmaline from Mozambique • 43.40 ct • 24.00 x 21.68 x 13.44 mm

Bloom from Pala International Grounds • Photo: Mia Dixon